Institute of Biotechnology and

Department of Biosciences, Division of Genetics

Faculty of Biological and Environmental Sciences and

Viikki Doctoral Program in Molecular Biosciences

University of Helsinki

Finland

Structural studies on viral receptor-binding proteins

Violeta Manole

ACADEMIC DISSERTATION

To be presented for public examination with the permission of the Faculty of Biological and Environmental Sciences, University of Helsinki, in the lecture hall 3 of Viikin infokeskus Korona, Viikinkaari 11, Helsinki, on September 28th 2012 at 12 o'clock noon.

HELSINKI 2012

Supervisor

Professor Sarah J. Butcher

Institute of Biotechnology

University of Helsinki

Finland

Thesis committee

Professor Dennis Bamford

Institute of Biotechnology and

Department of Biosciences

University of Helsinki

Finland

Principal Investigator Hideo Iwai

Institute of Biotechnology

University of Helsinki

Finland

Reviewers

Assistant Professor Shee-Mei Lok

Duke-NUS Graduate Medical School

Center for BioImaging Sciences

National University of Singapore

Singapore

Docent Janne Ravantti

Institute of Biotechnology and

Department of Biosciences

University of Helsinki

Finland

Opponent

Professor Elena Orlova

Institute for Structural and Molecular Biology

Department of Biological Sciences

Birkbeck College

London, U.K.

Custos

Professor Tapio Palva

Department of Biosciences and Division of Genetics

Faculty of Biological and Environmental Sciences

University of Helsinki

Finland

ISBN 978-952-10-8261-0 (paperback)

ISBN 978-952-10-8262-7 (PDF)

ISSN number 1799-7372

http://ethesis.helsinki.fi

Unigrafia

Helsinki 2012

To my family

TABLE OF CONTENTS

LIST OF ORIGINAL PUBLICATIONS

I Manole V., Laurinmäki P., Van Wyngaardt W., Potgieter A.C., Wright I.M., Venter G., van Dijk, A.A., Sewell T.B., and Butcher S.J. (2012). Structural insight into African Horsesickness virus infection. *J Virol* **86**, 7858-7866.

VM planned experiments, performed and interpreted homology modelling, electron microscopy and image reconstruction experiments and wrote the manuscript.

II Huiskonen, J.T., Manole, V. Butcher, S.J. (2007). Tale of two spikes in bacteriophage PRD1. *Proc Natl Acad Sci U S A* **104**, 6666-6671.

VM planned experiments, performed experiments to produce material and contributed to writing the manuscript together with JTH and SJB.

III Pietilä, M. K., Atanasova N. S.*, Manole V.*, Liljeroos L., Butcher J.S., Oksanen H.M., Bamford D.H. (2012). Virion architecture unifies globally distributed pleolipoviruses infecting halophilic archaea. *J Virol* **86**,5067-5079.

VM planned experiments, performed and interpreted electron microscopy and image reconstruction experiments. VM, MKP and NSA wrote the manuscript.

*These authors have equal contributions.

ABBREVIATIONS

3D	three-dimensional
2D	two-dimensional
3DEM	electron cryo-microscopy and three-dimensional image reconstruction
AHS	African horsesickness
AHSV	African horsesickness virus
BTV	Bluetongue virus
CA	capsid domain of Gag polyprotein
CCD	charge-coupled device
cryoEM	electron cryo-microscopy
cryoET	electron cryo-tomography
cryoTEM	transmission electron cryo-microscopy
CTF	contrast transfer function
DNA	deoxyribonucleic acid
ds	double-stranded
EM	electron microscopy
ET	electron tomography
Env	envelope glycoproteins of HIV-1
F	fusion protein of measles virus
FEG	field emission gun
H	hemagglutinin protein of measles virus
HHPV	*Haloarcula hispanica* pleomorphic virus
HIV-1	human immunodeficiency virus 1
HM	hemagglutinin

HRPV	*Halorubrum* pleomorphic virus
HSV-1	herpes simplex virus type 1
IN	integrase
kV	kilovolt
L	polymerase of measles virus
M	matrix protein of measles virus
MA	matrix domain of HIV-1 Gag polyprotein
MCNC	matrix-covered nucleocapsids
N	nucleoprotein of measles virus
NA	neuraminidase
NC	nucleocapsid domain of Gag polyprotein
NP	nucleoprotein of influenza virus
NS	non-structural protein
ORF	open reading frame
P	phosphoprotein of measles virus
PCA	principal component analysis
PR	viral protease
RNA	ribonucleic acid
RNP	ribonucleoprotein complex
rRNA	ribosomal ribonucleic acid
RRV	Rhesus monkey rhadinovirus
RT	reverse transcriptase
SAXS	small angle X-ray scattering
SDS-PAGE	sodium dodecyl sulphate polyacrylamide gel electrophoresis

SIRV	*Sulfolobus islandicus* rod-shaped virus
ss	single-stranded
STIV	*Sulfolobus* turreted icosahedral virus
SV40	Simian Virus 40
T	triangulation number
TBSV	tomato bushy stunt virus
TEM	transmission electron microscopy
TMV	tobacco mosaic virus
VP	viral protein
wt	wild type
ZPC-EM	Zernike phase-contrast electron cryo-microscopy
Å	Ångström
σ	sigma, standard deviation

THESIS SUMMARY

Structure. Almost everything around us has it. But why? What is it needed for? Since the early days of human enquiry people have tried to understand how things come together and stay assembled. As scientific discovery advanced, researchers from all fields of science have been at some point or another puzzled by problems related to structure. Among them, biologists discovered that there is more to the natural world surrounding us than meets the eye. Structural biology studies are often hypothesis-driven and require flexible methods to address specific questions on the relationship between structure and biological function. My thesis discusses three cases in which structure is fundamental to function, and presents three different approaches to solving the three-dimensional structure of entire viruses or virus proteins, going from relatively well-ordered systems to increasing heterogeneous ones.

The first study is the characterization of African horsesickness virus, a double-stranded RNA icosahedrally-symmetric virus causing a severe disease in horses. I used electron cryo-microscopy and icosahedral reconstruction to determine the virion structures of two serotypes to 11 and 14 Å resolution. The three-dimensional structures allowed us to map two domains of the receptor-binding protein VP2, an important step for the informed design of new subunit vaccines for African horsesickness virus.

The second study is a description of the spike complex of bacteriophage PRD1, a membrane-containing virus. Here, the major problem was to determine the organization of flexible, low abundance proteins involved in cell recognition and attachment. This sort of heterogeneity in biological systems is key to their function, but very unfavourable for structural analysis. We used a combination of different mutants, electron cryo-microscopy three-dimensional image reconstruction and atomic modeling to address the symmetry mismatch between the icosahedrally-symmetric capsid and the spike complex situated at the five-fold vertices and determined the architecture of the spike complex formed by protein P5 and the receptor-binding protein P2.

The third study is a comparative biological and structural study of seven recently isolated pleomorphic viruses, which infect extremely halophilic archaea. I established the pleomorphic nature of this novel virion type by electron cryo-tomography. Detailed analysis

using subtomographic processing showed the radial distribution of the membrane and the spike protein VP4, and led to an average structure of VP4.

1. INTRODUCTION

1.1. Why is structure important

Structure. Almost everything around us has it. But why? What is it needed for? People have tried to understand how things come together and stay assembled for a very long time. Researchers from all fields of science are puzzled by problems related to structure at some point or another. Biologists have discovered that there is more to the natural world surrounding us than initially meets the eye. Large objects seem to be put together from smaller building blocks, and these from even smaller blocks. It seems there is a natural tendency for things to start with a simple structure, to which more elements are being added, increasing in complexity with each new level of organization. But how small is small? In the field of biology, by the early 1900s many macroorgansims had been characterized and classified, as well as more and more microscopic organisms readily observable with the light microscopes of the age. Such studies into bacterial life led Twort (in 1915) and d'Herelle (in 1917) to observe and isolate organisms smaller even than bacteria, which they called "invisible antagonistic microbes" (Twort 1915; D'Herelle 2007). Later on, these microbes were named "bacteriophages", "eaters" of bacteria, and were shown to be "particles with a size of about 100 nm made of proteins and nucleic acid" (Wurtz 1992). It was thus that the very first viruses (the bacteriophages) were discovered. Subsequent studies leading to the understanding of their parasitic (viral) nature set the foundations of modern molecular biology.

When it comes to viruses, simplicity in structure is defined by the number of layers and components a virus possesses. We tend to consider viruses composed of nucleic acid and a protein shell as having a 'simple' structural organization. However, some viruses acquire additional protein coats, lipid layers and proteins with specialized functions containing more complex structures.

Viruses display a wide range of sizes and shapes and yet they are made up of similar building blocks with common features in assembly: the viral genome is protected by a capsid made out of proteins, sometimes together with lipids. Their genomes are composed of different types of nucleic acid: DNA or RNA, single- or double-stranded, linear or circular. The sole purpose of viruses is to survive in the environment long enough to find a new host into which the viral genome can be delivered to produce a new generation of

viruses. The majority of viral genomes encode the minimum number of necessary proteins for viral replication and assembly inside the host cell, often exploiting the host cell machinery. In simple viruses, a single gene product is responsible for capsid formation, for more complex viruses the capsid is formed by several different proteins. Virus capsids are often symmetric, utilizing many copies of the same or a few different proteins, and thus minimizing the coding capacity required in the genome.

Every step in the viral life cycle involves complex interactions of the viral proteins with each other, with host proteins and with the viral genome. Such intricate processes raise a number of questions concerning the specificity of the interactions, how viral assembly is controlled and which are the factors involved in virus-host cell interactions.

One of the main roles of the viral capsid is to protect the genome from the extracellular environment, and so it has to be big enough to contain a full complement of genes. In addition, it can be responsible for host recognition and entry, for example in the case of the African horsesickness virus (AHSV) and PRD1 presented in detail in this thesis (Section 1.5, Section 1.6, Studies I and II). Hence the detailed knowledge of the capsid protein structure and its organization has great importance for the study of virus life cycle and virus inhibition.

1.2. Common principles of virus architecture

Bacteriophages and other simple viruses like tobacco mosaic virus (TMV) and tomato bushy stunt virus (TBSV) were some of the first model systems utilized for the study of the architecture of macromolecular assemblies (Caspar 1956; Crick and Watson 1956). Crick and Watson were the first to suggest that viral genomes code for a number of small protein subunits that organize in a symmetric array to form the viral coat. They predicted that the subunits would make identical repeated contacts between each other, throughout the viral capsid and obey either helical or cubic symmetry. Experimental data obtained by X-ray diffraction and electron microscopy (EM) proved that viruses with such symmetries exist (Klug 1960; Horne 1961). Viruses with helical symmetry obeyed the theoretical predictions. The size of the viral capsid is determined by the length of the genome, as the protein subunits assemble in a helix around the nucleic acid molecule. The contacts formed by each subunit with its neighbors are essentially identical, the only exception being the

protein subunits located at each end of the viral capsid. Spherical viruses, on the other hand, are not the same. In order for the Crick and Watson theory to apply, the icosahedrally-symmetric capsids should be constructed out of 60 subunits, all identical and forming identical connections to each other. However, spherical viruses often displayed capsids with more than 60 identical subunits, a fact that challenged Crick and Watson's predictions. A theoretical solution to the puzzle was proposed by Caspar and Klug, when they introduced the "Physical principles in the construction of regular viruses" (Caspar 1962).

Inspired by the geometry of Fuller geodesic domes, Caspar and Klug imagined an explanation for the formation of icosahedrally-symmetric shells with more than 60 subunits using planar nets. These planar surfaces are made out of equilateral triangles grouped into hexagons. Curvature is introduced into the net by substituting some of the hexagons in specific positions with pentagons. This then induces curvature, folding the net up into a three-dimensional volume. Caspar and Klug also introduced the concept of "quasi-equivalence": predicting that the bonds formed by the protein subunits would be of the same type throughout the capsid, but slightly "deformed" to accommodate the "non-symmetry related environments" (Caspar 1962) (**Figure 1**). This concept was coined before the first atomic models of icosahedrally-symmetric viruses were solved. The "slight deformation" that was predicted is rarely fulfilled, instead there are major conformational switches invoked by alternative N- and C-termini conformations between subunits and even additional proteins that change the local environment (Hogle, Chow et al. 1985; Hadfield, Lee et al. 1997; Abrescia, Cockburn et al. 2004).

The different types of icosahedrally-symmetric volumes can be described by the triangulation number, $T= h^2 + hk + k^2$ (where h and k are positive integers and define the positions in the lattice where a hexagon is replaced by a pentagon). In simpler words, the T number defines the number of steps necessary to travel between two fivefold vertices passing through local six-fold axes of symmetry (**Figure 1**).

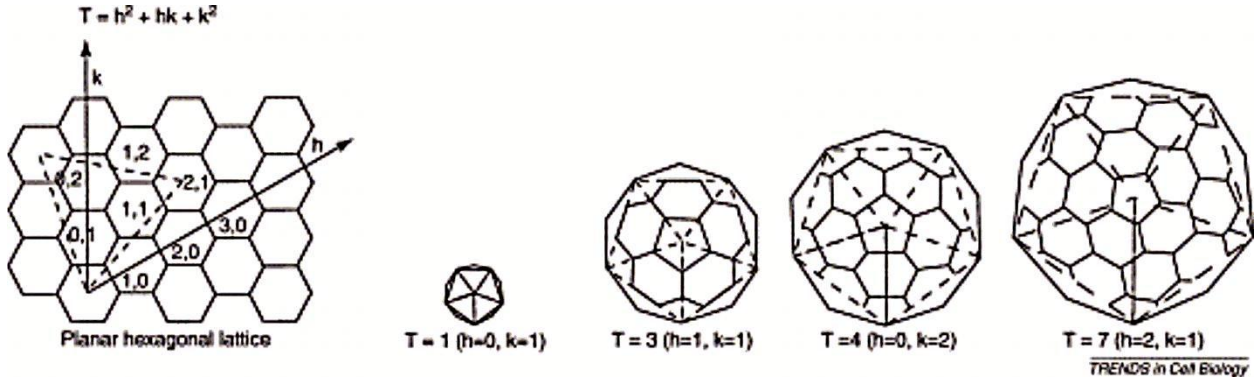

Figure 1. **Quasi-equivalence of subunits in shells of icosahedral viruses:** this principle (Klug 1960) explains how closed icosahedral capsids are constructed from multiples of 60 protein subunits (60T), organized as hexamer and pentamer units. Curvature can be introduced in a flat hexamer net by replacing some hexamers with pentamers. A closed shell is generated by inserting 12 pentamers in symmetrical positions. The multiplicity, T, depends on the vector (*h*,*k*) between the lattice points in the centres of hexagons in the sheet that become pentamers in the icosahedral shell. The subunits that make up the hexamers or pentamers interact with neighbouring subunits in T slightly different ways. Reprinted from Amos and Finch 2004 with permission from the publisher.

Thus, an icosahedrally-symmetric virus with twenty triangular facets has 3 x 20T asymmetric units (Caspar 1962). This has proven to be a very robust, useful theory for the description of many viruses. However, this calculation renders a discrete string of numbers which excludes certain values that have been experimentally observed in viruses. Some examples that illustrate this apparent contradiction between theory and practice are the inner core of bluetongue virus (Grimes, Burroughs et al. 1998) where an asymmetric dimer forms the inner capsid shell, thus using 120 subunits instead of 60, and the capsid structure of bacteriophage PRD1 which is a quasi T=25 structure, using trimers rather than hexamers to fill the lattice (Butcher, Bamford et al. 1995; Benson, Bamford et al. 1999; San Martin, Burnett et al. 2001; San Martin, Huiskonen et al. 2002; Abrescia, Cockburn et al. 2004). Thus, the quasi-equivalence theory elaborated by Caspar and Klug can often predict the correct localization of the capsomers, but it does not give information on their molecular composition (Caspar 1962). Another approach explaining virus symmetry is the tiling theory, which can be seen as a generalized principle of quasi-equivalence (Twarock 2004). The tiling theory states that any approximation of a spherical shape can have overall icosahedral symmetry given that the sphere is made up of tiles of the right shape. Thus, instead of considering only triangular tiles as in the Caspar-Klug theory, the tiling

theory takes into account shapes like kite, dart, large and small rhomb. The tiling theory has been used successfully to describe virus structures that did not obey the Caspar-Klug theory, like polyoma virus and Simian Virus 40 (SV40) where pentamers of the major capsid protein fill a T=7 lattice and L-A virus where asymmetric dimers of the major capsid protein form a T=1 shell (Rayment, Baker et al. 1982; Liddington, Yan et al. 1991; Twarock 2004)(**Figure 2**).

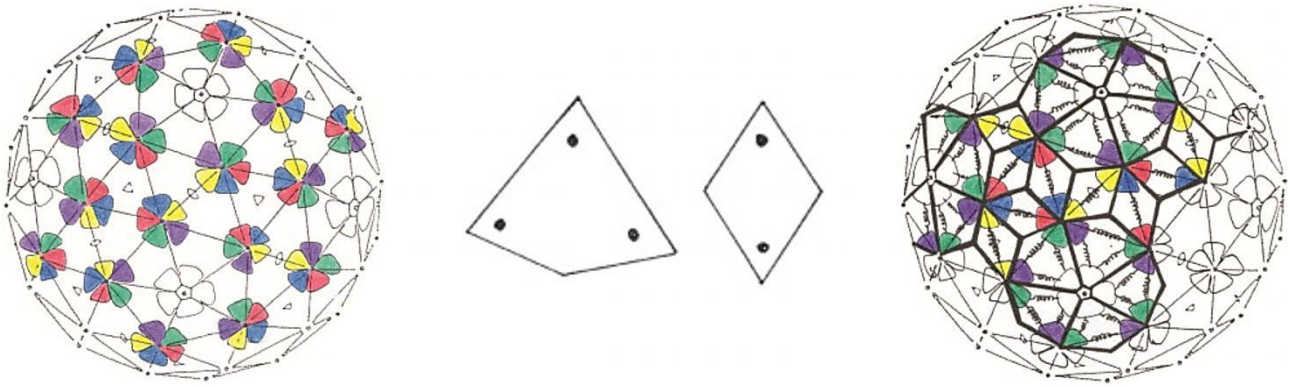

Figure 2. Viral tiling theory. A) Location of the protein subunits of polyoma virus on the 7d hexagonal lattice according to (Rayment, Baker et al. 1982); **B)** Tiles for the tesselation modelling the location of protein subunits for polyoma virus and Simian Virus 40; **C)** The tesselation for polyoma virus and Simian Virus 40 superimposed on the 7d hexagonal lattice. Spiral arms indicate the location of intersubunit bonds as observed in Modis, Trus et al. 2002. Reprinted from Twarock 2004 with permission from the publisher.

These common principles of virus architecture have led to an understanding of the basic construction of a viral capsid and of the importance of symmetry in its assembly. However, most viruses are much more complex than just a proteinaceous capsid, displaying a wide range of proteins decorating the capsid, to complexes consisting of tens of proteins such as the bacteriophage tail involved mainly in host entry and genome delivery. These special viral proteins vary in size, number, flexibility and position depending on the function, for example: they may only occupy some of the possible sites on the capsid, like the elongated structure decorating the capsid of the cyanophage Syn5 (Pope, Weigele et al. 2007). They may occupy all positions on the capsid, but have a symmetry mismatch compared to the local symmetry of the capsid where it is attached, like the hexameric packaging ATPase of phi8 attached to the five-fold vertices of the capsid (Huiskonen, Jaalinoja et al. 2007). They can be flexible like the tail fibers of bacteriophages or they can

be unique structures, for instance the unique packaging vertex of herpesvirus or PRD1 (Gowen, Bamford et al. 2003; Mesyanzhinov 2004; Chang, Schmid et al. 2007).

Most bacteriophages are called tailed viruses because of the presence of specialized host attachment structures. The overall morphology of a tailed phage consists of an icosahedrally-symmetric head packed with the genomic material, which connects to a helical tail through a complex connector structure. Only a few common tail morphologies are known: contractile or non-contractile long tails, and short non-contractile tails. The tail ends with a base plate, decorated with tail fibers. The main role of the fibers is to recognize the host receptors and to adsorb the virus on to the cell surface. Once the virus is bound to the cellular receptor, the base plate triggers a signal which causes the tail to contract and act as an injection needle through which the viral genome is delivered into the cytoplasm of the host (Mesyanzhinov 2004; Leiman, Arisaka et al. 2010). The components forming the tail complex have different symmetries with respect to each other. For example, in the case of the very well-studied phage T4, the dodecameric portal protein involved in genome packaging occupies one of the 12 five-fold vertices on the T4 icosahedral head. The tail connects to the packaging portal and has helical symmetry, which undergoes structural rearrangements during genome injection, when the tail contracts. The tail is assembled onto the hexagonal baseplate, which changes to a star-like conformation upon genome delivery. The six long tail fibers are elongated, rigid proteins, which can exhibit two different conformations - retracted or extended, and are the main structures for host cell recognition and adsorption (Mesyanzhinov, Leiman et al. 2004; Leiman, Arisaka et al. 2010).

Many eukaryotic viruses, as well as some bacteriophages and archaeal viruses, have a spherical capsid devoid of any tail structure. The host recognition and entry are driven by protein appendages situated on the outer surface of the viral capsid. Many of these different structures do not obey icosahedral symmetry and this symmetry mismatch induces a certain degree of instability in the overall virus structure. This is not a flaw in the virus architecture, but a means of making sure that the protective capsid will be able to disassemble and deliver the viral genome into the host cell. Such configurations are called metastable and are vital for dynamic biological processes. There are many such examples some of which are presented in detail later in the thesis (Section 1.4.5.1. Herpesvirus 1, Section 1.6. Bacteriophage PRD1).

Other receptor-binding proteins are assembled in metastable configurations that can be primed by protein cleavage and consequently triggered by specific interactions within the host to change conformation, resulting in for example, fusion with the host. This is typical of the pH-sensitive fusion proteins of many enveloped eukaryotic viruses such as Human immunodeficiency virus (HIV) (Section 1.4.5.2), influenza virus (Section 1.4.5.3), and AHSV (Section 1.5) which when exposed to low pH, fuse with the host endosomal membrane. Viral receptor-binding proteins of related viruses show the most sequence variability, even if the overall fold is conserved. Because of this, we cannot rely just on homology modelling based on sequence alignment to predict the structure of these critical proteins and so we are dependent on experimental structure determination methods such as EM and X-ray crystallography (Bertin, de Frutos et al. 2011).

1.3. Virus host-cell interactions

Viruses co-evolve with their hosts in what is a permanent battle for survival of the fittest. The wide genetic variation we see today in viruses partially reflects this evolutionary battle to escape from the continuously evolving host defense mechanisms. Receptor-binding proteins are generally the fastest evolving components of viruses. Their evolution allows evasion of the immune system, expansion of the host range by switching between hosts, and similarly is associated with developing different tissue tropisms (Pepin, Domsic et al. 2008). RNA viruses like influenza or HIV show high genetic variability, being able to adapt and escape host immunity by generating new variants of the receptor-binding proteins (Dai, Zhang et al. 2011).

In principle, any cell surface proteins can be used as receptors for virus attachment, and in many cases viruses have been observed to be able to bind more than one cellular receptor. The reasons for this are many fold. For instance, the virus could infect host cells in different organs where replication can be the most efficient or in some scenarios where maintaining dormant infection is advantageous. It is thus necessary for the virus to recognize different cellular receptors, for example, measles virus uses SLAM to infect B-cells, but nectin-4 on epithelial cells (Lentz 1990; Muhlebach, Mateo et al. 2011; Noyce, Bondre et al. 2011). In extreme cases, the virus may need to recognize cells from different species,for example the arthropod-borne viruses such as AHSV that infect both insect and

mammalian cells (Backovic and Rey 2012). Influenza also crosses the species barrier being able to infect humans, birds and swine with little modification of the receptor-binding proteins. This is an important adaptation occurring through genetic reassortment inside swines, the virus becoming highly virulent in the process (Rogers and Paulson 1983; Dai, Zhang et al. 2011).

Virus particles can adhere to carbohydrates, lipids and proteins and thus identifying cellular receptors is often very difficult. Phages of Gram-positive bacteria have been shown to recognize and bind to cell surface carbohydrates, those of Gram-negative bacteria to bind to the sugar moieties of lipopolysaccharides, and some of the viruses of archaea attach to glycoproteins from the cellular S-layer (Beumer 1984; Quiberoni, Stiefel et al. 2000; Eichler 2003). For eukayotic cells, it has been shown that apart from its biochemical composition, the membrane curvature can also influence virus attachment rates (Kunding, Mortensen et al. 2011). Virus tissue tropism is mostly determined by the nature, number and distribution of specific molecules on the cell surface. However, viruses can also use more than one receptor on one cell type. In this case, the distinction is often made between attachment molecules that bring the virus into contact with the cell surface where it can then roll around on the surface and then binding to a secondary receptor will induce cell entry as seen in SV40 (Kukura, Ewers et al. 2009). The attachment can be a transient interaction, the entry via receptor binding is usually irreversible. SPP1 is a bacteriophage that recognizes at least two cellular receptors on its host, *Bacillus subtilis* (Vinga, Baptista et al. 2012). One of the ways that viruses can infect many different cells is to use a common surface molecule, for instance, influenza virus recognizes and binds to specific sialyloligosaccharide structures (Rogers and Paulson 1983; Ramos and Fernandez-Sesma 2012).

The reason why viruses need to attach themselves to cell is the necessity of close contact with the cellular surface, which triggers the viral genome, a subviral particle or the whole virus to be internalized into the cell. The studies presented here focus on the first step of host recognition by the viral receptor-binding proteins. Many different methods have been developed to study the interactions between virus and host. In my thesis I have mainly used structural methods with the aim of linking the mature virus structure to its biological function, concentrating on the receptor-binding proteins. Three separate viral systems are described in Sections 1.5, 1.6, and 1.7.

The next section introduces the techniques used, followed by a description of relevant examples from the literature of applications used for studying viruses.

1.4. History and current status of electron cryo-microscopy of virus structure

The dimensions of viruses are a limiting factor with respect to the methods of choice for studying them. The objects of interest for structural biologists lie, as the name suggests, at the level of structural building blocks – from macromolecular complexes to single molecules. Such objects need to be visualized in the range of ~100 Å to near atomic resolution, where resolution is the limit at which two features in an object can still be distinguished. To image objects as small as viruses, such a resolution is achieved by X-ray crystallography and transmission electron microscopy (TEM). Until recently, X-ray crystallography was the method rendering the highest resolution in the viral structure research field, with 280 X-ray structures (with resolution values ranging from 1.5 Å or less to about 10Å) deposited in the RCSB Protein Data Bank (www.pdb.org) accessed on the 06.7.2012 (Berman, Westbrook et al. 2000; Berman, Henrick et al. 2003). However, X-ray crystallography is limited by several important factors such as the need for very homogeneous samples, sample tolerance to certain buffers, the difficulty of empirically determining the conditions in which good diffracting crystals grow, sensitivity of the crystals to handling especially with whole viruses and the phase problem (Bamford, Cockburn et al. 2002; Cockburn, Bamford et al. 2003). At present, transmission electron cryo-microscopy (cryoTEM) combined with three-dimensional (3D) image processing is able to reach a similar level of detail as X-ray crystallography, as was demonstrated recently by two very interesting studies describing the 3D structure of human adenovirus (Liu, Jin et al. 2010; Reddy, Natchiar et al. 2010). Thus TEM, and in particular cryoTEM, is my method of choice and has been used in all the studies reported in this thesis. As all scientific methods, it too has its strengths and weaknesses. In the following sections cryoTEM is described in detail, along with its application in the virus structure research field.

1.4.1. Electron cryo-microscopy

Using the first commercial electron microscope ever produced, Helmut Ruska published images of a tailed bacteriophage (1940; reviewed in (Kruger, Schneck et al. 2000)) and allowed the first glimpses into viral structure. The development of the negative-stain procedure was especially useful in the visualization of viruses (Brenner and Horne 1959). Advances in computing power and software development led to the possibility of reconstructing in three dimensions the viral architecture, using TEM micrographs and the principle of common lines (Crowther, Amos et al. 1970a; Crowther 1971; Crowther 1971). The development of vitrification techniques for specimens and the advent of electron cryo-microscopy (cryoEM) (Adrian, Dubochet et al. 1984; Dubochet, Adrian et al. 1988) has since allowed the study of viral preparations under native hydrated conditions. Now it is regularly possible to solve the structures of icosahedrally-symmetric viruses at subnanometer resolution where we can identify major elements of secondary structure such as in the herpesvirus capsid (Zhou, Dougherty et al. 2000), Bam35 (Laurinmäki et al. 2005), coxsackievirus A7 (Seitsonen et al. 2012) and the enveloped Semliki Forest virus (Mancini, Clarke et al. 2000). The first tracing of a complete Cα backbone was in the α-helical hepatitis B capsids at around 7.5 Å resolution (Bottcher, Wynne et al. 1997; Conway, Cheng et al. 1997). Lately, there have been further improvements with a number of detailed structures determined including those of adenovirus (Liu, Jin et al. 2010), cytoplasmic polyhedrosis virus (Yu, Jin et al. 2008), rotavirus (Zhang, Settembre et al. 2008; Chen, Settembre et al. 2009; Settembre, Chen et al. 2011), aquareovirus, (Zhang, Jin et al. 2010), P22 (Parent, Khayat et al. 2010; Chen, Baker et al. 2011), Venezuelan equine encephalitis virus (Zhang, Hryc et al. 2011), bacteriophage epsilon15 (Jiang, Baker et al. 2008), and the podovirus P-SSP7 (Liu, Zhang et al. 2010). Recently, this high-resolution work has given insight into the bullet-shaped vesicular stomatitis virus (Ge, Tsao et al. 2010) and the helical tobacco mosaic virus (Sachse, Chen et al. 2007) as well.

One of the reasons why we have seen advancements in the structure determination from cryoEM-micrographs is due to improvements in the electron microscope. These include improvements in electronic stability, in the electron source size and coherence, in the physical stability through vibration isolation, better manufacturing and increased accelerating potentials. A schematic representation of a transmission electron microscope is illustrated in **Figure 3**.

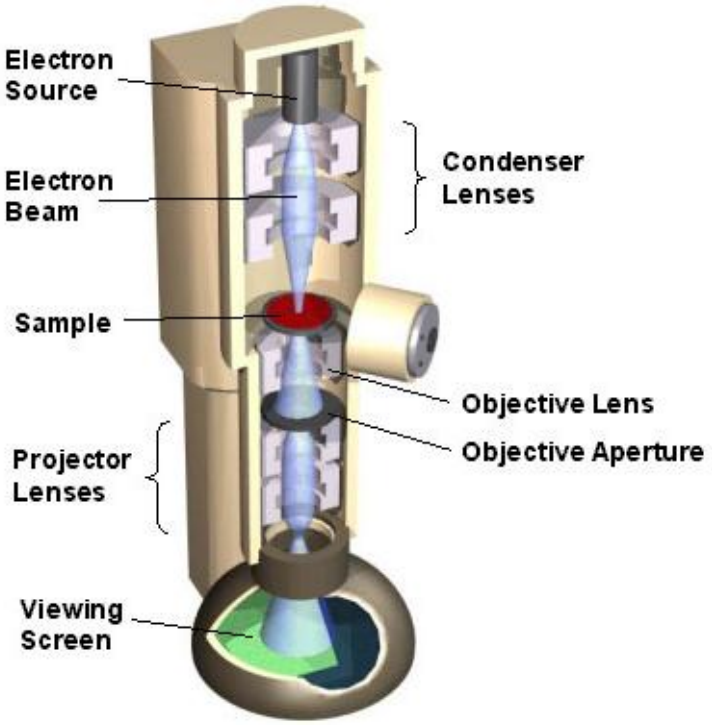

Figure 3. Schematic representation of a transmission electron microscope. Modified with permission from http://barrett-roup.mcgill.ca/tutorials/nanotechnology/nano02.htm accessed on 05.07.2012.

In the upper part of the microscope is the electron source, which can be either a heated metal filament or a field emission gun (FEG). Having a FEG as the electron source of the microscope is beneficial because the emitted electron beam is highly coherent, a property that improves the resolution of the data sets collected (Siegel 1971; Orlova and Saibil 2004). Similar to light microscopes, the electron microscope is equipped with lenses. These lenses are not optical ones, but magnetic coils that control and focus the electron beam. The first magnetic lens, the condenser lens, focuses the electron beam onto the specimen. After the beam has traversed the specimen plane, the objective lens collects the electrons and the final image is formed by the projector lens. The imperfections of these magnetic lenses (for example, the spherical aberration Cs of the objective lens) affect the achievable resolution. Recently, there have been advances in aberration correction, with commercial systems becoming available (Hosokawa, Tomita et al. 2003; Yu, Lentzen et al. 2012). As yet they have not made their mark on the virus structure field. The electron microscope column is kept under high vacuum maintained by a complex system of valves and pumps. The electrons would otherwise interact with air molecules as well as with the sample. The image formed in the microscope is recorded on sensitive film, which is subsequently digitized by scanning. Images can also be collected on charge-

coupled devices (CCD) or on direct electron detectors (Faruqi and Subramaniam 2000; Bammes, Rochat et al. 2012), an important development for automated data collection such as that used in electron cryo-tomography (cryoET) (Mastronarde 2005), and when very large data sets are collected.

One of the challenges of TEM is to preserve the structure of the specimen in the high vacuum of the column, under the high intensity of the electron beam. Biological samples contain water essential for structural integrity. The water has to be carefully removed during sample preparation to minimize distortion or collapse. In addition, there must be some contrast between the embedding medium and the sample so the structural detail is revealed. One of the first rapid and successful methods of visualizing the sample under the electron beam and vacuum of the microscope was negative staining, which creates a metal replica of the sample (Horne and Ronchetti 1974). The heavy metal coating scatters electrons very well, and this gives very good contrast in the image. However, the three-dimensional structural details can be completely lost because of sample flattening and dehydration partially induced by the high salt concentrations used (Boisset, Taveau et al. 1990; Harris and Scheffler 2002). A solution to maintaining the hydration in the sample for thin specimens came from the development of vitrification (Adrian, Dubochet et al. 1984; Dubochet, Adrian et al. 1988). This method relies on cooling the aqueous sample so rapidly that instead of ice crystals forming, the water is supercooled into an amorphous state (vitrified). This vitrified water has four main advantages, the sample stays hydrated even in the vacuum of the microscope, there are no ice crystals to disrupt molecular bonds, it can form a stable layer over a perforated support film and it is relatively transparent to electrons. A small aliquot (~3 µl) of sample suspended in an aqueous buffer is pipetted onto a holey carbon-coated copper grid that has been pretreated to reduce the hydrophobicity of the carbon film. The excess is blotted away leaving only a very thin layer of suspension. A thin layer is required to ensure maximal heat transfer during vitrification by plunging into a bath of ethane slush (-183°C) cooled by liquid nitrogen (Adrian, Dubochet et al. 1984; Dubochet, Adrian et al. 1988). This metastable state of vitrified water can be maintained by keeping the sample in liquid nitrogen to prevent devitrification (which occurs at a temperature between -133°C and -117°C) in all further steps. The grid is transferred to a cooled work station into a specially designed specimen cryo-holder. One end of the holder is attached to a dewar filled with liquid nitrogen. The cryo-holder enables us to transfer the grid into the microscope for imaging without heating the sample above

-133°C, where the vitrified water undergoes a transition to a crystalline phase (formation of cubic or hexagonal ice). To prevent water molecules in the microscope from building up on the cold sample as contamination (making the sample too thick to see through), the microscope has a cooled anticontaminator present. This is a “moisture trap” with a large surface area cooled with liquid nitrogen protecting the sample (Dubochet et al. 1988). Imaging the sample at liquid nitrogen temperature (-196°C for boiling nitrogen) or even better at liquid helium temperature (-269°C) protects it from radiation damage caused by the electron beam (Kuo and Glaeser 1975; Hayward and Glaeser 1979; Baker, Olson et al. 1999).

The sample is inspected in a low-dose imaging mode, to minimize the radiation damage. The first step is to search for a suitable area on the grid, with thin ice and a good sample concentration and distribution. This is done at low magnification and illumination. The next step requires focusing the image on an area adjacent to the area that will be imaged at high illumination and electron dose to avoid destroying the specimen. The area of interest is then exposed and the image is captured either on film or on CCD. The maximum total dose for one exposure has been calculated to be 20 electrons $Å^{-2}$. Exceeding this electron dose causes radiation damage to the specimen leading to a decrease in resolution (Kuo and Glaeser 1975; Hayward and Glaeser 1979).

1.4.2. Image formation

Image formation in transmission electron microscopy is not straightforward. For thin specimens assumed to be weak phase objects, the image obtained with the microscope is in fact a two dimensional (2D) projection of a three dimensional (3D) object (De Rosier 1968). During imaging, the electrons from the beam pass through the sample and interact with its components. The electrons colliding with the sample’s atoms are scattered either elastically or inelastically. Elastically scattered electrons keep their energy but have a modified trajectory. Inelastic scattering happens under small angles and the electrons in these types of collisions transfer their energy to the sample. This is the reason for beam damage (Kuo and Glaeser 1975). Some of the inelastically scattered electrons are removed by the microscope’s apertures, and some by using energy filters (Angert, Majorovits et al. 2000; Schroder 1992). All these events participate in the formation of a

projection on the image plane. The different ways electrons are scattered defines the contrast present in the image, which is defined by two components: amplitude contrast and phase contrast. Amplitude contrast is obtained when samples are stained. However, in cryoEM no staining is carried out and therefore amplitude difference contributing to contrast is minimal. Phase contrast arises from the fact that elastically scattered electrons have different phases than unscattered electrons. How much electrons are scattered depends on the sample. Under native conditions, biological samples are formed by light atoms which do not scatter electrons strongly. However, phase contrast can be enhanced by acquiring images with the electron beam focused under the image plane (under-focus settings). Focusing the beam above the image plane (over-focus) would lead to the cancellation of the amplitude and phase contrast effects, the two having opposite signs at over-focus. The relationship between the two contrast effects is described by the contrast transfer function (CTF), described by the following formula (Baker, Olson et al. 1999):

$$CTF(\nu) = -\{\left(1 - F_{amp}^2\right)^{\frac{1}{2}} \cdot \sin\left(\chi(\nu)\right) + F_{amp} \cdot \cos\left(\chi(\nu)\right)\} \cdot e^{-(\delta\nu)^2}$$

The CTF function is comprised of two terms added together: sin(χ(v)) is the phase contrast and cos(χ(v)) is the amplitude contrast term. F_{amp} is a constant (Toyoshima and Unwin 1988) and is the fractional amplitude contrast. $e^{-(\delta\nu)^2}$ describes the envelope function, an attenuation of the signal as a function of spatial frequency (v) and beam coherence (δ). χ(v) is a phase shift function introduced by the imperfections occurring in the microscope and described as follows:

$$\chi(\nu) = \pi \cdot \lambda(\Delta f \cdot \nu^2 - 1/2C_s \cdot \lambda^2 \cdot \nu^4)$$

where λ is the electron wavelength in the microscope, Δf is the defocus value, v is the spatial frequency and C_s is the spherical aberration caused by the imperfections of the magnetic lenses, and is specific to the microscope. In other words, the electron beam is limited in size and energy spread and this leads to a partial coherence that attenuates the contrast transfer function at higher spatial frequencies. This is one of the major factors that limit the resolution in TEM.

Figure 4 shows the shape of a CTF for a microscope with a 200 kV electron gun and a spherical aberration of 2.0 mm. The function is periodical and has negative terms as well as positive. In practical terms, this means the contrast in the image at different spatial frequency is reversed – black becomes white and vice versa. This can be corrected for by flipping the negative terms so they become positive (phase flipping). To fill the frequency spaces where the CTF is zero, images are collected at different defocii, or as focus pairs. Further compensation for the CTF is applied during the calculation of the reconstruction using a Weiner filter (Yan, Sinkovits et al. 2007). The decay can be compensated by the application of a temperature factor to the high resolution frequencies (Rosenthal and Henderson 2003; Fernandez, Luque et al. 2008).

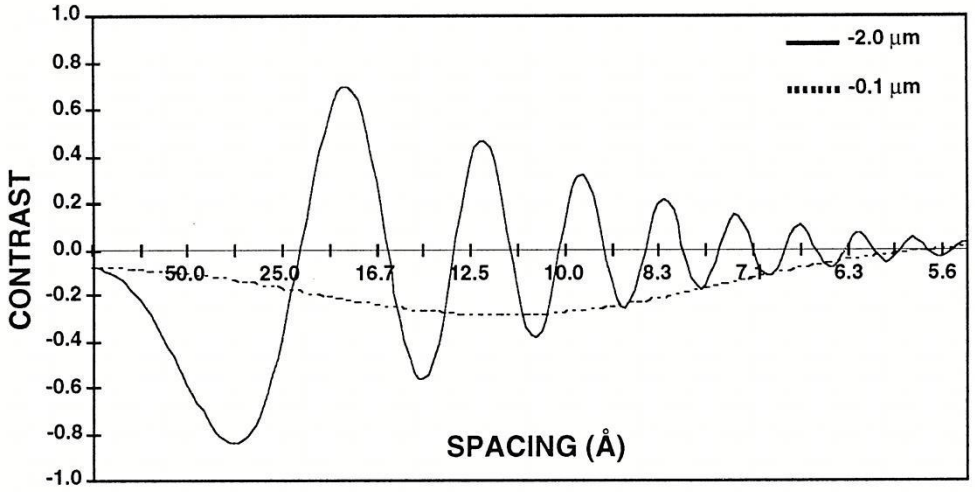

Figure 4. The CTF for a Philips CM200 FEG at 200 kV is plotted as a function of resolution in angstroms for an underfocus of 2 µm and an underfocus of 1,000 Å and a magnification of 336,000x. The decrease in the amplitude of the function with increased resolution reflects the measured attenuation due to the lack of coherence in the source, specimen movement, and other optical effects. The value of -0.1 at the origin is the amplitude contrast portion of the function. Reprinted from Baker, Olson et al. 1999 with permission from the publisher.

1.4.3. Image processing and 3D reconstruction

There are many factors that influence the quality of the cryoEM data. The sample purity, the buffer requirements, the ice thickness after vitrification, the temperature variations during sample handling, the small movements of the tip of the specimen holder due to

contraction or expansion of the metal under temperature shifts, and the movement (drift) of the specimen under beam irradiation or holder vibration. The quality of the electron micrographs can be assessed based on their Fourier transforms (Erickson and Klug 1971). Normally the Fourier transforms are computationally determined and they can be squared to generate a Fourier power spectrum. A Fourier power spectrum shows the contrast inversions of the CTF as Thon rings (Thon 1971). If the rings are elliptical, the image is astigmatic. If they are weak in one direction the image is drifted in the perpendicular direction. Thon rings can give a measure of the resolution limit in the image: the more the rings spread outwards, the higher resolution information is present in the micrograph. In practice the micrograph quality is assessed based on a comparison between the CTF calculated for the raw image and a theoretical CTF calculated at the same defocus level (Angert, Majorovits et al. 2000; Mindell and Grigorieff 2003). The selected micrographs show strong and even Thon rings that also reach the target resolution (approximately 8 Å as a lower limit). In the next processing step particle sub-images are identified and extracted automatically from the selected micrographs (Kivioja, Ravantti et al. 2000). The recorded micrographs are 2D projections of 3D objects and so the extracted particles are also 2D projections. To reconstitute the 3D structure of the original object it is necessary to sample the 3D space with a number of 2D projections at different angles (ideally from all possible views of the 3D object). There are different methods of getting these different views and they are sample dependent. If the object has an irregular, non-symmetric shape or a preferred orientation in the vitrified water, tilting the sample is required to obtain different views, and this is the approach used in random conical tilt and electron tomography (ET) data collection (Radermacher 1988; Chang, Liu et al. 2012). If the sample consists of identical objects, randomly oriented in the vitrified water, multiple views can be acquired in one image, and multiple images from different specimen areas can be combined together, thus the overall dose can be effectively limited (Crowther, Amos et al. 1970a; Crowther 1970b). Symmetry is a helpful property of the sample, since missing information can be recovered even when only a small number of different views of the object are available. For example, one icosahedrally-symmetric virus particle contains 60 identical copies of the asymmetric unit with known angular relationships. However, in order to increase the signal for image processing, many such images should be combined and thus, the angular relationship between the different projections must be calculated in order to reconstruct the 3D object of interest. There are three commonly used approaches for icosahedrally-symmetric viruses: the “common lines” method, the polar fourier transform

method with projection matching and the “random model” method (Crowther, Amos et al. 1970a; Crowther 1971; Crowther 1971; Fuller, Butcher et al. 1996; Marinescu 2003; Yan, Dryden et al. 2007; Yan, Sinkovits et al. 2007). The common lines approach is based on the projection theorem, which states that Fourier transforms of 2D projections are central sections through the Fourier transform of the original 3D object. So the 2D transforms of two projections at different angles intersect and the intersection line is a “common line” (Fuller, Butcher et al. 1996). Identifying these common lines leads to the determination of the angle between projections. Objects with icosahedral symmetry, have 37 pairs of common lines per projection, and 60 pairs between two projections. The polar fourier transform method was developed to speed up and to simplify the orientation determination by bringing in projection matching between a noise-free model and the data, with an icosahedrally-symmetric model being used to generate the initial projections and was used in Article II of my thesis. The third approach, the random model method, takes this one step further, to avoid model bias, the boxed-out particle images are centered and then, random orientations are assigned to a small subset of particles far from focus, several 3D reconstructions are calculated and each used independently as a model for refining the orientations (Marinescu 2003; Yan, Dryden et al. 2007; Yan, Sinkovits et al. 2007). In the next steps the best random model, having the highest resolution, is used to assign orientations for the entire data set. Further iterative rounds of model building and refinement are carried out until no improvement in the model is achieved. This method was used in Article I. This random model approach is very powerful for highly symmetric objects, but can also be used for objects with lower symmetry (Sanz-Garcia, Stewart et al. 2010). In contrast to many other single particle approaches, one does not need to generate class averages prior to orientation determination and the center and orientation of each particle is refined individually. The use of class averages for orientation determination also works very efficiently (Orlova, Dube et al. 1999; Orlova, Gowen et al. 2003). **Figure 5** summarizes the steps followed in solving the 3D structure of icosahedrally-symmetric particles.

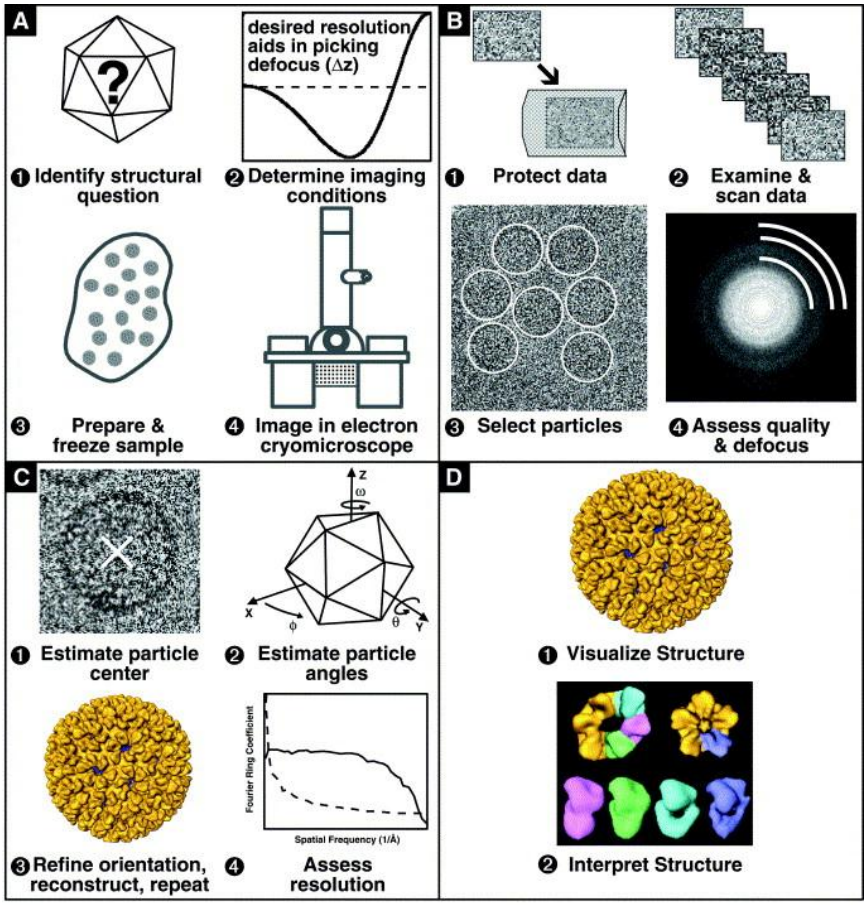

Figure 5. Overall scheme for structural studies of icosahedral particles using electron cryo-microscopy. (A) Virus particles are frozen and imaged in an electron cryo-microscope using imaging conditions determined based upon the specific biological questions being addressed and the desired resolution necessary to address those questions. **(B)** To ensure only high quality images are processed, data assessment is performed both before and after digitization. **(C)** The three-dimensional structure is determined in an iterative orientation determination process that is completed after assessment of the final resolution. **(D)** Last, a detailed structural analysis is performed to identify important structural features and to interpret the biological significance. Reprinted from Thuman-Commike and Chiu 2000 with permission from the publisher.

Even in objects displaying symmetry there are features that do not follow that symmetry. In viruses, the genome does not follow the icosahedral symmetry of the viral capsid so it appears as a compact mass of density, even though there may be very specific interactions between the capsid and the nucleic acid such as those found in MS2 where a number of hairpin loops in the genome dictate the co-assembly of the capsid with the RNA genome (Basnak, Morton et al. 2010; Morton, Dykeman et al. 2010; Rolfsson, Toropova et

al. 2010; Toropova, Stockley et al. 2011). Functional capsid proteins, such as viral spikes and packaging motors, are often present in non-stoichiometric amounts, do not follow the capsid symmetry and can also be flexible. For these problems, two approaches have been utilized in this thesis. The first method is called vertex reconstruction, the second one is cryoET. Vertex reconstruction was initially developed to deal with the issue of partial occupancy on viral vertices (de Haas, Paatero et al. 1999; Briggs, Huiskonen et al. 2005) and then expanded to explore symmetry mismatches (Huiskonen, Jaalinoja et al. 2007). In Article II of my thesis it was used in combination with homology modeling to look at the occupancy and flexibility of the PRD1 spike complexes on the five-fold vertices. The method utilizes icosahedral orientations determined for an icosahedrally-symmetric virus to pinpoint the locations of the five-fold vertices in the 2D images. These vertices are then extracted from the raw micrographs, retaining the information about the orientation with respect to the capsid, thus reducing the orientation search. As the signal is now from a very small object embedded in a thick specimen, the vertices must now be classified into similar projection classes, their orientations determined from class averages and then they can be used to generate a three-dimensional reconstruction by weighted back projection (van Heel, Gowen et al. 2000). The classification is done using principal component analysis (PCA), a type of multivariate statistical analyses that reveals the internal structure of a dataset starting from the variance within that dataset. Datasets with a multitude of variables, expressed as a set of coordinates in an N-dimensional space, can be simplified by PCA, which reduces the number of dimensions to the first principal components (hence the name of the method) thus simplifying the data interpretation. The PCA method applies to EM datasets analysis because of the many sources of variation within the EM images: noise, different orientations, irregular features etc. Mathematically, these variations are described by vectors called eigenvectors. The images corresponding to these vectors are called eigenimages and are further used to classify the data according to the orientation and the presence or absence of a spike complex for example.

Single particle processing is so well established, and the interpretation is also relatively straight forward because the structural elements, individual proteins, secondary structure, and even backbone can be discerned (detailed examples are given for two groups of viruses, Orbiviruses and Tectiviridae in Sections 1.5 and 1.6). However, tomographic reconstruction is methodologically at the level that single particle was twenty years ago, with basic questions of CTF estimation and correction, best data collection practices, and

software development in its infancy. Hence, showcases of what can be done will mainly be discussed in the tomography section (Section 1.4.5).

1.4.4. Homology modeling

Working with proteins is challenging and despite great advances in high throughput structural biology initiatives in recent years, more often than not solving the protein structure eludes the scientist (Matthews 2007). A way around this problem is to use homology modeling to generate an atomic model of the protein of interest. Homology modeling allows the construction of such a model starting from the protein amino acid sequence and a known tertiary structure of a similar protein (homologue). The way the model is generated depends on the availability of template structures in the protein databanks (Zhang 2008; Roy, Kucukural et al. 2010). If the protein of interest and the template from the database are similar in tertiary structure but not at the secondary structure level, the method used for generating the homology methods is called threading. This method matches the amino acid sequence of the target protein directly to known tertiary structures available in databases and generates several models with similar folds (Zhang 2008). For proteins with no matching secondary structures or folds in the databases, the models are built *ab initio*. Confidence in a homology model can be assessed based on scores defining the accuracy of the threading alignments and the convergence of the refinement simulations (Roy, Kucukural et al. 2010). Even models with low scoring can be used in predictions regarding the overall shape of the molecule and the presence of α-helices and β-sheets. One of the goals of homology modeling is to use the structure in determining the biological function of the protein of interest (Roy, Kucukural et al. 2010). In electron cryo-microscopy and three-dimensional image reconstruction (3DEM), homology modeling and data from atomic models of individual proteins is often used to help understand the complex densities that arise from the reconstruction of objects containing sometimes thousands of individual molecules. Hence it is possible to generate quasi-atomic models of much of the density, giving biological context to individual protein molecules that would otherwise be missing (Baker, Olson et al. 1999; San Martin, Burnett et al. 2001; San Martin, Huiskonen et al. 2002; Huiskonen, Jäälinoja et al. 2007; Jäälinoja, Roine et al. 2008; Seitsonen, Susi et al. 2010).

1.4.5. Electron cryo-tomography

When one starts to image irregular objects such as tissue samples, whole cells, cellular substructures or pleomorphous viruses, then averaging over long distances, or over many objects all of which are structurally incongruent requires different data collection and processing strategies, and most commonly electron tomography is used (Baumeister and Steven 2000). Electron tomography data collection is very similar to that of transmission electron microscopy, except that the data collection strategy defines the angular relationship between the multiple images that are taken from one area of a grid. Electron tomography (and in this case cryoET) requires a sample holder that can be tilted at different angles under the electron beam to collect serial projections (or tilt series) of the 3D object of interest (**Figure 6**).

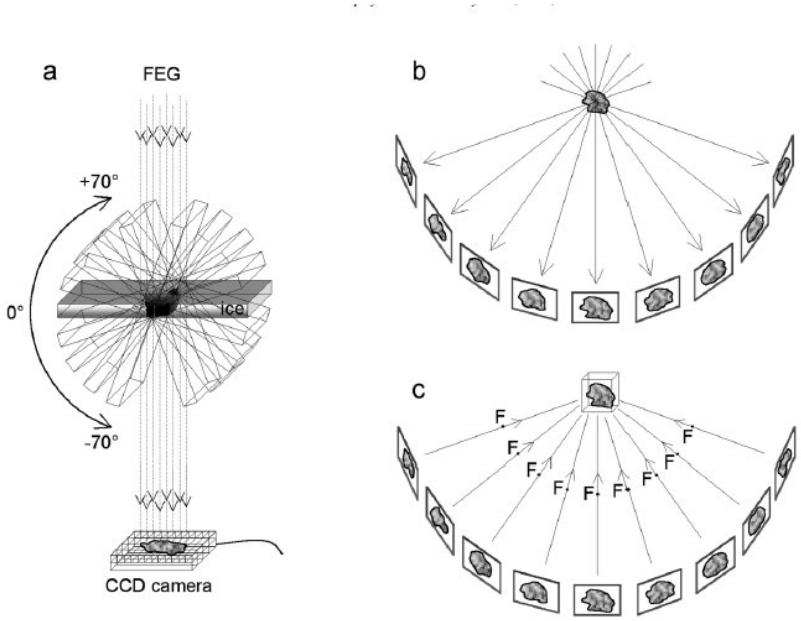

Figure 6. Principle of electron tomography. The basic idea underlying this method is to record series of 2D transmission electron micrographs (projection images) at different tilt angles for individual 3D objects. In practice **(a)**, the specimen holder is tilted incrementally around an axis perpendicular to the electron beam and projection images of the same specimen area are recorded on a CCD camera at each position. Tilt increments are typically 1.5–5.0^0 and the tilt range is approximately ±70^0. A more schematic diagram **(b)** illustrates the images projected by a specimen at successive tilt angles. After mutual aligning all of these projection images, they are synthesized into a density map (the tomogram) by a 'weighted backprojection' procedure **(c)**, effected in Fourier space. This map represents the distribution of density through the specimen volume. Reprinted from Grünewald, Medalia et al. 2003 with permission from the publisher.

The tilt angle is physically limited to ±70° because at higher angles the tip of the sample holder, the grid bars and the thickness of the vitrified water layer can all obscure the view. The tilt series is collected at a certain step size, according to the sample and expected resolution, ranging typically from 1.5° to 5.0° (Grünewald, Medalia et al. 2003). Another limiting factor in tomography is the repeated exposure of the sample to the electron beam and the accumulation of beam damage with every new projection in the tilt series. Tomographic tilt series are collected on CCD, using automated data collection which helps to correct for specimen drift (using tracking), and allows autofocusing and minimizes the electron dose used. This speeds up the process considerably (Mastronarde 2005). Electron cryotomography has a few shortcomings, which limit the resolution of the tomographic reconstruction. An accurate and reliable reconstruction would require a complete sampling from -90° to +90° using a step size as small as possible. In practice this is impossible because of the physical limitations of the sample holder and because of the beam damage the sample would be exposed to if too many steps are used. Since the highest tilt angle is ±70°, in a single-axis tilt tomography there will be information missing from the dataset: - the “missing wedge” effect. The limited tilt angle imposes a limit in the corresponding sections in Fourier space, which results in a wedge-shaped region with no information content (Carazo et al. 2005). This can be reduced to a cone by collecting double-tilt series. Due to the very low dose used in cryoET, each acquired image has very low signal-to-noise ratio. Because sample tracking during data collection is not very accurate, projections from a tilt series are normally aligned based on fiducial markers added to the sample before vitrification (Masich, Ostberg et al. 2006). Nanometer-sized (5 to 10nm) gold beads are commonly used as fiducial markers, because gold is electron dense and therefore gives very good contrast in cryoEM microscopy. Fiducial-less alignment of the tilt series is also possible, by aligning structural elements within the sample (Liu, Penczek et al. 1995; Brandt, Heikkonen et al. 2001). The final tomograms (the 3D reconstructions) are calculated using the aligned images and weighted back-projections. If single particle techniques can give resolutions of 3 or 4 Å, the best resolution tomography could offer until recently is around 50 Å (Grünewald, Medalia et al. 2003; Masich, Ostberg et al. 2006). With CTF correction and subtomogram averaging it is possible to achieve 20Å resolution (Zanetti, Riches et al. 2009). Subtomogram averaging requires the extraction of subvolumes from the tomographic reconstructions, which are subsequently aligned and averaged together. This method increases the signal to noise ratio and leads to an increase in resolution (Schmid 2011). Technological advances in

recent years have made it possible to implement an idea initially proposed by Zernike (1942) for light microscopy. The frequency of the scattered electrons can be modified by placing a phase plate in the back-focal plane of the objective lens, generating very high contrast of the sample at focus. Currently this method is limited by the lifetime of the phase plate (often only one series may be collected with one phase plate), and the difficulties incurred by having to recenter the phase plate for each new tilt. The maximum resolution that can be achieved using a phase plate is around 9 Å, so it is ideally suited for tomographic data (Liu, Zhang et al. 2010).

Electron tomography has been used very successfully to examine pleomorphic viruses such as herpes simplex virus type 1 (HSV-1), influenza A virus, human immunodeficiency virus 1 (HIV-1), measles virus etc. and these will be discussed in the next section.

1.4.5.1. Herpesvirus.

The alphaherpesvirus, HSV-1, is a human pathogen with a complex structure. It is one of the best characterized viruses by 3DEM using a combination of icosahedral symmetry averaging, vertex reconstruction, and cryoET. In addition, extensive genetic and biochemical experiments have also been conducted thereby unraveling its basic structure and life cycle. HSV-1 has an icosahedrally-symmetric nucleocapsid sheltering the viral genome, a lipid envelope containing glycoproteins, and a region between the capsid and the envelope called the tegument. The nucleocapsid is composed of 150 hexons, 11 pentons and a portal located at one vertex. The hexons and pentons are connected by triplexes, a unique structure to herpesviruses, involved in capsid growth and stability (Zhou, Chiu et al. 1998; Zhou, Dougherty et al. 2000; Baker, Jiang et al. 2003; Chang, Schmid et al. 2007; Deng, O'Connor et al. 2007; Rochat, Liu et al. 2011). The portal is a unique feature of the capsid and, since it does not follow the capsid symmetry, it was not readily identified using cryoEM and icosahedral reconstruction. However the virion has been characterized by cryoET and Zernike phase-contrast electron cryomicroscopy (ZPC-EM) and within the virion, the portal was shown to be similar in structure to portal connector complexes seen in other viruses like bacteriophages Epsilon15, P22 or Φ29 (Tang, Olson et al. 2008; Lander, Khayat et al. 2009; Chang, Schmid et al. 2010; Chen, Baker et al. 2011). The viral capsid looks different around this unique vertex, and the penton density is clearly missing. The portal appears to have 12-fold symmetry and is

located inside the capsid shell (Chang, Schmid et al. 2007; Deng, O'Connor et al. 2007; Rochat, Liu et al. 2011)(**Figure 7**).

Figure 7. Tomographic reconstruction of HSV-1 B capsid. **(a)** Radially colored icosahedral reconstruction of the HSV-1 B capsid showing the characteristic T=16 capsid shell; **(b)** The 12-fold average of the portal density shown in panel a sitting within the HSV-1 B capsid shell; **(c)** External view of the portal density extracted from the map showing 12 radially arranged densities. Modified from Rochat, Liu et al. 2011, with permission from the publisher.

Although the herpesvirus capsid interacts with the nuclear pore prior to the genome entering the nucleus (Ojala, Sodeik et al. 2000), no tail-like proteins, equivalent to those found in bacteriophages for host recognition and genome delivery were visible outside the herpesvirus capsid. This indicates that the main roles for the portal are for capsid formation, genome packaging and as a conduit for genome release into the nucleus. In herpesviruses, glycoproteins embedded into the envelope and tegument proteins connected with the viral capsid are responsible for host recognition, binding and entry (Deng, O'Connor et al. 2007). The hexons are decorated by the smallest capsid proteins which are, probably involved in capsid interactions with the tegument and cellular cytoskeletal proteins (Lo, Yu et al. 2003; Yu, Shah et al. 2005). The variability in shape and protein composition of envelope and tegument raised the same problems as the unique packaging vertex and were also addressed by cryoET. Using this approach it was shown that the HSV-1 capsid has an off-centered position with respect to the envelope, with the tegument forming a cap on one side of it (Grünewald, Desai et al. 2003). There are protein connections between the capsid pentons and the inner side of the tegument

through UL36, a protein shown to have a scaffolding role during tegumentation. UL36 was also shown to maintain the structural integrity of the tegument during viral infection, until the tegument disintegrates during infection (Newcomb and Brown 2010; Cardone, Newcomb et al. 2012). From the tomographic reconstructions, it was also possible to distinguish the reticular structure of the tegument and its connections to the envelope at the sites of the glycoproteins (Grünewald, Desai et al. 2003). In alphaherpesviruses the connections between the tegument and the viral capsid have an icosahedral arrangement and appear to anchor one end of the pentons to the adjacent triplexes (Zhou, Chen et al. 1999; Kim, Huang et al. 2011). In gammaherpesvirus the connections between the tegument compartment and the viral capsid do not have symmetric contacts, and the tegument is organized in two layers, an inner and an outer sub-compartment (Yu, Shah et al. 2011). Betaherpesvirus displays different types of contacts between the inner layer of the tegument and the capsid, forming a thin net surrounding the capsid (Zhou, Chen et al. 1999). These differences could also be related to differences in the outer regions of the capsid, observed for example in the case of Rhesus monkey rhadinovirus (RRV) A-capsid when compared to alphaherpesvirus capsid organization (Yu, O'Connor et al. 2003). Despite these differences in organization, it seems that the tegument serves similar roles in all three types of herpesviruses (Dai, Jia et al. 2008). The life cycle of a gammaherpesvirus has been studied by dual-axis electron tomography, and has confirmed observations from previous publications on other herpesviruses. It showed viral entry through endocytosis, endosome transport to the nucleus, genome injection, formation of intranuclear inclusion bodies following viral genome replication and protein expression, egress of viral nucleocapsids from the nucleus and the envelopment and de-envelopment process, tegumentation taking place in the cytoplasm, acquisition of the final envelope and egress from cell through exocytosis. The three dimensional reconstructions allowed direct observation of the events taking place during viral life cycle and eased the biological interpretation of the results (Peng, Ryazantsev et al. 2010). Another recent study employing cryoET has showed the tegument role in axonal transport of non-enveloped particles, and events taking place at the secondary envelopment sites of HSV-1 (Ibiricu, Huiskonen et al. 2011). Similarly to bacteriophages, it has been hypothesized that capsid assembly and maturation is initiated through the interaction of the portal complex with the major capsid protein, which in turn recruits the scaffolding protein.

1.4.5.2. Human immunodeficiency virus 1 (HIV-1).

HIV-1 is a well-studied human pathogen and another example of where understanding the structure has aided the understanding of the biological functions of different viral components. HIV-1 is a pleomorphic retrovirus with an RNA genome enclosed in a cone-shaped proteinaceous core. Upon budding the virus acquires its envelope, decorated with viral and host membrane proteins (Briggs and Krausslich 2011)(**Figure 8**).

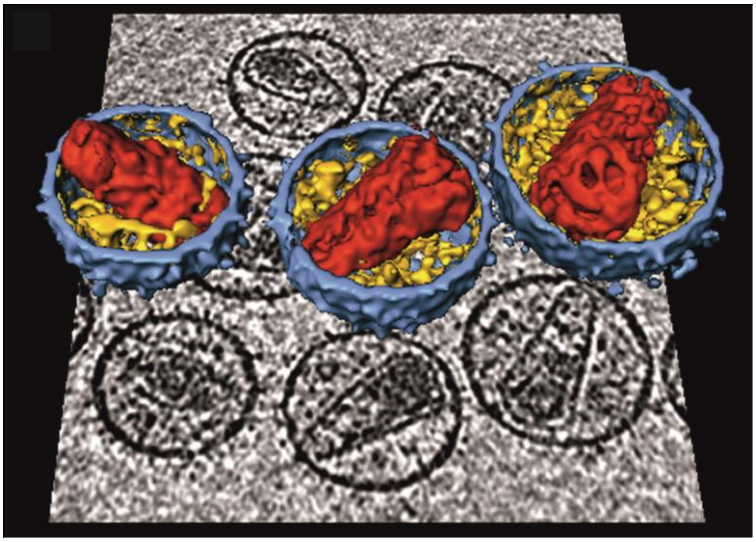

Figure 8. 3D Reconstruction of HIV-1 virions from cryoET. 3D rendering of three sample virions from the tomogram. Blue, viral membrane; yellow, density between the membrane and the core; red, viral capsid. Half of the blue and yellow densities have been computationally removed to reveal the core. The rendered virions are shown above a central slice through the reconstruction. Modified from Briggs, Grünewald et al. 2006, with permission from the publisher.

The trimeric envelope glycoproteins (Env) of HIV-1 are the receptor-binding proteins, interacting with the cellular receptor CD4 and a coreceptor. They are also sites targeted by neutralizing antibodies (Zanetti, Briggs et al. 2006). The Env spikes are heterodimers of gp120, a surface glycoprotein, and gp41, a transmembrane glycoprotein (White, Bartesaghi et al. 2010; Harris, Borgnia et al. 2011). The trimeric nature of Env spikes located on the virus surface was first shown by EM tomography of negatively stained virions (Zhu, Chertova et al. 2003). Recent cryoET investigations have reported the detailed structure of the Env trimer *in situ*, on the viral surface, showing three gp120 globular domains sitting upon a gp41 stem. The globular domains have a right-hand twist and seem to be separated from the gp42 stem density, as indicated by a cavity at the

center of the spike density (Zanetti, Briggs et al. 2006). The conformation of the Env trimer changes radically upon binding of CD4 and a 17b Fab fragment. The gp120 domains rotate in respect to the central three-fold axis, in addition to an out-of-plane rotation and a vertical movement of the three gp120 domains. There are also structural changes in the stem region, the opening of the upper globular domains of gp120 allowing the center of the gp41 stalk to be exposed. It has been proposed that upon binding to CD4, the globular part of the Env spike opens up and draws the virus in close contact with the cell. The closed structure of the unbound spike has the role of protecting the viral epitopes from making contact with antibodies, and helps the virus to elude the immune system (Liu, Bartesaghi et al. 2008; Liu, Wright et al. 2010). HIV-1 has two different architectures, depending upon the stage of the maturation process. The first step in HIV-1 maturation process involves assembly of uncleaved Gag polyproteins in an immature form of the virus. Uncleaved Gag polyprotein has three domains matrix (MA), capsid (CA) and nucleocapsid (NC) and three shorter peptides. MA, CA and NC are released as independent smaller proteins upon proteolytic cleavage of Gag. CryoET analysis of this HIV-1 form shows a network of hexameric Gag polyproteins interrupted by gaps, which allow the lattice to curve into a shell (Wright, Schooler et al. 2007; Briggs, Riches et al. 2009). X-ray structures of Gag domains fitted into the electron density (or density map) of the hexamers show a tight packed lattice in the immature HIV-1 particle and indicate that forming the cone-shaped core would require disassembly and rearrangement of the subunits rather than mere tightening of the immature shell (Briggs and Krausslich 2011). The approximate orientations of the Gag domains, derived from this fitting, show the N-terminus of CA domain arranged around the 6-fold positions in the lattice and delineating an opening at the center of the hexamer. The C-terminal part of the CA domain connects two adjacent hexamers at the 2-fold positions of the lattice. A helical bundle seems to contact the NC layer. The second step in the virus life cycle represents the maturation process, which requires proteolytic cleavage of Gag at five different sites. The structural changes occurring during maturation have been studied by cryoET of mutants for different cleavage sites. Thus it has been shown that disassembly of the immature Gag lattice requires cleavage at two sites, between the Gag CA domain and one of the peptides. Disorganization of the lattice allows access for viral protease (PR) to the remaining cleavage sites. At the very center of the mature HIV-1 particle is the ribonucleoprotein (RNP) complex, composed of two copies of positive-sense RNA coated by numerous copies of the NC protein, the reverse transcriptase (RT), integrase (IN) and viral accessory

protein. The RNP is protected by a conical shell, which contains 250 hexamers and 12 pentamers of the CA protein. Although the majority of cores are conically shaped, some tubular or aberrant shapes have also been observed. The narrow end of the core touches the matrix, composed of a few thousand copies of MA, which in turn lines the inner layer of the viral membrane (Benjamin, Ganser-Pornillos et al. 2005; Briggs and Krausslich 2011). Electron tomography of plastic-embedded sections, as well as cryoET and subtomogram averaging has given insight into events taking place at the assembly and budding sites. A continuous Gag shell forms under the plasma membrane, the large gap facing the cell and marking the place of the scission point. It has been suggested the cone assembly starts at the narrow end and its elongation is limited by the diameter of the virion (Briggs, Grünewald et al. 2006). Different stages of assembly have been observed and there is also evidence indicating that maturation can occur prior to particle release from the cell (Briggs and Krausslich 2011).

1.4.5.3. Influenza virus.

Flu is one of the most important and widely spread diseases in the world, constantly threatening to become pandemic. The pathogenic agent causing this disease is influenza virus, an enveloped RNA-containing pleomorphic virus. When it comes to pleomorphicity, influenza virus takes it one step further. Herpesvirus or HIV particles vary in size or protein composition, but the virions have a roughly spherical shape. Influenza virions vary even in this respect: round as well as elongated particles have been observed, both varying in size as well (Harris, Cardone et al. 2006; Calder, Wasilewski et al. 2010). As has been the case for the aforementioned HSV-1 and HIV-1, the best method for studying the 3D structure of influenza virus in close-to-native conditions on its own and during fusion is cryoET (Lee 2010). Most influenza virions have a lipid envelope covered irregularly with glycoprotein spikes and a dense proteinaceous matrix layer situated under the envelope and enclosing the viral RNPs (Harris, Cardone et al. 2006). The virus has a segmented genome formed by 8 RNA segments of negative polarity, associated with the nucleoprotein (NP) and with the viral polymerase (Calder, Wasilewski et al. 2010). Some virus particles show an incomplete matrix layer or the layer missing altogether. It has been shown that the M1 protein forms an ordered helical matrix under the viral envelope of filamentous influenza viruses and is responsible for determining virion morphology (Calder, Wasilewski et al.

2010; Fontana, Cardone et al. 2012). The spikes are formed by two different glycoproteins: hemagglutinin (HM) and neuraminidase (NA), and an ion channel protein M2. The viruses have less NA spikes than HA, which tend to cluster in patches on the virion opposite to the RNPs attachment point (Calder, Wasilewski et al. 2010). NA tetramers may have a role in both virus entry and egress from the cell (Fontana, Cardone et al. 2012). High resolution X-ray structures of HA at neutral (Wilson, Skehel et al. 1981) and low pH (Bullough, Hughson et al. 1994), as well as of NA (Varghese, Laver et al. 1983) helped to understand the molecular functions of these proteins. However, little was known about their behavior and conformational changes in the context of the native virus, a state best explored by cryoEM and cryoET (Fujiyoshi, Kume et al. 1994; Harris, Cardone et al. 2006; Calder, Wasilewski et al. 2010; Fontana, Cardone et al. 2012)(**Figure 9**).

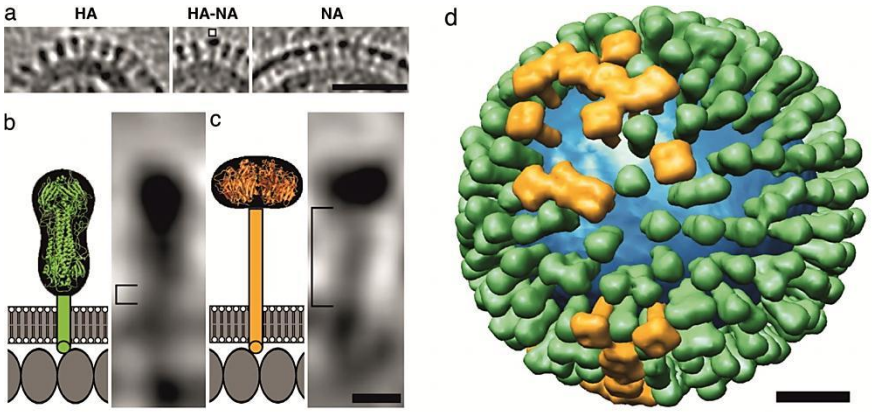

Figure 9. Distributions and shape-based differentiation of HA and NA spikes. (a) HA cluster (Left); single NA (marked) in a cluster of HAs (Center); and cluster of mainly NA spikes (Right). (Scale bar, 50 nm.) **(b and c)** The stem lengths of HA and NA (square brackets in **b** and **c**, respectively). The structures of the stems, transmembrane segments, and endodomain tails are not known, and they are shown schematically. Molecules in the matrix layer are inferred to be packed in a monolayer with a spacing of 4 nm. Scale bar, 5 nm. **(d)** Model of the distribution of glycoprotein HA (green) and NA (gold) on a single influenza virion. The lipid bilayer is blue. Scale bar, 20 nm. Modified from Harris, Cardone et al. 2006, with permission from the publisher.

The trimeric HA is a class I fusion protein required for cell entry, the HA0 precursor being activated by proteolytic cleavage by a cellular enzyme. The resulting subunits HA1 and HA2 remain connected by a disulfide bond. HA recognizes and binds cellular receptors containing sialic acid, and the virus is internalized by receptor-mediated endocytosis (Calder, Wasilewski et al. 2010).The low pH of the cellular endosome modifies the HA

structure further, leading to the dissociation of the outer-membrane domains of HA1, the fusion peptides are relocated towards the distal end of the HA molecule following a modification in the B-loop, and the transmembrane domains are positioned on the same side as the fusion peptides after a modification in the kinked loop of HA2. These structural modifications occurring in influenza A virus in a low pH environment were followed by cryoET and subtomogram averaging (Fontana, Cardone et al. 2012). It was observed that first the HA ectodomains disorganize and then the RNPs and the matrix layer M1 become condensed and cannot be distinguished from each other. The order in which the HA structural modifications occur, as well as the existence of intermediate states which might be reversible or not is still under debate. However, subtomogram averaging revealed two reversible intermediates during HA fusion process at low pH which suggest the movement of the fusion peptide and some part of HA2 domain outward, reaching state 1 conformation, followed by the lowering of the HA1 domains and their moving outwards in the state 2 conformation. This would allow access of the peptide fusion and the kinked loop to the exterior of the molecule, while the B-loop remains “unclamped” (Fontana, Cardone et al. 2012). It was proposed that these rearrangements are important during the endosomal passage of the virus, when it is exposed to a low pH environment. The model stipulates that HA adopts the reversible conformational change observed by cryoET and protons are being pumped inside the virus through the M2 ion channel, weakening the interactions between the matrix and the viral envelope. These modifications make the envelope more fusion-compatible with the endosomal membrane. The binding of matrix to the RNPs is also disrupted, allowing them to be released into the cytoplasm of the cell (Fontana, Cardone et al. 2012). Based on the structural information obtained for filamentous influenza virus an assembly mechanism has been proposed. The localization of the RNP assembly, distally from the viral membrane, could be one of the factors to trigger budding, which is driven afterwards by the polymerization of the matrix helix. The matrix protein could also be involved in concentrating the glycoproteins at the budding site, in their distribution on the surface of the envelope and in the interaction with the RNPs (Harris, Cardone et al. 2006; Calder, Wasilewski et al. 2010). The viral M2 protein, as well as cellular factors like actin may also be involved in the formation of influenza filamentous viruses.

1.4.5.4. Measles virus.

Measles virus is a member of the *Paramyxoviridae* family, along with other human pathogens and displays a pleomorphic structure. It has a segmented genome of single stranded, negative sense RNA. The genome is bound to the nucleoprotein (N) forming a helical nucleocapsid. Also bound to the nucleocapsid are the viral polymerase (L) and the phosphoprotein (P) (Jensen, Communie et al. 2011). The N protein has two domains, an intrinsically disordered N_{TAIL} domain interacting with P, and an RNA binding domain N_{CORE}. It has been suggested that N_{TAIL} could act as a hook for the viral polymerase complex in solution and attach it to the nucleocapsid, initiating transcription and replication of the genome (Jensen, Communie et al. 2011). Measles also has a matrix protein (M), and a lipid envelope decorated with two types of glycoproteins, fusion (F) and hemagglutinin (H) (**Figure 10**) (Liljeroos, Huiskonen et al. 2011).

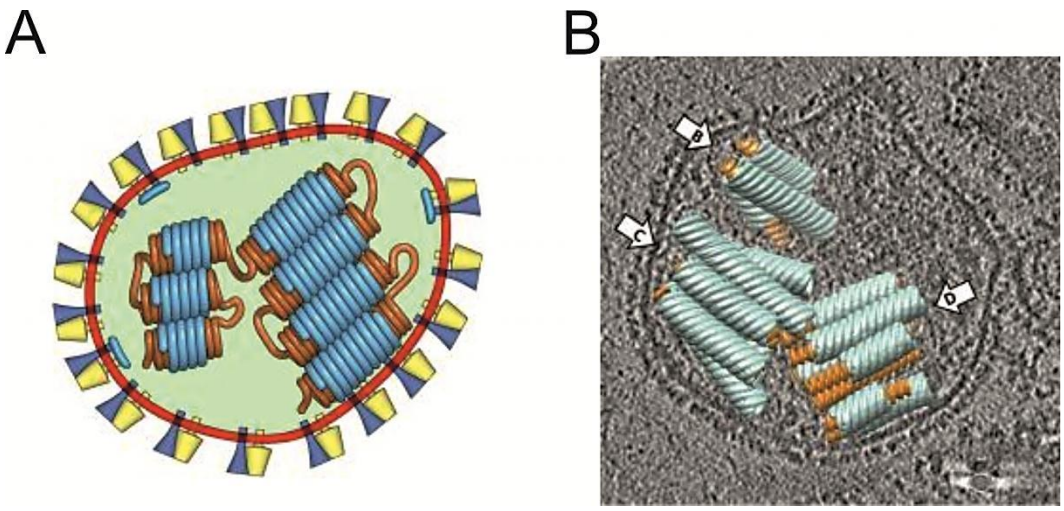

Figure 10. (a) Schematic diagram illustrating the organization of measles virus; **(b)** The averaged structures for the matrix (blue) and nucleocapsid (orange) filaments were placed back into the density map of a virion (one section is shown in gray scale, positive density is black). Modified from Liljeroos, Huiskonen et al. 2011, with permission from the publisher.

The glycoproteins are involved in viral recognition of the host and entry. Unlike other viruses from the family, measles H protein binds to the cellular receptor SLAM (CD150) which does not contain sialic acid (Hashiguchi, Ose et al. 2011). Vaccine strains of measles can also use an alternate receptor, CD46 (Dorig, Marcil et al. 1993). H probably

forms dimers and tetramers on the viral surface, and the partial disassembly of the trimers could be the mechanism triggering fusion with the cell. Binding of the H tetramers to the cell receptor would induce a conformational change in H protein, allowing the virus to come into close proximity with the cellular membrane. This would allow F protein trimers to undergo conformational change and initiate fusion (Hashiguchi, Ose et al. 2011). Until recently, based on its similarities to Sendai virus, it was believed that the matrix protein coats the inner surface of the membrane in a non-continuous layer (Loney, Mottet-Osman et al. 2009). The fact that M is translocated and binds to cell membranes also supported this interpretation (Riedl, Moll et al. 2002; Pohl, Duprex et al. 2007). Liljeroos et al. conducted a tomographic reconstruction study of the measles virus, showing that the matrix protein does not reside under the viral envelope but mostly coats the nucleocapsids as a second helical layer together forming matrix-covered nucleocapsids (MCNC). Similarly to the nucleocapsid helix, the M layer is a left-handed helix, with a larger pitch and with a probable repeating structural unit of dimers (**Figure 10**). These observations allow a renewed interpretation of the measles assembly pathway. It seems possible that the nucleocapsids associate with matrix already in the cytosol before being transported to the cellular membrane. The tight packing of bundles of MCNC suggests that M proteins can interact with each other, contributing to the compact packing of the viral genome. Since most of the matrix is localized on the surface of the nucleoproteins, it seems that it is not the major factor inducing membrane-curvature at the budding site. This might be a cellular protein working in concert with the glycoproteins. It has also been suggested that the ribonucleocapsid nucleates the assembly of the M helix, but its elongation depends on M-M interactions (Liljeroos, Huiskonen et al. 2011).

1.5. African horsesickness virus

African horse sickness (AHS) is a non-contagious, infectious disease of the *Equidae* family, with a mortality rate of over 90% in susceptible horses (those that have not been previously exposed to the disease or vaccinated) and only rarely manifesting clinical signs in donkeys, mules or zebra (Erasmus 1973). AHS is endemic to regions in sub-Saharan Africa and the Arabian Peninsula, but sporadically causes epidemics as far away as India and Southern Europe (Mellor and Hamblin 2004). The aetiologic agent of AHS is the African horsesickness virus (AHSV), a member of the *Reoviridae* family in the genus

Orbivirus. Like many other orbiviruses, AHSV is an arthropod-borne virus, generally transmitted from one host to another by some species of midges in the genus *Culicoides*. *Culicoides imicola* is considered to be the most important of the arthropod vectors for AHSV, *C. bolitinos* being recently implicated as a second important African vector (Mellor, Boorman et al. 2000; Paweska, Venter et al. 2002).

Weather and climate have a strong influence over the host and vector distribution through temperature, humidity and wind (Sellers 1980). As a global phenomenon, climate change has a direct and important effect on biodiversity and disease range. This fact is reflected in the changing patterns of arbovirus (insect-transmitted viruses) distribution worldwide, demonstrated by the spread of Bluetongue virus (BTV) into northern Europe, and the emergence of Schmallenberg and African horsesickness viruses in Europe (Mellor and Hamblin 2004; Slenning 2010; Gibbens 2012). Both AHSV and BTV are transmitted by *Culicoides* sp midges, and it seems highly likely that Schmallenberg virus has the same arthropod vector, although it is a different viral species closely related to orthobunyaviruses (Gibbens 2012). The wide dispersal of BTV and AHSV could be attributed to a raise in both humidity and temperature in areas inhabited by the midges, increasing the vector persistence throughout winter and thus extending the infection time span. BTV overwinters in cattle as well, being able to cross the placenta and infect the fetus, thus maintaining a reservoir for the vector. Wind dispersal of *Culicoides* has been shown to spread both AHSV and BTV (Pedgley and Tucker 1977; Gould and Higgs 2009).

Micrographs of negatively-stained neurotropic AHSV preparations and biochemical investigations have shown that it is a non-enveloped, icosahedrally-symmetric virus with a linear double-stranded RNA (dsRNA) genome of ten segments (Polson and Deeks 1963; Oellermann 1970; Bremer 1976). Out of the ten genomic segments, eight code for single proteins only (Grubman and Lewis 1992). Nine AHSV serotypes have been isolated and described (Howell 1962). Seven structural proteins (VP1 to VP7) make up the AHSV particle, arranged into three layers around the viral genome (Grubman and Lewis 1992). Apart from an atomic model of the top domain of VP7, there is no available structure of any AHSV component (Basak, Gouet et al. 1996). The organization of AHSV has been inferred based on indirect evidence coming from negatively-stained electron micrographs, comparative genomics and proteomics of the orbiviruses and from the first atomic structure of an orbivirus, that of the BTV1 core (Grimes, Burroughs et al. 1998). In the case of BTV1, the genome is surrounded by a proteinaceous layer of 60 asymmetric

dimers of VP3. A similar arrangement was observed, for example, in reovirus, rotavirus and Broadhaven virus (Schoehn, Moss et al. 1997; Reinisch, Nibert et al. 2000; Chen, Settembre et al. 2009). The transcriptase complex, formed by the minor proteins VP1 (polymerase), VP4 (capping enzyme) and VP6 (helicase), sits under the five-fold vertices (Nason, Rothagel et al. 2004). The transcriptase complex was not defined in the X-ray structure of the BTV core, being averaged out where icosahedral symmetry was imposed. However, based on information obtained from BTV core-like particle studies and comparison to similar features observed in rotavirus and reovirus particles, it has been postulated that the polymerase might account for the bulk of the complex density, while the rest of it would be assigned to the capping enzyme VP4 and the VP6 helicase (Prasad, Rothnagel et al. 1996; Grimes, Burroughs et al. 1998; Zhang, Walker et al. 2003; Nason, Rothagel et al. 2004). The BTV core undergoes conformational changes during transcription, allowing the newly synthesized RNA to emerge through a pore in the VP3 layer, located at the five-fold axes (Gouet, Diprose et al. 1999). The BTV VP6 helicase is organized as a hexamer in solution, similarly to many other known helicases (Kar and Roy 2003). Its role is to unwind the dsRNA segments and make them available for the VP1 polymerase, which has been shown to have both replicase and transcriptase activity (Boyce, Wehrfritz et al. 2004; Roy 2005). The capping enzyme VP4 is a dimer having methyltransferase, guanylyltransferase and RNA triphosphatase activies, indicating that the complete capping process relies on this single core protein (Martinez-Costas, Sutton et al. 1998; Ramadevi, Burroughs et al. 1998a; Ramadevi and Roy 1998b; Ramadevi, Rodriguez et al. 1998c).

The AHSV transcriptase complex is not as well studied. Based on sequence analysis and comparison to the BTV and other RNA polymerases, the AHSV VP1 has been assigned as the putative viral RNA polymerase of AHSV (Vreede and Huismans 1998). VP6 has been shown to bind nucleic acid and it is believed to be the AHSV helicase (de Waal and Huismans 2005). The genomic segment coding for VP4 has been sequenced, but there is little known about the protein itself (Mizukoshi, Sakamoto et al. 1993).

The BTV VP3 layer is covered by 260 trimers of VP7, organized as a T=13 lattice (Grimes, Burroughs et al. 1998; Diprose, Burroughs et al. 2001). The crystal structure of the top domain of AHSV VP7 shows a trimeric molecule very similar to the corresponding fragment of VP7 of BTV (Basak, Gouet et al. 1996). One interesting property of AHSV VP7 is the spontaneous assembly of the pure protein into two dimensional hexagonal arrays, a

similar property being observed for the corresponding VP7 protein of Broadhaven virus (Burroughs, O'Hara et al. 1994; Schoehn, Moss et al. 1997).

The outermost layer of BTV is composed of 120 VP5 globular trimers interlaced with 60 VP2 trimers forming protruding triskelions on the viral surface (Hewat, Booth et al. 1992; Nason, Rothagel et al. 2004; Zhang, Boyce et al. 2010). The predicted coiled-coil motifs of BTV VP5 are typical of membrane fusion proteins and they indicate the role VP5 has in pore formation during cell entry (Zhang, Boyce et al. 2010). VP2 is the cellular receptor-binding protein, raising neutralizing antibodies in the host and giving the virus its serotype specificity and hemagglutination activity (Huismans and Erasmus 1981; Fukusho, Ritter et al. 1987; Ghiasi, Fukusho et al. 1987). Little is known about the role and structure of AHSV VP5, except that it is an early serological marker in AHSV infections, thus indicating its positioning on the viral surface, with access to host antibodies (Martinez-Torrecuadrada, Diaz-Laviada et al. 1997). AHSV VP2 has the highest variability of any of the viral proteins between serotypes and triggers the formation of virus-neutralizing antibodies, marking it as the putative receptor-binding protein (Burrage and Laegreid 1994; Williams, Inoue et al. 1998). Similarly to BTV VP2, AHSV VP2 undergoes proteolytic cleavage, either by the insect vector proteases or by those present in the host serum (Marchi, Rawlings et al. 1995; Darpel, Langner et al. 2011).

In addition to the major structural proteins, BTV genome codes for four non-structural proteins NS1, NS2, NS3/NS3A and NS4. NS1 and NS2 are involved in virus replication and assembly in virus assembly factories. In BTV infected cells these represent sites within the cell where newly synthesized viral proteins, as well as assembly intermediates, accumulate (Roy 2005). These assembly sites are located near the cell nucleus (Brookes, Hyatt et al. 1993). NS2 is synthesized early in the infection cycle and in its phosphorylated form is associated predominantly with the virus assembly sites, both in BTV-infected cells as well as in *in vitro* experiments (Thomas, Booth et al. 1990; Brookes, Hyatt et al. 1994). It has an important role in recruiting ssRNA for replication and in capsid assembly, by associating with both structural proteins and assembling particles (Thomas, Booth et al. 1990; Roy 2005). NS2 recognizes specific BTV RNA structures unique in each of the segments and thus may be involved in the packaging of the genome (Lymperopoulos, Wirblich et al. 2003).

NS3 is produced in two different forms, NS3 and NS3A, because of the presence of a second in-frame initiation codon in the coding RNA segment. These proteins accumulate in high concentrations in insect cells and could be involved in the release of BTV from the insect cell through a budding mechanism rather than by cell lysis (French, Inumaru et al. 1989). NS3/NS3A are transported to and embedded in the cellular membrane, being localized at the site of virus release (Hyatt, Zhao et al. 1993). At the membrane level, NS3 interacts with the light chain (p11) of calpactin, which in turns belongs to the Annexin II complex. NS3 replaces the heavy chain (p36) of Annexin II in this complex, playing a role in membrane fusion. NS3 has motifs implicated in recruiting cellular proteins present in the pathway of multivesicular body formation and can bind the major capsid protein, VP2 (Beaton, Rodriguez et al. 2002).

NS4 is the product of a recently identified overlapping ORF in genomic segment 9 of orbiviruses and has the ability to bind dsRNA. During infection, NS4 starts by accumulating in the cell cytoplasm and nucleus, only to be seen later associated with the cellular membrane. These two observations suggest a role for NS4 both in the early steps of the infection as well as, possibly together with NS1 and NS3, in virus egress (Belhouchet, Mohd Jaafar et al. 2011).

There is no evidence yet for AHSV NS1 function in viral replication in the cell. It also differs in primary structure and biochemical characteristics from those of BTV and other orbiviruses. It has been speculated that the NS1 tubules seen in virus preparations might play a role in virus transport from the assembly sites to NS3 in the membrane (Maree and Huismans 1997). AHSV NS2 can bind ssRNA and forms multimeric complexes and is believed to be functionally equivalent to BTV NS2 (Uitenweerde, Theron et al. 1995). After VP2, AHSV NS3 shows the most variation across serotypes. It functions as a viroporin (viral protein which destabilizes membranes) permeabilizing cellular membranes to allow the release of virions from the cell (Meiring, Huismans et al. 2009).

Many questions arise regarding the assembly of multilayered viruses such as BTV or AHSV, which is an intricate process because of the complexity of the protein-protein interactions required for construction of the different shells. Studies on BTV entry, assembly pathways and egress provided some answers to these questions. VP2 is the receptor-binding protein of BTV. VP2 has two sites for binding to the host cell, one of which has an affinity for sialic acid. Binding triggers the receptor-mediated internalization

of the virus into clathrin-coated endocytic vesicles. Endosomal acidification activates VP5, a fusogenic protein that undergoes conformational changes leading to the destabilization of the endosomal membranes and the release of the uncoated viral core into the cellular cytoplasm (Forzan, Marsh et al. 2007; Roy 2008). The core is transcriptionally active and releases newly synthesized RNA through pores at the five-fold axes, RNA which is translated into new viral building-blocks. The individual proteins aggregate at the assembly site created by NS2, where VP3 recruits the minor proteins of the transcriptase complex. The VP3 shell is stabilized by the attachment of VP7 trimers and assembly of the VP7 layer at multiple initiation sites. VP5 and VP2 are acquired independently of each other and attach on the outer surface of the VP7 protein layer. The interaction of VP2 with both vimentin filaments and NS3 facilitate virus egress from the cell (Bhattacharya, Noad et al. 2007; Roy 2008). The AHSV life cycle is presumed to be similar to that of BTV, but more studies are required to clarify that, especially as they infect different hosts, so the differences in cell tropism need to be explored.

1.6. Bacteriophage PRD1

PRD1 is the best characterized member of the Tectiviridae family (Caldentey, Bamford et al. 1990; Bamford, Caldentey et al. 1995). PRD1 is a bacteriophage infecting Gram-negative bacteria containing a conjugative IncP, IncN or IncW plasmid, which codes for the bacterial receptor. It has an icosahedrically-symmetric protein capsid decorated with spikes and enclosing a lipid membrane which, in turn, contains the linear, double-stranded DNA genome (Butcher, Bamford et al. 1995). An atomic resolution structure of PRD1 particles showed in detail the overall arrangement of the majority of capsid proteins, the distribution of the lipid bilayer and the close interaction between the membrane and dsDNA genome (Abrescia, Cockburn et al. 2004). 240 copies of the major capsid protein P3, with a double β-barrel fold, assembles into trimers onto a pseudo T=25 surface lattice. Single β-barrel pentamers of P31 occupy 11 out of 12 pentavalent positions in the capsid and form the base of the viral spikes (Rydman, Caldentey et al. 1999). A network of 30 dimers of P30, a minor capsid protein located under the shell formed by P3, acts as a cementing protein and stabilizes the contacts between the capsid facets and, together with integral membrane protein P16, fixes the vertices into place (Rydman, Bamford et al. 2001; Abrescia, Cockburn et al. 2004; Jaatinen, Viitanen et al. 2004). Spikes are evident

on the capsid vertices in electron cryo-micrographs of PRD1 virions, and analysis of $P2^-$ and $P5^-$ deficient mutants showed that they were probably formed of P2 and P5 attached to P31 (Butcher, Bamford et al. 1995; Grahn, Caldentey et al. 1999; Rydman, Caldentey et al. 1999). An atomic model of P2 showed that it is an elongated monomer with an overall shape resembling a sea horse. The distal end of the molecule is formed by a pseudo β-propeller and most likely constitutes the receptor-binding part of the spike (Xu, Benson et al. 2003). Small angle X-ray scattering has shown P5 to be an elongated protein, with the C-terminal part extending outside from the virus surface, while the N-terminus seems to interact with the P31 pentamer (Sokolova, Malfois et al. 2001). An atomic model of the P5 C-terminus showed that it forms trimers composed of a stalk region with a fold similar to that of the adenovirus fibre and a β-barrel head region with a TNF-like fold, connected by a collagen-like motif and a hinge region of eight glycine residues (van Raaij, Mitraki et al. 1999; Merckel, Huiskonen et al. 2005). The flexibility and the tendency of P5 to associate into oligomers made it impossible to crystallize the full-length protein. Mutation of the P5 shaft by removal of the glycine hinge region, reducing flexibility, allowed a slightly longer fragment to be crystallized. This reduction in flexibility also slowed the attachment of PRD1 to its host (Huiskonen, Laakkonen et al. 2003; Merckel, Huiskonen et al. 2005). Proteins P31, P5 and P2 are probably missing from the unique packaging vertex of PRD1, which includes a different set of proteins: the membrane proteins P20 and P22, P6 and the packaging ATPase P9 (Gowen, Bamford et al. 2003; Stromsten, Bamford et al. 2003; Jaatinen, Viitanen et al. 2004). The atomic model of the full PRD1 virion shed no light on either the packaging complex of the virion or on the association of the two spike proteins (P2 and P5) with the capsid. P2 was missing because ordered crystals were only formed from mutant PRD1 capsids lacking P2, P5 was not visible in the electron density and the packaging vertex was averaged out when icosahedral symmetry was applied during the crystallography (Bamford, Cockburn et al. 2002; Abrescia, Cockburn et al. 2004; Cockburn, Abrescia et al. 2004). Several attempts have been made to try to understand the relative orientation of these proteins with respect to each other and to the viral capsid. Based on the available evidence, four different models can be considered. The first model considers the P5 N-terminus forming a heteropentamer with P31, based on a sequence identity of 38% between P31 and P5 (Caldentey, Tuma et al. 2000; Sokolova, Malfois et al. 2001). It also places a P2 monomer sitting on top of a P5 trimer, its position as the most distal spike component supported by the fact that P2 is involved in host recognition and binding, while P5 seems to have no obvious role in infection under *in vitro* conditions

(Grahn, Caldentey et al. 1999; Bamford and Bamford 2000; Caldentey, Tuma et al. 2000). The second model describing the PRD1 spike structure considers P5 sitting on top of the P31 pentamer and contacting it at three positions, a structure similar to that of adenovirus penton and trimeric fiber (Zubieta, Schoehn et al. 2005). The third and fourth models incorporate the experimental results obtained from the small angle X-ray scattering studies and propose that there is no observed connection between the P5 C-terminus and P2 (Sokolova, Malfois et al. 2001), and therefore no experimental evidence that places P2 on top of P5, except genetic evidence that P5- mutants assemble P2 at much reduced levels (Bamford and Bamford 2000). These latter models present the P2 monomer being wedged between P5 and P31, while P5 can be either contacting the P3 capsid shell or sitting on top of P31 (**Figure 11**).

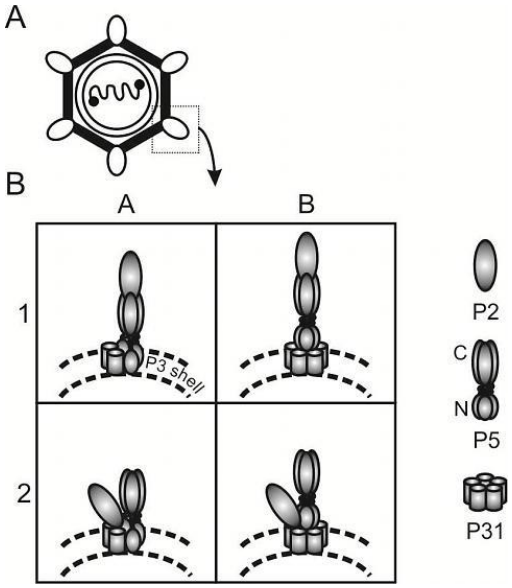

Figure 11. Schematic model of PRD1. (A) Schematic model of the whole virion. The linear dsDNA is encapsulated by a membrane covered by an icosahedral capsid. One spike complex is boxed. **(B)** Spike-complex models. The three vertex proteins (P2 monomer, P5 trimer, and P31 pentamer) and their possible organizations are illustrated schematically in four different models (referred to as 1a, 1b, 2a, and 2b). In models 1a and 1b, the P2 monomer is bound to the distal tip of the P5 trimer. In contrast, in models 2a and 2b, the P2 monomer is wedged between the P5 trimer and the P31 pentamer. Also, in models 1a and 2a, the N-terminal domain of P5 is buried in the P3 shell, whereas in models 1b and 2b, P5 sits on top of P31. Reprinted from Huiskonen, Jäälinoja et al. 2007, with permission from the publisher.

PRD1 spike proteins are the main molecules required for viral adsorption. P2 is the receptor-binding protein, recognizing the host cell receptor encoded by a conjugative plasmid (Mindich, Bamford et al. 1982a). Mutations affecting P5 seemed only to prolong

the infection time, and so P5 might only act as an initial non-specific recognition protein, helping the primary receptor-binding protein P2 in finding the cellular target receptor (Butcher, Manole et al. 2012). During genome delivery into the host, the spike complex is disassembled and the inner viral membrane, with the help of viral proteins P11, P14, P18, and P32 forms a tube-like structure acting as a DNA injection device (Bamford and Mindich 1982; Mindich, Bamford et al. 1982a; Mindich, Bamford et al. 1982b; Butcher, Bamford et al. 1995; Rydman, Caldentey et al. 1999; Grahn, Daugelavicius et al. 2002a; Grahn, Daugelavicius et al. 2002b). The genome is replicated by the viral DNA polymerase via a protein-primed mechanism (reviewed in Butcher, Manole et al. 2012). The assembly process continues with the expression of P3, P5, and P31 in the cell cytoplasm along with some viral chaperones, while the virus-encoded membrane proteins are embedded into the inner membrane of the bacterium. The procapsids are assembled in the cytoplasm including P31, P2 and P5. P2 and P5 assemble on to the procapsid only in the presence of P31. The procapsid is then filled with viral DNA, as the genome is translocated through the unique packaging vertex by the P9 ATPase in a process probably analogous to the mechanism used by herpes simplex virus 1 (see Section 4.5.1 Herpesvirus). In the case of PRD1 P9, P6 and the terminal protein P8 were all shown to be essential in an *in vitro* packaging system. The progeny virions are released from the host cell via a holin-endolysin lysis system (reviewed in Butcher, Manole et al. 2012).

1.7. Pleomorphic archaeal viruses

The world of archaeal viruses is populated by viruses with great morphological diversity, matching the very diverse and often extreme environments from which they have been isolated. Electron microscopy studies have shed light on the different kinds of archaeal virus morphologies, with several virus and virus-like particle structures solved by 3D image reconstruction and X-ray crystallography (Rice, Tang et al. 2004; Haring, Rachel et al. 2005; Haring, Vestergaard et al. 2005; Vestergaard, Haring et al. 2005; Prangishvili, Vestergaard et al. 2006; Akita, Chong et al. 2007; Jäälinoja, Roine et al. 2008; Happonen, Redder et al. 2010). The morphologies of archaeal viruses can roughly be divided into three different types: i) spherical viruses with icosahedral symmetry, and head and tail viruses with an icosahedrally-symmetric head and a helical tail; ii) viruses with different regular morphologies lacking icosahedral symmetry, like rod-shaped, lemon-shaped or

bottle-shaped viruses; and iii) pleomorphic viruses. In the first category we find spherical archaeal viruses like STIV, STIV2 or SH1. The 3D structures of these viruses have been solved by cryoEM and shown to have an icosahedrally-symmetric capsid enclosing a lipid layer which in turn protects the dsDNA genome. The vertices are decorated by spikes which differ in size and shape between the three viruses, but they all might serve similar functions in host recognition (Rice, Tang et al. 2004; Jäälinoja, Roine et al. 2008; Happonen, Redder et al. 2010). In the same category we find archaeal viruses with an apparently icosahedral head and a helical tail based on micrographs of negative stained samples (Witte, Baranyi et al. 1997; Pagaling, Haigh et al. 2007).

The second category comprises numerous viruses, some of which have been characterized by electron tomography and which will be presented in the following section. One such virus is an archaeal virus infecting hosts in the genus *Acidianus*, which has a very interesting life cycle and exhibits a unique ability: the virus exits the host as a lemon-shaped particle and develops one tail at each end of the capsid extracellularly. Prangishvili et al. noted that this can be likened to the maturation of the HIV1 core after budding (discussed previously in Section 1.4.5.2) or the tube formation during bacteriophage PRD-1 infection (Butcher, Bamford et al. 1995; Prangishvili, Vestergaard et al. 2006). Another structure of an *Acidianus*-infecting virus has been solved by electron tomography of negative stained samples, showing a conical-shaped virus (or bottle-shaped) with thin filaments at the broad end of the particle, surrounded by a bell-like envelope (Haring, Rachel et al. 2005). The third structure of an *Acidianus* virus characterized by electron tomography is that of a rod-shaped virus with an apparent helical structure and three tail fibers at each end (Prangishvili, Arnold et al. 1999; Vestergaard, Haring et al. 2005).

The third category of archaeal viruses comprises members with pleomorphic appearance. Only two isolates have been characterized, both isolated from environments saturated in salt. Biochemical investigations and images of negative stain preparations of *Halorubrum* pleomorphic virus 1 (HRPV-1) and *Haloarcula hispanica* pleomorphic virus 1 (HHPV-1) showed that, although the viruses have different types of genomes (circular ssDNA for HRPV-1 and circular dsDNA for HHPV-1), they share similar morphologies and have similar structural proteins sequences (Pietilä, Roine et al. 2009; Pietilä, Laurinavicius et al. 2010; Roine, Kukkaro et al. 2010). HRPV-1 and HHPV-1 are composed of a lipid membrane containing the genome and are decorated with glycosylated spikes (**Figure 12**). Most of the lipids present in the viral membrane are acquired from the host. Two

major viral proteins, VP3 and VP4, have been identified both with predicted transmembrane domains. Based on the fact that VP4 is proteolyticaly cleaved and shows higher amino acid sequence divergence than VP3 in these two viruses, it has been proposed that VP4 is the receptor binding protein, sitting on the outer surface of the viral membrane. The other major viral protein, VP3, has been proposed to be integrated into the viral membrane, with domains exposed to both its inner and outer surface. Neither of the viruses lyses the host cells, causing instead growth retardation of the host (Pietilä, Roine et al. 2009; Pietilä, Laurinavicius et al. 2010; Roine, Kukkaro et al. 2010). A recent study probing the worldwide distribution of viruses in hypersaline environments has characterized forty nine new virus isolates, three of which displayed similar morphology to the previously described HRPV-1 and HHPV-1 (Atanasova, Roine et al. 2012).

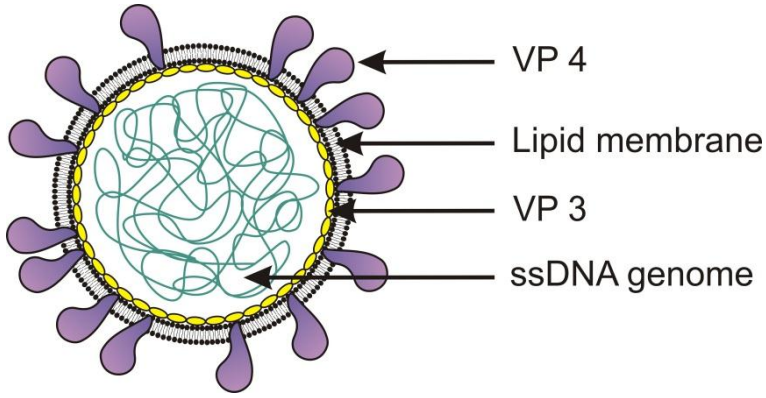

Figure 12. Schematic of HRPV-1 organization.

Despite this wealth of information on archaeal virus structure, little is known about their life cycles in the context of the host. The most comprehensively studied in this respect are *Sulfolobus islandicus* rod-shaped virus 2 (SIRV2) and *Sulfolobus* turreted icosahedral virus (STIV) (Quax, Krupovic et al. 2010; Quax, Lucas et al. 2011). The infection process of STIV was followed by cryoET in vivo. STIV, like SIRV2, has an unusual egress mechanism which could be related to the host architecture. Virus-associated pyramid structures form on the cellular surface even before viral particles could be observed in the cytoplasm (Fu, Wang et al. 2010; Quax, Lucas et al. 2011), and eventually open up towards the cell exterior, allowing the release of the virions from the host (Prangishvili, Arnold et al. 1999; Quax, Lucas et al. 2011).

2. OBJECTIVES

1) Characterization of AHSV VP2 structure from two isolates to aid in vaccine development.

2) Understanding the spatial distribution of the two spike proteins of PRD1 within the context of the virion.

3) Characterization of novel pleomorphic archaeal viruses by electron tomography, focusing on the architecture and distribution of the putative receptor binding protein of HRPV1.

3. MATERIAL AND METHODS USED IN THE STUDIES.

The cell lines and viral strains used in this study are listed in **Table 1**. The experimental methods used in this study are summarized in **Table 2**. A full description is available in the original articles.

Table 1. Cell lines and viral strains used in this thesis

Cell line	Plasmid	Reference for cell line	Viral strain	Reference for viral strain
Salmonella enterica serovar *typhimurium* LT2				
DB7156	pLM2	(Mindich, Bamford et al. 1982b)	PRD 1*sus539*P2$^-$	(Grahn, Caldentey et al. 1999)
PSA	pLM2	(Mindich, Bamford et al. 1982b)	PRD 1*sus690* P2$^-$ P5$^-$	(Bamford and Bamford 2000)
DS88		(Bamford and Bamford 1990)	PRD 1 wt P5Δ8G PRD1*sus539* P2$^-$ PRD1*sus690* P2$^-$P5$^-$	(Huiskonen, Laakkonen et al. 2003) (Grahn, Caldentey et al. 1999) (Bamford and Bamford 2000)
Halorubrum sp. PV6		(Pietilä, Roine et al. 2009)	HRPV-1	(Pietilä, Roine et al. 2009)
Halorubrum sp. SS5-4		(Atanasova, Roine et al. 2012)	HRPV-2	(Atanasova, Roine et al. 2012)
Halorubrum sp. SP3-3		(Atanasova, Roine et al. 2012)	HRPV-3	(Atanasova, Roine et al. 2012)
Halorubrum sp. SS7-4		Study III	HRPV-6	Study III
Halogeometricum sp. CG-9		(Atanasova, Roine et al. 2012)	HGPV-1	(Atanasova, Roine et al. 2012)
Haloarcula hispanica ATCC 33960		(Juez 1986)	HHPV-1	(Roine, Kukkaro et al. 2010)
			His2	(Bath, Cukalac et al. 2006)
Vero cells		(Yasumura 1963)	AHSV-4 HS 32/62	(Erasmus 1973)
Baby hamster kidney cells BHK-21		(Macpherson 1963)	AHSV-4 AHSV-7 tVP2	Study I Study I

Table 2. Methods used in this thesis

Method	Used in Study
Virus growth and purification	I, II, III
SDS polyacrylamide gel electrophoresis	I, II, III
Tomographic reconstruction	III
Asymmetric three-dimensional reconstruction	II
Icosahedrally-symmetric three-dimensional reconstruction	I, II
Subtomogram averaging	III
Fitting of X-ray structures into EM density maps	I, II
Difference imaging	I
Protein modeling	I, II
Cryo-electron microscopy	I, II
Automated cryo-electron tomography	III
Dissociation of virus particles	III
Protease treatment of virus particles	III
Western blotting	II
Agarose gel electrophoresis of RNA	I
DNA sequencing	I
Cell culture	I
Protein concentration measurement	I, II, III
Lipid analysis	III
Agarose gel electrophoresis of DNA	III

4. RESULTS

This thesis presents the structures of three different viral receptor-binding proteins belonging to AHSV (Study I), PRD1 (Study II) and HRPV-1 (Study III). Each study employs a different method of three-dimensional reconstruction, fitted to the characteristics of the viruses: icosahedrally-symmetric 3D reconstruction in Study I, image classification and multivariate statistical analysis in Study II, and tomographic reconstruction and subvolume averaging in Study III.

4.1. The architecture of African Horsesickness virus

4.1.1. Virus purification and biochemical characterization

Two strains of AHSV were used in this study. AHSV-4 strain is a field isolate, while AHSV-7 tVP2 is an isolate identified during a large sequencing project. The dsRNA of both strains was isolated and compared to other AHSV strains, including AHSV-4. The genome segment 2 coding for the receptor-binding protein VP2 of AHSV-7 tVP2 is 675 nucleotides shorter than the corresponding segment 2 of AHSV-4. This in-frame deletion at the genome level was confirmed by SDS-PAGE (sodium dodecyl sulphate-polyacrylamide gel electrophoresis) analysis of the protein profiles of both AHSV-4 and AHSV-7 tVP2, the latter having a receptor-binding protein VP2 with a deletion of 225 amino acids between residues 280-504. The deletion in VP2 causing AHSV-7 tVP2 VP2 to migrate faster than AHSV-4 VP2 is the major difference in the otherwise very similar protein profiles. Interestingly, this change in VP2 confers a competitive advantage in AHSV-7 tVP2 compared to AHSV-4 in Vero cell culture when mixed together in either equal amounts or with a ten-fold or a hundred-fold excess of AHSV-4.

4.1.2. Homology modeling of the AHSV core

Bluetongue virus is the best study orbivirus and a model system for the family, and was used as a comparison to validate our results. Based on amino acid sequence alignment, we observed that BTV1 and AHSV-4 VP3 share a 58% sequence identity, which shows

that VP3 is the most conserved protein within the AHSV virus. This identity allowed us to generate reliable homology models (a C-score of 0.53, where values range from -5 to 2) using the I-TASSER server for AHSV-4 VP3 A and B monomers (**Figure 13 D, F**). Alignment of the BTV1 VP3 and AHSV-4 VP3 model gave a root mean square deviation of the α-carbon backbones of 0.2 Å for the A monomer and 0.3 Å for the B monomer (Zhang 2008; Roy, Kucukural et al. 2010). The homology models were compared with the reconstructions and used to generate quasi-atomic models of the AHSV VP3 shell The VP3 icosahedrally-symmetric shell fitted well into the EM density, with the exception of a stretch of 100 amino acids at the N-terminus of VP3 monomer A (**Figure 13 A, B, F**). Since residues 1-56 in this region are also missing from the X-ray structure, we decided to remove the whole 100 residues region from the homology model. The predicted amino acid sequence for AHSV-4 VP7 was also submitted to the I-TASSER server, returning a reliable full-length homology model (a C-score of 1.87) of one VP7 monomer (root mean square deviation of the α-carbon backbone of 0.5Å)(**Figure 13 E**). This model was used to generate a full VP7 shell, which also fitted well into the corresponding EM density (**Figure 13 A, C, G**). No reliable models could be generated for VP5 and VP2 due to a lack of suitable structural homologs.

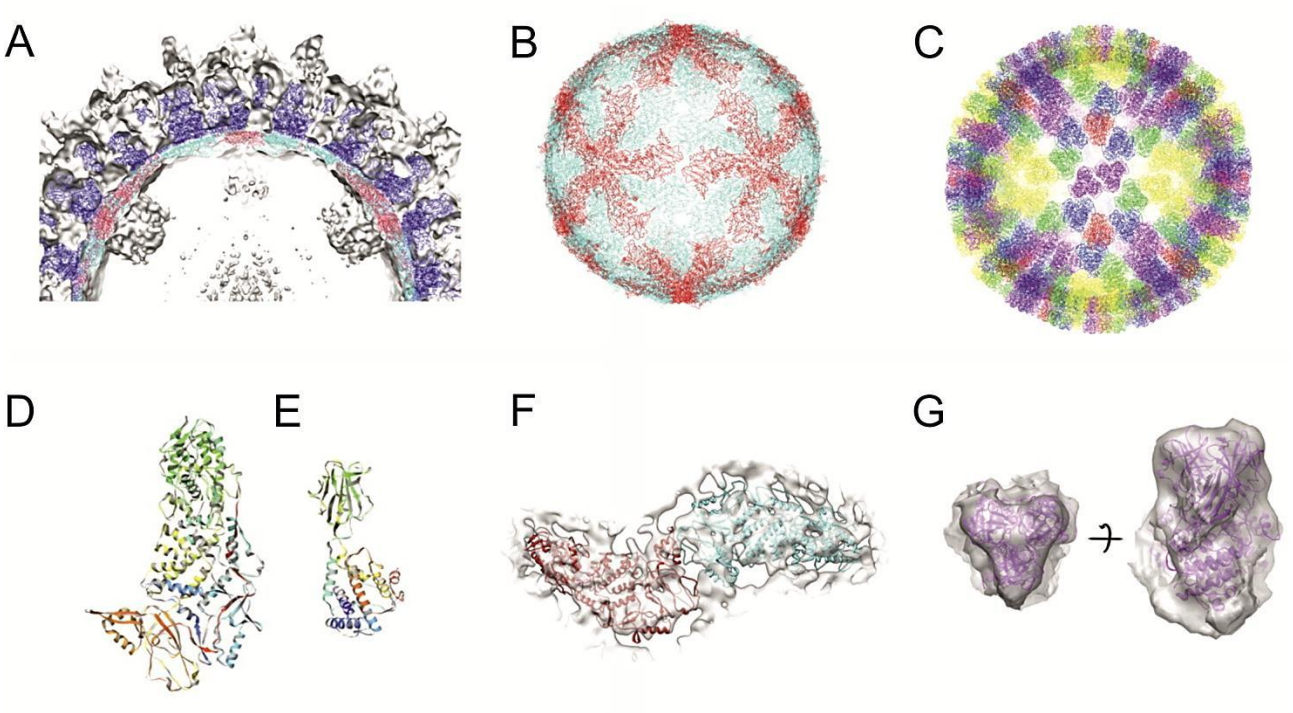

Figure 13. Modeling of VP3 and VP7. (A) Slabbed isosurface representation of the AHSV-7 tVP2 empty-particle reconstruction, rendered at 1 σ above the mean with the fitted homology models of VP3 (cyan and red string) and VP7 (blue string). The densities correspond very well. The transcription complexes can be seen as protruding lumps of density beneath VP3 penetrating into the interior of the capsid. **(B)** Homology model of the VP3 shell, containing 120 molecules in a T=1 arrangement. The two copies of VP3 within one asymmetric unit are colored cyan and red. **(C)** Homology model of the VP7 shell, containing 780 molecules in a T=13 arrangement. The asymmetric unit contains 13 copies of VP7. The 5 trimers (P, Q, R, S, and T) contributing to the asymmetric unit are colored yellow, green, blue, purple, and red. Trimer T sits on an icosahedral 3-fold axis, so it contributes only one monomer to the asymmetric unit. **(D)** Superposition of the AHSV-4 VP3 A monomer homology model on the BTV VP3 A monomer, using ribbon representation. **(E)** Superposition of the AHSV-4 VP7 homology model on the BTV VP7 A monomer, using ribbon representation. AHSV-4 VP3 and VP7 are colored from the N terminus (blue) to the C terminus (red), according to amino acid sequence. BTV VP3 and VP7 are presented as gray ribbons. **(F)** Homology model of a VP3 dimer (cyan and red) fitted into the EM density of the VP3 shell from filled AHSV-7 tVP2 (gray isosurface), shown at a threshold of 1.7 σ above the mean. The density was cut out using a 20-Å zone radius around the homology model, using Chimera (Pettersen, Goddard et al. 2004). **(G)** Homology model of a VP7 trimer (magenta) fitted into the EM density of the VP7 layer from empty AHSV-7 tVP2 (gray isosurface), shown at a threshold of 1.9 σ above the mean, from the top and from the side. The density was cut out using a 14-Å zone radius around the homology model, using Chimera (Pettersen, Goddard et al. 2004). Reprinted from Manole, Laurinmäki et al. 2012, with permission from the publisher.

4.1.3. AHSV electron cryo-microscopy reconstruction

3D reconstructions were calculated for both AHSV-4 and AHSV-7 tVP2. They are very similar to each other, showing an icosahedrally-symmetric virus of approximately 87 nm (**Figure 14 A-C**).

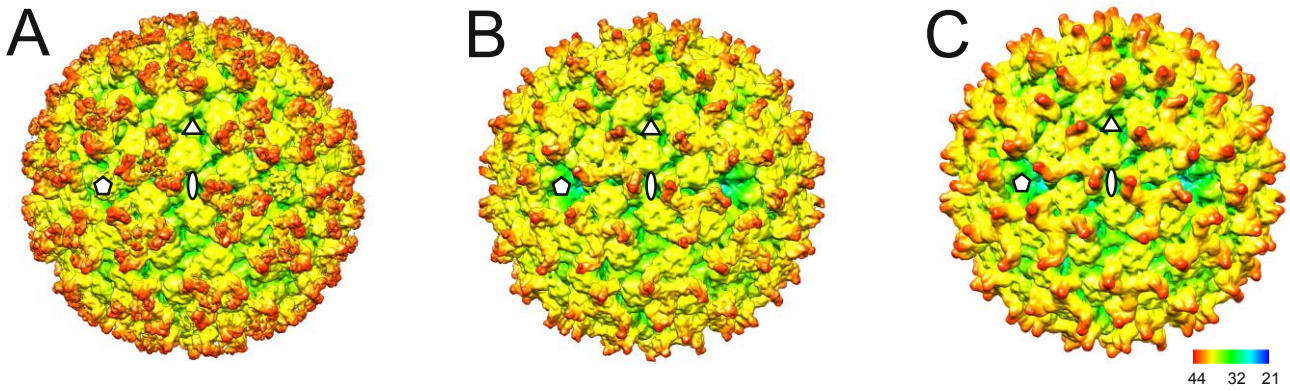

Figure 14. Radially depth-cued isosurface representation of the reconstructions viewed down a two-fold axis of symmetry. The isosurfaces were drawn at 1σ above the mean density level. The structures were radially depth-cued in Chimera (Pettersen, Goddard et al. 2004). **(A)** AHSV-4 at 14.4 Å resolution, **(B)** empty AHSV-7 tVP2 at 15.8 Å resolution, **(C)** filled AHSV-7 tVP2 at 11.4 Å resolution. **(A-C)** Radial depth-cueing scale bar in C in nm. A five-fold (pentagon), a three-fold (triangle) and a two-fold (ellipse) symmetry axis are marked on each representation. Reprinted from Manole, Laurinmäki et al. 2012, with permission from the publisher.

The viral capsid has a triple-layered structure, enclosing the ten dsRNA genomic segments. Immediately under the VP3 shell the first three layers of RNA appear well-ordered, with a spacing of 3nm. The AHSV-7 tVP2 reconstruction missing the RNA density revealed the position of the transcription complex under the five-fold vertices (**Figure 13 A**). The innermost layer of AHSV is a T=1 shell formed by 60 asymmetric VP3 dimers. The VP3 layer is covered by 260 trimers of VP7 organized on a T=13 lattice, and together the VP3 and VP7 layers form the viral core. The outermost layer of the virion is formed by the major structural proteins VP5, a mainly α-helical protein organized as globular trimers positioned between VP7 and VP2, and the major immunogen VP2, organized as 60 trimers called triskelions. The biochemical analyses indicated that the AHSV-7 VP2 is considerably smaller than AHSV-4 VP2, and thus there must be a difference in the

structure of the triskelions. To confirm this, we first aligned the deletions in AHSV-7 tVP2, BTV1 and AHSV-4 by comparing the amino acid sequences of 24 related proteins from AHSV, BTV and epizootic hemorrhagic disease virus. Next we superimposed the 3D structures of the VP2 trimers from AHSV-4, AHSV-7 tVP2, and BTV1. These data combined allowed us to show that each central domain present in AHSV-4 and missing in AHSV-7 tVP2 and BTV1 is formed primarily by residues 368-483, and the distal tip density of the AHSV-4 triskelion (lacking from AHSV-7 tVP2 reconstruction) comes primarily from residues 279-368 (**Figure 15 A-G**).

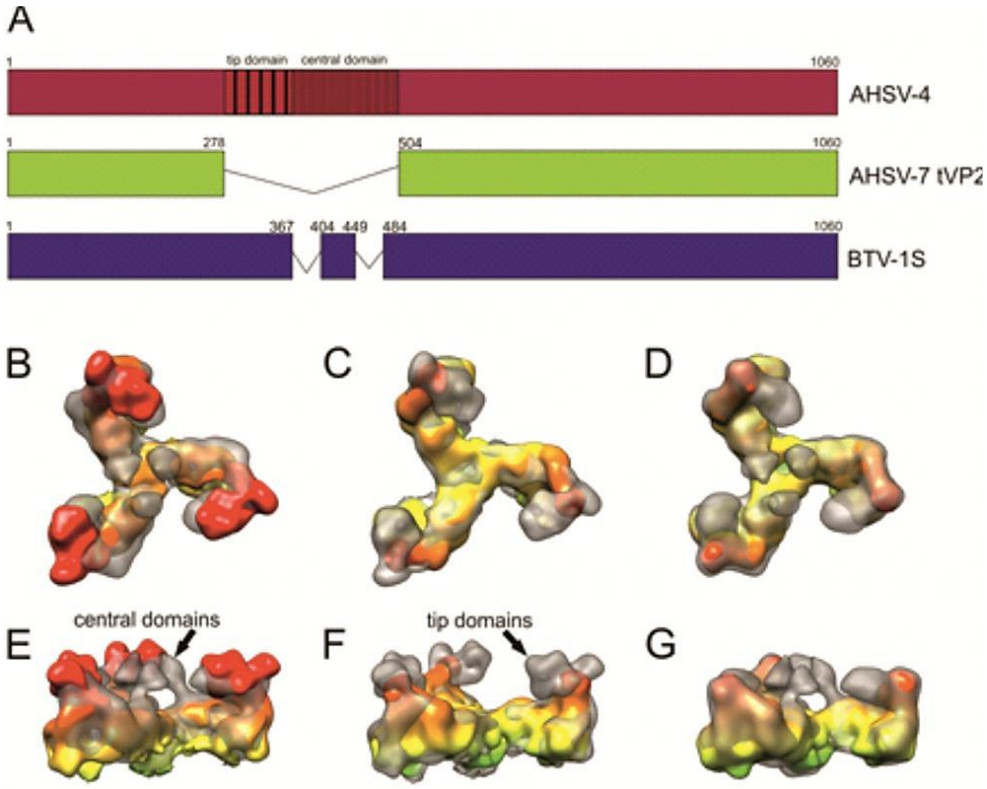

Figure 15. Mapping of deletions in VP2. (A) The schematic shows the positions of the major deletions in AHSV-7 tVP2 and BTV 1 compared to AHSV-4 from the multiple sequence alignment (Supplementary Figure S1 in Study I). Numbers indicate the amino acid residue according to the AHSV-4 sequence **(B & E)** Superposition of VP2 from AHSV-4 (gray transparent density) and BTV (radially depth-cued) from the top **(B)** and from the side **(E)**. The main additional density in AHSV-4 is in the center of the triskelion on top of the hub, coming from residues 368-483 in AHSV-4. **(C & F)** Superposition of VP2 from BTV 1 (gray transparent density) and the empty AHSV-7 tVP2 reconstruction (radially depth-cued) from the side and from the top. Main additional density is in the distal ends of the triskelion coming from residues 279-367 in BTV 1 and AHSV-4. **(D & G)** Superposition of VP2 from AHSV-4 (gray transparent density) and AHSV-7 tVP2 (radially depth-cued) from the side and from the top. Main additional density is in both the center and in the distal ends of the triskelion coming from residues 279-367 and 368-483 in AHSV-4. Reprinted from Manole, Laurinmäki et al. 2012, with permission from the publisher.

4.2. The receptor-binding complex of PRD1 – a tale of two parts

4.2.1. Modelling the full-length spike protein P5

The full-length spike protein P5 has proved impossible to crystallize most likely due to flexibility (see Section 1.6). However, a low-resolution SAXS model and X-ray data for separate fragments of the protein were available, and this allowed us to create an atomic model of the whole P5 (Sokolova, Malfois et al. 2001; Merckel, Huiskonen et al. 2005). First, we exploited the fact that the P5 N-terminal fragment and P31 share a 38% amino acid sequence identity and generated a homology model of the N-terminal fragment of the P5 monomer using SWISS-MODEL (Schwede, Kopp et al. 2003). The homology of P5 to P31 also allowed us to predict the monomer-monomer interface in P5 and to generate a trimeric form of the P5 N-terminal fragment, which was then fitted into the SAXS model density. Eight glycine residues forming a hinge-like structure and a collagen-like region were also missing from the X-ray model. Atomic models were generated for both these regions using a collagen fiber as template. The likely interactions between the N-terminal base, collagen-like region, shaft, glycine hinge and C-terminal head fragments were established by first determining the orientation of the P5 full-length molecule. This was achieved by fitting the X-ray model of the C-terminus fragment into the SAXS density of the full-length P5. The rest of the atomic model was then assembled independently of the SAXS density and rendered as a P5 trimeric molecule 170 Å in length. The SAXS model of P5 was 270 Å long, so it is possible that there is an alternative conformation of P5, where the N-terminal base is extended (Sokolova, Malfois et al. 2001).

4.2.2. The interaction between P5 and the P31 penton base.

CryoEM and 3D image reconstruction were used to determine the way P5 binds to the PRD1 capsid. For this purpose we used two PRD1 amber mutants; *sus539* lacking P2, and *sus690* which lacks P5 and as a consequence it shows much reduced assembly of P2 (Bamford and Bamford 2000). Both strains were propagated on their respective suppressor strains (Mindich, Bamford et al. 1982b) and the purified particles were analyzed by SDS-PAGE. Western blotting analysis of the purified material performed with PRD1 polyclonal sera against P2, P5, and P31 (Hänninen, Bamford et al. 1997; Grahn, Caldentey et al. 1999; Rydman, Caldentey et al. 1999), indicated a small fraction of the

purified preparations still assembled the P2 and P5 proteins, despite the amber mutations in those respective genes, and the fact that the purified virus preparation titres on the non-suppressor host were ~10^6 times lower than on the suppressor host. A mixture of particles with and without the spike complex would have posed a serious problem later in the image processing and 3D reconstruction steps, and so careful attention to the quality control of the purified virus preparation by Western blotting analysis was a crucial step prior to data collection and imaging. Wild type PRD1 and P5Δ8G, (a PRD1 mutant with the glycine hinge region removed making P5 less flexible and thus more amenable to image processing) were used (Huiskonen, Laakkonen et al. 2003) as controls to find the relative positions of P2 and P5. Icosahedrally-symmetrized three-dimensional reconstructions were calculated for all four particle types, showing a P31 penton surrounded by five trimers of the major coat protein P3. In all of the reconstructions except $P2^-P5^-$, the spike was only partially resolved, because of the five-fold symmetry imposed on the 3D reconstructions as a knob-like density at the center of the P31 penton. These results indicated that it is the P5 trimer and not P2 which apparently binds directly to the center of the penton base.

4.2.3. PRD1 has two separate spike proteins

Imposing icosahedral symmetry (five-fold symmetry in particular) made it impossible to resolve completely the different components of the spike, which do not obey the same symmetry. To address this issue, we used multivariate statistical analysis and image classification in an approach similar to subvolume averaging methods used in tomography. We extracted only the vertex images out of the images of entire particles, utilizing the previously determined icosahedral orientations of each particle image. Only those images of vertices roughly perpendicular to the view point were used further. The variation in the images allowed us to group together similar conformations and orientations of the spikes and calculate 2D class averages of the spike side views, using a limited orientation search (Briggs, Huiskonen et al. 2005; Huiskonen, Jäälinoja et al. 2007; Jäälinoja, Roine et al. 2008)(**Figure 15 A-C**). This revealed the presence of two spikes instead of one at each vertex, one perpendicular to the capsid and with a knob at the distal end, the other at an angle to the first and connected to it at the base (**Figure 15 A, B**). The 2D projections of the $P2^-$ particles were missing the density of the angled spike and allowed us to tentatively assign this density to P2 (**Figure 15 C**). Next we imaged the $P2^-P5^-$ particles (**Figure 15**

D). This mutant lacked the spikes entirely, which allowed us to verify our results and conclude that the upward-pointing spike is formed by P5 and the angled spike by P2.

4.2.4. Modelling the PRD1 double spike.

Because of the inherent protein flexibility and variability of their interactions, we were only able to model the spike complex at about 20 Å using the P5Δ8G data set (**Figure 16 A-D**). When the trimeric atomic model of P5 was fitted into the EM density, the head and shaft domain corresponded well with the electron density (**Figure 16 A, B**). The collagen-like region remained unresolved, but we observed that its fold fits well with the knob-like density at the center of the P31 penton (**Figure 16 C, D**). Also, our model indicated that the N-terminal fragment of P5 is embedded within P31. Fitting the P2 atomic model into the second spike density indicated that this protein is attached as a monomer, and is flexible. This shows that P2 has some degree of movement with respect to P5, resulting in four different solutions for the fitting (**Figure 11** Section 1.6, **Figure 16 A**). P2 flexibility made it impossible to establish the exact interactions between P2 and the other vertex components, as there was no density to correspond to the base of the P2 spike. However, it did give the orientation of P2 with the pseudo β-propeller distal to the particle, in line with protease treatment of the virion which has previously been shown to cleave the C-terminus of P2 (Xu, Benson et al. 2003).

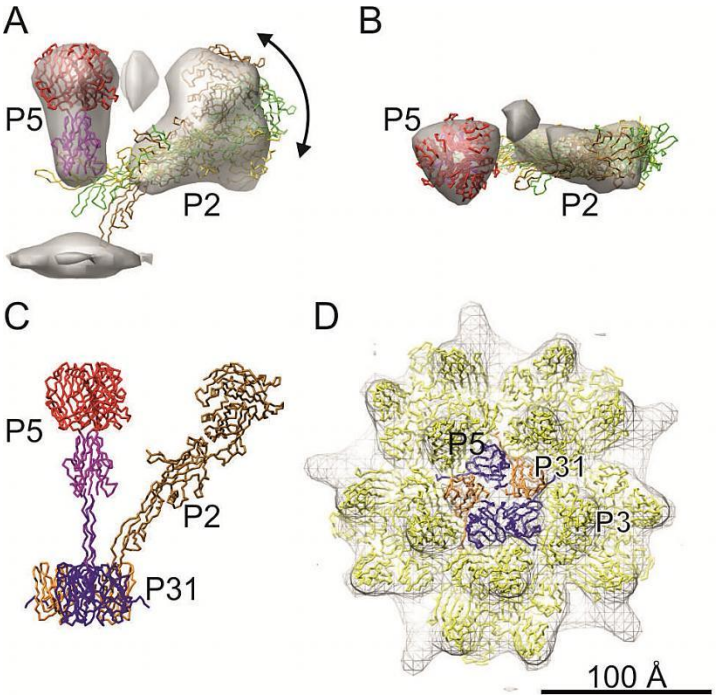

Figure 16. Model for the spike complex. (A and B) Spike-complex reconstruction (gray surface) from P5Δ8G (wt-like) data are shown from the side in A and from the top in B. Ribbons represent P2 (PDB ID code 1N7V) and the P5Δ8G C-terminal fragment (PDB ID code 1YQ8) fitted to the reconstruction. The P5Δ8G structure is colored to correspond with the C-terminal head (red), shaft (magenta) and N-terminal base (blue). Three possible fits of five are shown for P2 in green, brown, and dark brown. The arrow illustrates different conformations of the P2 head relative to P5. The P5 collagen-like region and P2 tail are unresolved in the reconstruction. **(C)** Model for the spike complex shown from the side. The P5–P31 interaction was modeled as a heteropentamer with two P31 subunits replaced by P5 and one P5 monomer in an extended conformation penetrating into the virion (not modeled). P5 monomers are shown in blue, and P31 is shown in orange. **(D)** The heteropentamer is shown from the top, together with the surrounding P3 trimers (yellow). The mesh surface represents the fivefold symmetric P5Δ8G reconstruction. Reprinted from Huiskonen, Manole et al. 2007, with permission from the publisher.

4.3. Glimpses into the structure of a pleomorphic virus infecting halophilic archaea

4.3.1. Isolation and biochemical characterization of seven virus isolates

This study compared seven different pleomorphic archaeal viruses infecting extreme halophilic hosts to give a general view on the characteristics of these poorly understood new types of virions. Three of these isolates had been recently identified by Atanasova et al in 2012, three more had been previously described in studies by Pietilä et al in 2009, Roine et al in 2010, and Bath et al in 2006. One isolate was described for the first time in this study. All seven isolates and their hosts are listed in Table 3. The new virus reported in this study was isolated, together with its host, from a salt crystal collected in Thailand. The host strain was designated as *Halorubrum* sp. SS7-4, based on 16S rRNA sequence similarities with *Halorubrum chaoviator* (AM048786) and *Halorubrum sodomense* (D13379) of 99.4%, and 99.2%, respectively. Accordingly, the new virus was designated *Halorubrum* pleomorphic virus 6 (HRPV-6).

Table 3. Viruses and their host strains used in this study

Virus			Host archaeon	
Name	**Origin**	**Reference**	**Strain**	**Reference**
HRPV-1	Italy, Trapani	Pietilä *et al*., 2009	*Halorubrum* sp. PV6	Pietilä *et al*., 2009
HRPV-2	Thailand, Samut Sakhon	Atanasova *et al*., 2011	*Halorubrum* sp. SS5-4	Atanasova *et al*., 2011
HRPV-3	Israel, Sedom ponds	Atanasova *et al*., 2011	*Halorubrum* sp. SP3-3	Atanasova *et al*., 2011
HRPV-6	Thailand, Samut Sakhon	This study	*Halorubrum* sp. SS7-4	This study
HGPV-1	Spain, Cabo de Gata	Atanasova *et al*., 2011	*Halogeometricum* sp. CG-9	Atanasova *et al*., 2011
HHPV-1	Italy, Margherita di Savoia	Roine *et al*., 2010	*Haloarcula hispanica* ATCC 33960	Juez *et al.*, 1986
His2	Australia, Victoria	Bath *et al*., 2006	*Haloarcula hispanica* ATCC 33960	Juez *et al.*, 1986

The small size of the virus plaques and their hazy appearance indicated that these seven archaeal viruses may be non-lytic. This observation was further supported by one-step growth curves where host cell growth continued throughout the infection.

SDS-PAGE analysis of the protein profiles of the purified viruses showed the presence of three major structural proteins for His2 and HGPV-1 and two for HRPV-1, HRPV-2, HRPV-3, HRPV-6, and HHPV-1. Sudan Black B staining of the protein gel showed the presence of viral lipids, as well as of two lipid-modified proteins, His2 VP28 and HGPV-1 VP4. Thin-layer chromatography analysis of the lipid composition of His2, HRPV-2, HRPV-3, HRPV-6, and HGPV-1 indicated they were acquired from the host membranes, the virus-host pairs showing only minor differences in the lipid patterns. The lipid content of HRPV-1 and HHPV-1 was determined previously (Pietilä, Roine et al. 2009; Pietilä, Laurinavicius et al. 2010; Roine, Kukkaro et al. 2010). Based on these results we concluded that all seven viruses contained lipid membranes.

The position of the viral proteins with respect to each other and to the lipid membrane was determined biochemically by dissociation studies. The viruses were incubated at either 37^0C or 60^0C in the presence or absence of proteinase K, dissociated at low salt concentrations or subjected to a combination of these two methods. Similar dissociation methods were previously used to describe HRPV-1 (Pietilä, Laurinavicius et al. 2010). Based on the dissociation results we established the presence of surface proteins

sensitive to proteases and membrane-embedded proteins that were more resistant (**Figure 17 A-F**).

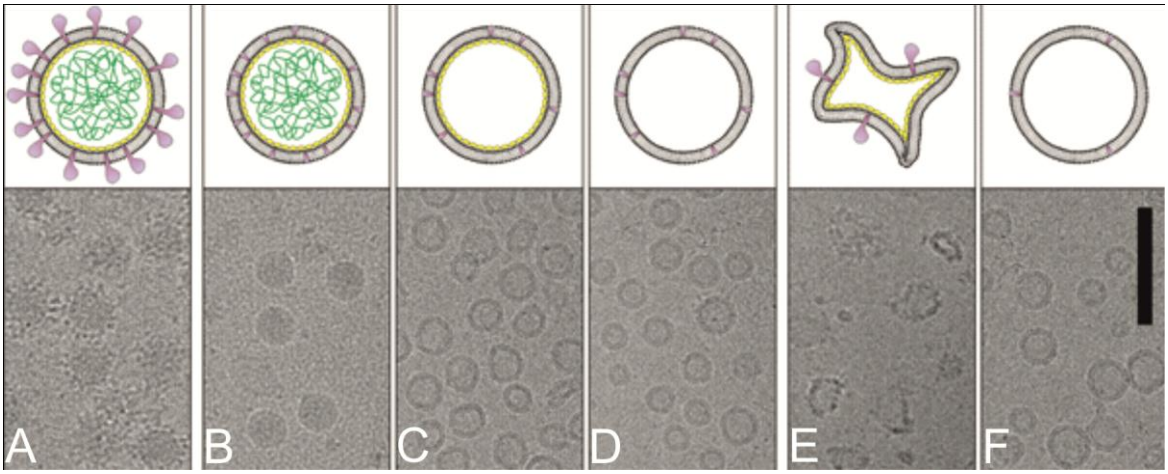

Figure 17. Dissociation products of HRPV-1 analysed by cryo-EM. Cryo-electron micrographs of the particles are shown on the left and schematic presentations on the right. Colours indicate the VP4 protein (purple), the VP3 protein (yellow), and the genome (green). The two membrane-associated domains of VP3 are not indicated in the schematic presentations. **(A)** Untreated '1× purified' virions. **(B)** Virions treated with proteinase K at high salinity at 37°C. **(C)** Proteinase K treated particles further dissociated at low salinity at 37°C. **(D)** Virions treated with proteinase K at low salinity at 37°C (48). **(E)** Virions treated at low salinity at 60°C. **(F)** Particles produced at low salinity at 60°C further treated with proteinase K at low salinity at 37°C. Scale bar, 100 nm. Reprinted from Pietilä, Atanasova et al. 2012, with permission from the publisher.

4.3.2. HRPV-1 viral architecture

HRPV-1 is the best characterized model system for pleomorphic archaeal viruses (Pietilä, Roine et al. 2009; Pietilä, Laurinavicius et al. 2010; Roine, Kukkaro et al. 2010) and in this study we specifically set out to compare the architecture of HRPV-1 with the other isolates, using cryoEM for the first time on any of these viruses. It was rapidly evident that all the seven viruses are roughly similar in shape with the membranes and spikes visible when imaged in high salt (**Figure 18**).

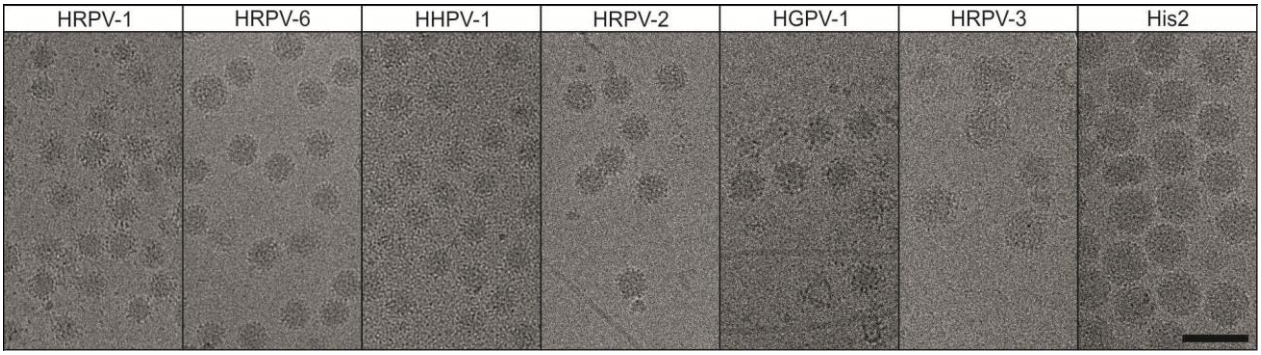

Figure 18. Virion morphology by cryoEM. The viruses are placed in increasing particle size. Either the '1× purified' virions (HRPV-1, HRPV-2, HGPV-1, HRPV-3, and His2) or the '2× purified' virions (HRPV-6 and HHPV-1) are shown in the cryo electron micrographs. For HRPV-6 and HHPV-1, the '2× purified' virions were used because of ribosome impurities in the '1× purified' material. The micrographs of HRPV-2 and HGPV-1 contain some host cell flagella. Scale bar, 100 nm. Modified from Pietilä, Atanasova et al. 2012, with permission from the publisher.

The spikes seen on the HRPV-1 surface were assigned to the protease-sensitive VP4 based on the biochemical and cryoEM observations. The membrane-embedded VP3 was not directly evident in the cryoEM. The genome was evident inside the membrane vesicle by following the appearance of the particle during step-wise dissociation of the virus (**Figure 17 A, B**) (Pietilä, Laurinavicius et al. 2010). The three-dimensional structure of HRPV-1 was investigated by cryoEM and image reconstruction. Images of purified HRPV-1 particles of similar diameter and apparently ordered were collected and processed using single-particle averaging methods. The orientation searches did not render a single model and so we decided to use cryoET and subtomographic averaging instead. Intact HRPV-1 virions, as well as HRPV-1 subviral particles of known composition were imaged by cryoET and seventeen tomograms were computed (**Figure 19 A, B**). The tilt angles varied in the range of $\pm 48^0$ to $\pm 60^0$ with increments of 1^0 to 4^0. The best 3D tomographic reconstruction showed approximately spherical and intact HRPV-1 particles with protruding spikes covering the surface of a continuous membrane layer (**Figure 19 A**).

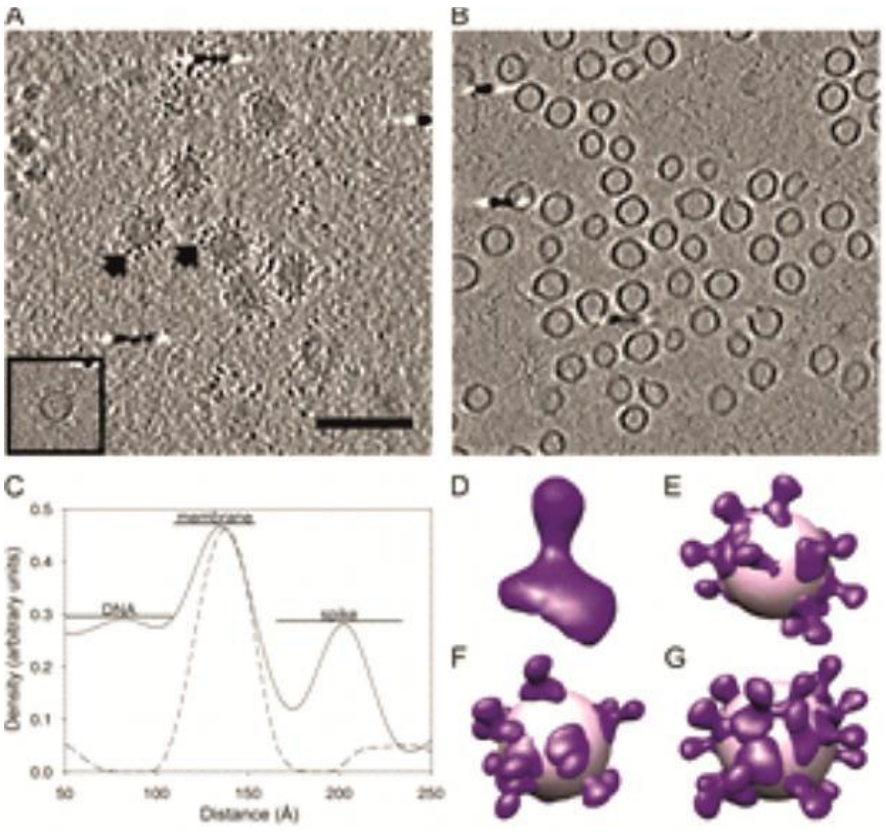

Figure 19. Structural organization of HRPV-1. (A) Tomographic slice of HRPV-1 showing intact spherically-shaped virions containing the genome and spikes projecting out from the surface of the membrane (black arrows). An empty particle image is in the insert. Scale bar, 100 nm (same for B). **(B)** Tomographic slice of HRPV-1 subviral particles composed of the lipid membrane and VP3 protein. The slices are 5.7 nm thick in A and B. **(C)** The density distribution over the membrane calculated from the aligned extracted subvolumes for HRPV-1 virions (solid line) and subviral particles containing the membrane and VP3 (dotted line). The membrane peaks were normalized. **(D)** Isosurface representation of a single VP4 spike. **(E-G)** The model of the VP4 spike protein (violet) was placed into individual virion tomograms based on the refined spike positions that contributed to the averaged VP4 model. The viral surface (light pink) was approximated by a sphere of 35 nm in diameter. Reprinted from Pietilä, Atanasova et al. 2012, with permission from the publisher.

The structural features of HRPV-1 were analyzed in more detail by subtomogram averaging. Thus we obtained an average structure of VP4 and we were able to calculate a radial profile of the membrane layer and of the VP4 spike. For comparison, we also computed a 3D tomographic reconstruction of HRPV-1 subviral particles composed only of the lipid vesicle and the membrane protein VP3. At the current resolution we could not differentiate between the membrane density and the density belonging to VP3. However, we were able to determine that the membrane together with VP3 forms a 4.2-nm-thick continuous layer, and that the VP4 spike is approximately 7nm long when embedded into the membrane (**Figure 19 C**). Further refinement of the averaged subvolumes of VP4 revealed a club shaped protein, with a knob at the distal end from the membrane (**Figure 19 D**). We reconstructed the overall organization of the spikes on the virus surface by

cross-correlating the averaged VP4 structure with the virions in the tomograms. Based on these results, we generated three 3D models of HRPV-1 virions in CHIMERA (Pettersen, Goddard et al. 2004; Goddard, Huang et al. 2007)(**Figure 19 E-G**). The models show a relatively spherical membrane layer randomly decorated with spikes which form irregular arrays across its surface. There are low spike densities in two opposing areas on the volumes, a result of the missing wedge of information in the tomographic reconstructions (**Fig 19 E-G**).

5. DISCUSSION

5.1. On the architecture of African Horsesickness virus

The recent emergence of the Schmallenberg virus in Europe, as well as the increased European area affected by BTV has focused attention on the emergence of new pathogens in previously unaffected areas. Particularly such viruses have been shown to have a devastating effect on susceptible livestock and the livelihoods of their owners. African horsesickness virus is considered endemic to the African continent, but has already caused major economic losses to the equine industry in southern Europe (Coetzer 1994; Mellor and Hamblin 2004). It is known that BTV and AHSV are transmitted by the same insect vectors, and recently this has been postulated for the Schmallenberg virus (Mellor 1992; Mellor, Boorman et al. 2000; Slenning 2010). Hence it is high time that effective measures for the prevention and treatment of AHSV are also developed. This was a major driving force to study the structure of AHSV to gain insight into its biology and to the similarities and differences to the well-studied BTV.

We have shown that although the overall structure of AHSV resembles that of BTV, there are some significant differences. The current conformation of the AHSV-4 and AHSV-7 tVP2 VP3 layer prevents the mRNA strands from exiting via the five-fold vertices, which has been show as the route of exit during BTV transcription (Grimes, Burroughs et al. 1998; Diprose, Burroughs et al. 2001). AHSV-4 has an additional density blocking the five-fold vertices, density that could correspond to an incorrectly averaged VP5 trimer or to one part of the VP2 arms surrounding the five-fold (**Figure 14 A**). The quasi-atomic model of the core particle allows a testable model of the VP3-VP7 interactions that could be exploited in the design of antiviral drugs to AHSV (**Figure 13 A, B, C**).

As the receptor-binding protein, VP2 is exposed on the viral surface and thus is the first of the viral proteins to be encountered by the host immune system. This selective pressure favors mutational events at the amino acid sequence level of VP2, while still maintaining the overall protein architecture. This explains why VP2 has the least conserved sequence among the AHSV and BTV structural proteins (see Table 2 in Study I). Mapping of some of the known immunogenic sites (variable regions in the sequence) showed that these are all on the exposed surfaces of VP2. Due to VP2 sensitivity to equine serum proteases we believe that an endoproteolytic cleavage of the VP2 trimer can also occur in the salivary

glands of the vector (Marchi, Rawlings et al. 1995; Darpel, Langner et al. 2011). This activation of VP2 is very important for virus entry. It may well destabilize the VP2 structure allowing new sites for receptor binding to be exposed on VP7, VP5 or VP2 along with activation of VP5 (putative fusion protein). The deletion of 225 amino acids from the AHSV-7 VP2 structure occurs in a region known to contain immunogenic epitopes and residues implicated in tissue tropism and virulence (Martinez-Torrecuadrada and Casal 1995; Bentley, Fehrsen et al. 2000; Potgieter, Page et al. 2009). For the first time we showed that for AHSV these epitopes are located at the tips of the triskelions, in a region free from interaction with either VP5 or VP7 (**Figure 15 C-F**). We also located the other major immunogenic epitopes (residues 368-403 and 450-483) at the top of the AHSV-4 triskelion hub (Bentley, Fehrsen et al. 2000)(**Figure 15 B-E**). It is possible that this central domain is a target for the serum proteases (Burroughs, O'Hara et al. 1994; Marchi, Rawlings et al. 1995). The central domain of VP2 probably covers the putative sialic acid binding site (tentatively identified in BTV1). The central domain is absent in both BTV1 and AHSV-7 tVP2 (Zhang, Boyce et al. 2010)(**Figure 15 C, F**). This would allow direct accessibility to the binding site of VP2 and could explain why AHSV-7 tVP2 outgrows AHSV-4 in tissue culture.

BTV VP5 was shown to function similarly to a fusion protein and we believe that AHSV VP5 might have the same role in virus entry (Hassan, Wirblich et al. 2001; Forzan, Wirblich et al. 2004). Apart from being a preponderantly α-helical protein, the secondary structure prediction for AHSV VP5 showed an N-terminal amphipathic helix (residues 1-41), with the putative function of a fusion peptide (Lupas, Van Dyke et al. 1991). Considering these structural clues, we propose a likely series of events for AHSV cell entry: VP2 is proteolitically cleaved either in the salivary glands of the vector or in the host serum, the putative sialic acid receptor binding region of VP2 interacts with the cellular receptor, the virion is internalized via an endocytic pathway, VP5 gets activated by the low pH environment leading to possible conformational changes and the exposure of the fusion peptide, which leads upon insertion into the endosomal membrane to the release of the transcriptionally-active core into the cytoplasm. This would be a pathway very similar to that described for BTV (Forzan, Wirblich et al. 2004; Zhang, Boyce et al. 2010) and requires experimental validation.

5.2. Discussing the proposed model for the PRD1 spike complex

PRD1 is one of the best characterized membrane-containing viruses (Caldentey, Bamford et al. 1990; Bamford, Caldentey et al. 1995). Its overall architecture was solved both by cryoEM and X-ray crystallography and is described in detail in Section 1.6. of the Introduction (Butcher, Bamford et al. 1995; Benson, Bamford et al. 1999; San Martin, Huiskonen et al. 2002; Abrescia, Cockburn et al. 2004; Cockburn, Abrescia et al. 2004). However, because the methods applied to study PRD1 virion structure previously which all imposed icosahedral–symmetry, all other protein complexes and the DNA which did not obey the imposed symmetry were averaged out during image processing. This study provided the first in-depth analysis of the PRD1 spike structure *in situ* and offers a realistic atomic model of how the protein complex is organized within the capsid (**Figure 16 A-D**). The analysis allowed us to deal with heterogeneity coming from the occupancy of the spikes, from symmetry mismatch, and to some extent from flexibility. Most of the virion vertices were found to have P2 and P5 present, next to each other, connected with the capsid at the level of the P31 penton, oriented so that the narrow end of the spikes is proximal to the particle, and the bulky heads distal (**Figure 15 A, B**). This agrees with a truncation study of gene *V* which has shown that the N-terminal 149 amino acids of P5 can still assemble into the particle, and to digestion of the whole virion with trypsin that has shown that the C-terminus of P2 is exposed (Bamford and Bamford 2000; Xu, Benson et al. 2003). We could not accurately show the position of P2 binding at the capsid level, but there are only a few likely possibilities: it can either bind to the N-terminus of P5, to P31 or P3. The genetic dependency of P2 assembly requiring the presence of both genes *XXXI* and *V*, is only indirect evidence that P2 attaches directly to P5. No association has been shown in vitro, unlike the P5-P31 association (Caldentey, Tuma et al. 2000; Sokolova, Malfois et al. 2001). Thus further experiments are required to determine the exact nature of the interaction. The presence of only one copy of P2 on most vertices could be explained by the asymmetric environment created by the interaction between P5 and P31, either by P5 replacing one or more copies of P31 in the pentamer (they are predicted to have similar folds), or by the N-termini of the P5 trimer being in a more extended state, passing through the P31 pentamer. PCA of the vertices from the virions also revealed a class that apparently did not contain spikes. It has previously been observed that there is a unique packaging vertex in PRD1, which can be identified by antibody labeling of mildly detergent-treated virions and mutants (Gowen, Bamford et al. 2003). This PCA class may

represent the packaging vertex, in which case there is no clear portal evident, or it may represent broken vertices, where the metastable vertex containing P31 has been released (Rydman, Caldentey et al. 1999)(**Figure 15 D**, last class in the row).

The orientation of P2 adds weight to the argument proposed when the atomic model of P2 was determined, that the pseudo-β propeller is the receptor-binding domain, most distal to the particle and facilitates host attachment, recognition and entry (Grahn, Caldentey et al. 1999; Xu, Benson et al. 2003). In laboratory conditions, the P5 trimer is not involved in binding to the cellular receptor, since mutant virus particles with P2 missing from the vertex complex are not infectious (Bamford and Bamford 2000). Also, we showed that P5 is not a pedestal for P2, exposing it more distally from the particle (Xu, Benson et al. 2003), since the two proteins are arranged as two different spikes (**Figure 16 A-C**). So what is the role of P5? It is possible that P5 gives the virus an advantage in the wild as an auxillary attachment protein that keeps the virus in contact with the host until P2 binds (Butcher, Manole et al. 2012). This would explain why the P5Δ8G mutant has slower attachment kinetics as the glycine hinge removal makes P5 less flexible and thus slows the attachment process (Huiskonen, Laakkonen et al. 2003). Still the binding of P2 to the host is reversible, so as there is a packaging vertex, this could also be the place that the genome has to exit the particle (Grahn, Caldentey et al. 1999; Grahn, Daugelavicius et al. 2002a). Hence rolling of the virus on the cell could be required to allow the packaging vertex to bind irreversibly giving a plausible explanation for the unusual architecture of the majority of the vertices. It has been observed directly, for instance, with SV40 that the virus moves over the surface of the cell, rolling and reversibly attaching until it finally enters the cell (Kukura, Ewers et al. 2009).

5.3. What does the HRPV-1 structure tells us?

The structural biology of viruses infecting archaea is a fast developing field of study. Nevertheless, the number of solved structures for these viruses is very low. This can be partly explained by the fact that many archaea species inhabit prohibitive environments, such as acidic hot springs or bodies of water with high salt content, and thus the conditions required for virus stability are not conducive to structural work. Another reason is the wide variety of shapes displayed by archeal viruses, many of them posing challenges for current

methods of data collection and 3D image processing (see Section 1.7 of the Introduction). This latter reason explains why so far the only structures solved by cryoEM are those of icosahedrally-symmetric archaeal viruses such as STIV, SH1, and STIV2 (Rice, Tang et al. 2004; Jäälinoja, Roine et al. 2008; Happonen, Redder et al. 2010). Structure determination attempts have also been made on irregularly-shaped viruses, using electron tomography of negatively-stained samples (Prangishvili, Arnold et al. 1999; Haring, Vestergaard et al. 2005; Vestergaard, Haring et al. 2005; Prangishvili, Vestergaard et al. 2006). Our study describes the first structure of a pleomorphic archaeal virus solved by cryoET and subtomographic averaging. The virions were imaged in their native hydrated state to avoid shape distortions, after checking that the specimen purification did not induce such changes. The tomographic reconstruction of HRPV-1 showed roughly spherical particles decorated with spikes on the surface of a lipid membrane enclosing the viral genome (**Figure 19 A, E, F, G**). VP3 protein seems to be mainly embedded into the membrane, without forming any regular arrays. We found several potential sources for the pleomorphicity seen in HRPV-1 and the other isolates, including size differences, and the apparent random distribution of VP4 on the membrane outer surface, indicating only weak lateral interactions between individual spikes. An aspect of the HRPV-1 biology that most likely affects pleomorphicity, is that the virus apparently buds from the cells, rather than lysing them. What are the mechanisms in virus budding that could be the basis for such flexible assembly? In other pleomorphic viruses, such as influenza, measles and HIV, there are three basic steps in budding: initiation of the bud, elongation of the patch of membrane that will be incorporated into the virus, and scission of the bud (Calder, Wasilewski et al. 2010; Rossman and Lamb 2011). This is a complex process, where both the envelope glycoproteins and the matrix proteins have been shown to have an influence on membrane curvature and budding and, where cooperativity is required between the glycoproteins and the matrix. Importantly, host proteins are also involved, for instance the host ESCRT complex proteins are required for the final act of scission (Harris, Cardone et al. 2006; Bruce, Medcalf et al. 2009; Watanabe and Lamb 2010; Rossman and Lamb 2011). The result of this complex set of interactions is that the virus takes over the export processes of the cell, without specifically defining the final virus shape. As a consequence, the resulting particles vary tremendously in shape and size. This is in contrast to enveloped viruses such as Semliki Forest virus and dengue virus where there are very specific viral protein interactions occurring that dictate the shape and size of the final particle (Mancini, Clarke et al. 2000; Kuhn, Zhang et al. 2002). A similar mechanism could

be controlling the morphology in HRPV-1 resulting in “sloppy” assembly due to the virus exiting the host cell by budding. In this case, the interactions between the membrane-embedded protein VP3, the spike protein VP4, the viral genome and host proteins could all be key factors for assembly. The identification of conserved regions either in the primary sequence or in the three-dimensional structures of the viral proteins between different pleomorphic archaeal viruses may help in dissecting this process further (Sencilo, Paulin et al. 2012).

6. CONCLUSIONS

When fast, automated techniques such as PCR or whole genome sequencing became widely available, everybody got excited every time a new genome of an entire organism was released, culminating with the sequencing of the human genome (Venter, Adams et al. 2001). It quickly became obvious to scientists that having the genome map is merely the beginning, and it opened new exciting avenues of research. It also raised a lot more complicated questions. The story of structure determination followed a similar path, and while structures are becoming more readily available from structural genomics initiatives, for instance, putting them back in their biological context remains just as tricky. My thesis illustrates this point by addressing the relationship between the structures of three different types of receptor-binding proteins belonging to three viruses and their biological implications for the viral life cycle. I found that especially in the case of animal pathogens, that understanding the structure of these proteins is essential for understanding how one could disrupt protein-protein interactions for vaccine development or blocking different stages in the virus life cycle. The method of choice for each study was based on the biological complexity of the system and the hypotheses to be tested. This is the reason why I used three different computational approaches for *in situ* determination of the 3D structure of the virus receptor-binding proteins, resulting in different levels of detail, but in each case shedding light on the biology.

In the first study, which describes the detailed icosahedrally-symmetric reconstructions of African horsesickness virus (AHSV), the amount of detail in the final structure comes from the advantage of the very high symmetry which contributes to accurate orientation determination and to increasing the signal to noise ratio. The homology models for several of the viral proteins which we were able to generate, used in combination with the structure of a naturally-occurring mutant of the spike protein, enabled us to add to the detail that could be extracted from the reconstructions. The limiting factor in this study was the relatively low number of virus particles in the data sets, caused by both the fact that eukaryotic viruses are difficult to purify and that the viruses had to be imaged in South Africa, where AHSV is endemic and can be worked with on the bench, unlike in Finland where it is a strictly regulated, notifiable virus.

In the second study, the 3D organization of the spike complex of the bacteriophage PRD1 was determined using two single particle approaches. The image processing was helped

by using the initial information from the icosahedral orientations of the virus particles as a constraint to identify the positions of the vertices in the original images and limit the degrees of freedom in the refinement. In the final classification and averaging, the thickness of the specimen clearly added a lot of noise to the data, considering the huge size difference between the capsid and the individual spikes. The interpretation of the results was further hindered by the flexibility of the two spike proteins with respect to each other. We overcame these shortcomings by combining our results with information from known atomic models of individual components to generate a model of the spike complex.

The last study dealt with a sample showing enough heterogeneity in shape and size to render single particle methods obsolete. This problem was addressed by using cryoET, and local averaging of individual spikes carried out from the tomographic data. The resolution was limited in this case by the small size of the virus and spikes, the lack of classification analyses, the random distribution of the spikes on the viruses and especially the very low signal to noise ratio in the sample due to the high salt background, which forced us to collect tilt series at high underfocus values. Still, the result gave indications that the assembly of HRPV-1 and other pleomorphic archaeal viruses may be much more closely related to viruses infecting eukaryotes than to those infecting bacteria.

The ability to interpret the biological significance of the structures described in my thesis is influenced by all of those limiting factors mentioned above. However, the limitations of one method can be overcome using one or more different, though complementary methods. Thus, a combination of biochemical studies, structure determination and homology modeling allowed us to assign the location of the different proteins of AHSV in the EM density, tentatively locate the major immunogenic epitopes in VP2, and propose a realistic pseudo-atomic model for the PRD1 spike complex. Because of the scarcity of archaeal homologous sequences in the databases, we were not able to find any similar protein structure that would help validate our reconstruction of HRPV-1. However, even at this limited resolution, HRPV-1 structure remains informative.

Of course, there are also situations when even a wealth of information does not guarantee only one solution for a given structure. This was the case in retrovirus research when trying to establish the structure of the glycoprotein trimer gp120 in the context of the virion. CryoET structures of the trimer were published by two different groups, and imaged in different conformations with ligands bound or not. In spite of the fact that X-ray structures

of the complexes were available, the way the two groups interpreted their structures differed considerably. One disagreement concerned the conformation of the gp41 region, another referred to the packing density of the gp120 domains in the trimer (Liu, Bartesaghi et al. 2008; Zhu, Winkler et al. 2008; Schief, Ban et al. 2009). Partly these conflicting results could be explained by the different implementations used in subtomogram averaging, which emphasizes the infancy of this field of image processing. When we think about the biological function of a protein or a macromolecular complex, we also have to consider the difference of analyzing it *in situ* or as a purified entity, separated from the overall structure it belongs to. It seems a small thing to consider, but it can make a huge difference when we think in terms of conformational changes that occur during virus assembly and entry in the quaternary structure interactions (Li, Lok et al. 2008).

The take-home message of the three studies presented in my thesis is that there is a great deal of complexity in dealing with biological systems. In terms of image processing, there is still no generally applicable method to deal with heterogeneity and flexibility. In terms of biology, it is exactly this heterogeneity that is biologically relevant, and thus must be addressed.

7. FUTURE PERSPECTIVES

Although I have achieved the proposed goals for my thesis, this study is far from being exhaustive. Considering the AHSV structure, the next obvious step for continuation is to calculate a 3D structure at subnanometer resolution to reveal the fold of the individual proteins, which would aid understanding of key interactions for vaccine development (Schief, Ban et al. 2009). Such a high resolution structure does not necessarily imply collecting a huge data set. Three essential factors must be fulfilled: excellent specimens, excellent imaging conditions and robust data processing to find the best data to incorporate (Liu, Jiang et al. 2007). Modern electron microscopes, operating at voltages of 300 kV and equipped with multispecimen holders and energy filter are very stable and enable very high quality data collection (Zhang, Settembre et al. 2008). An impediment in my study of AHSV was that as it is a controlled pathogen in Europe, it requires high biosafety levels for handling. To avoid this I carried out the imaging in South Africa, where the disease is endemic and the virus can be handled on the bench, but this was also not ideal. In order to study the virus more conveniently, one should develop either a way to inactivate the virus so that it loses its infectivity, or use a reverse genetics system (Matsuo, Celma et al. 2010) to introduce different types of mutations to modify only the spike protein VP2 in a stable genetic backbone. Thus this would provide a basis for exploring the regions required to generate neutralizing antibodies, and for differences in cell tropism and virus fitness in different hosts. A reverse genetics system could also considerably improve our chances of cloning and expressing individual proteins for crystallization trials as an alternative to atomic-level cryoEM. An X-ray structure of the receptor-binding protein VP2 or of VP5 would add considerably to our current knowledge of AHSV (and BTV), since there are no homology models for these proteins. Another challenge we faced and which needs to be addressed in the future is to develop a new purification protocol for the wild type AHSV-7. This strain could not be purified during our studies. The structural studies must also be complemented by cell biology studies, since at the moment very little is known on the cellular aspect of the life cycle of AHSV in either insect or mammalian cells, or why BTV and AHSV have similar vectors, but different host tropisms (Erasmus 1973; Mellor, Boorman et al. 2000; Paweska, Venter et al. 2002). One reason could be due to differences in the protease susceptibility of VP2. Comparative studies between the AHSV and BTV life cycles are likely to be very informative (Forzan, Wirblich et al. 2004; Roy 2005; Forzan, Marsh et al. 2007). We know AHSV VP2 is protease sensitive, so three-

dimensional reconstruction of protease-treated particles, and determination of the exact cleavage sites by mass spectrometry could be exploited in a reverse genetics system to help explore different stages in VP2 activation and shed light on the initial steps of viral infection.

In the case of PRD1, one of the questions still to be addressed is the location and the *in situ* structure of the unique packaging vertex. One possibility is to try to analyze all the vertices from tomographic reconstructions of PRD1 to find the packaging vertex. This approach has been used most successfully to identify the herpes virus portals (Deng, O'Connor et al. 2007; Rochat, Liu et al. 2011). The component proteins of the vertex complex have been identified biochemically, and thus one might consider incubating intact PRD1 virions with antibodies raised against the proteins most likely to be exposed or closest to the virus surface. This technique has given excellent results for measles virus, for instance, where immunosorbent EM was used to discriminate between the matrix protein and the nucleocapsid (Liljeroos, Huiskonen et al. 2011). Integrin-labeling and subsequent image analysis allowed localization of the RGD motif on the surface of Human parechovirus 1, proving once again the validity of this approach (Seitsonen, Susi et al. 2010). Another approach could take into account imaging whole bacterial cells during PRD1 infection, similar to the study of Epsilon15 infection of Salmonella cells (Chang, Schmid et al. 2010). In this case, the vertex from which the genome enters the cell would be most likely oriented closest to the cell surface, and if this is the same as the packaging vertex, would facilitate the analysis, such as in studies of MS2 bound to pili (Toropova, Stockley et al. 2011). CryoET would thus be the method of choice for trying to locate the packaging vertex and resolve its *in situ* conformation. The recent technical advances that allowed electron microscopes to be equipped with energy filters, the exciting results coming from studies using the Zernike plate and the development of new direct detectors hold great promise for improved cryoET results in the future (Murata, Liu et al. 2010; Bammes, Rochat et al. 2012).

The study of pleomorphic archaeal viruses would also benefit greatly from these new technical advances in imaging as well as from the development of robust tomographic data processing, such as the implementation into already established software of image classification and CTF correction algorithms (Winkler 2007; Xiong, Morphew et al. 2009; Zanetti, Riches et al. 2009). However, in the case of HRPV-1, the high salt concentration in the sample will always be a limiting factor for image quality, regardless of the

capabilities of the microscope or image processing software. Lowering the salt concentration of HRPV-1 buffer at any stage during purification leads to the loss of the virus structural integrity, possibly because of a big difference in the osmotic pressure between the inside of the virus and the outer environment. A lower salt concentration also means lowering the ionic strength of the buffer, which could also disrupt the protein-protein interactions. Thus it is of interest for this study to check the tolerance of other pleomorphic archaeal viruses for low salt conditions without losing structural integrity, since sample optimization is the first rule for high resolution microscopy studies. HRPV-2 could be a good candidate in this respect, with only 9% salt concentration in the optimal buffer compared to a range of 12% to 18% salt concentration for the other isolates. The size of the sample can also make a difference in imaging, and since His 2 is the largest archaeal pleomorphic virus isolated thus far, it would make a good choice for further tomographic investigations. Apart from the overall viral architecture, one should also look at individual components of the virus. For example, HRPV-1 spike protein VP4 could be proteolytically cleaved from the virus surface and purified for crystallization trials, thus by-passing the need for an archaeal cloning and expression system. A similar approach led to a 3Å resolution X-ray structure of influenza hemagglutinin, after the ectodomain of the glycoprotein was separated from the virus via proteolytic cleavage (Wilson, Skehel et al. 1981). As an integral membrane protein, purification protocols for HRPV-1 VP3 could pose a challenge for obtaining soluble purified protein for X-ray crystallization trials. As an alternative, one could study the 3D structure of such proteins by employing cryoEM of 2D crystals followed by image processing. An advantage of this method is that the protein is embedded into a closer-to-native environment of a lipid bilayer, thus maintaining its native conformation (Ubarretxena-Belandia and Stokes 2012). This is a very powerful method, which generated atomic-resolution structures such as that of the junctional aquaporin-0 at 1.9 Å resolution (Gonen, Cheng et al. 2005). All these different studies would be perfectly complemented by whole-cell cryoET of the archaeal host during viral infection, which would shed light on the assembly principles of these archaeal pleomorphic viruses.

ACKNOWLEDGEMENTS

The work for this thesis was carried out at the Finnish Centre of Excellence in Virus Research (2006 - 2011), at the Institute of Biotechnology and Department of Biosciences at the University of Helsinki, under the supervision of Professor Sarah Butcher. The work was financed by the Viikki Doctoral Programme in Molecular Biosciences (VGSB).

I want to thank Sarah, the best supervisor anyone could wish for. She was there for me every step of the way, and always willing to offer support in both scientific and personal matters. She is a great teacher and an even greater scientist. Her energy and dedication to her work have pushed me forward when everything seemed to go nowhere.

I am much in debt to Dr. Jani Seitsonen, the first ever to explain to me what UNIX is. Without his advice and endless patience I would have probably graduated at 70 years old. And busted a few computers in the process.

I would also like to thank Prof. Dennis Bamford and Dr. Hideo Iwai for their support and advice as members of my follow-up group. Assistant Prof. Shee-Mei Lok and Docent Janne Ravantti are thanked for carefully, yet quickly, reviewing the thesis manuscript and for their valuable comments.

A very special thank you goes to Dr. Roman Tuma, for his expert supervision on the phi project and for introducing me to the HDX technique. Thank you for your patience and for the long hours put in at the mass spectrometer in Alabama.

I wish to thank my collaborators in all the projects that I had the pleasure to participate in. I have enjoyed very much working with Juha and I always admired his dedication and professional skills. To all my great collaborators in South Africa, thank you so much for making me feel so welcome and for your strong belief in our project, for your enthusiasm and for the great coffee. I also wish to thank you for the “extracurricular” activities we enjoyed together and which made my stay there so wonderful.

I am most grateful to Pasi, for professional microscope training and lots of patience with it. Also, I would like to thank him for being such a nice company during our South African trip.

The Electron Microscopy Unit is warmly acknowledged for excellent collaboration and expertise.

A group hug and thanks for the “Butcher’s arms”, present and former: Sarah, Lotta, Heini, Jani, Lassi, Shabih, Pasi, Ari, Veli-Pekka, Eevakaisa, Katarina, Noha, Kirsty, Juha, and Harri. My heartfelt thanks go also to Benita Löflund, whom heroically stood by me during frantic protein purification.

I would like to thank Riitta Tarkiainen for all her help during my early times in the “wet” lab.

The greatest outcome of this thesis is my wonderful group of friends, whom I met during these years. I will warmly remember all our talks and laughs in the lab or office, without which life would have been unbearable. So thank you, Virginija, Mart, Jani, Lotta, Heini, Lassi and Shabih. Thank you Virga and Mart for the great times we had together, in Ontario, Helsinki and Vilnius, for all the coffee breaks and the intellectually elevated discussions. Thank you, Jani, for everything, for our endless talks about everything and for being the one to spark the interest for building a super-computer. You are a true walking encyclopedia. Thank you, Lotta, for being there when I most needed someone. Thank you for everything. Thank you, Heini, for all your efforts to keep us in shape, for sharing your hobbies with me and for letting me pet your cat. Thank you, Lassi, for being such a great guy and great company in the lab and not only. Thank you for being my friend. Thank you, Shabih. Although you are the newest addition to our group, you have not escaped my endless yapping, which you bear with endless serenity. It’s so easy to talk to you and to be your friend.

To my “non-scientific” friends, Ruxi, Oana, Bogdan, Friedi thank you for keeping me sane all these years and for being you.

My family has a special place in my heart, and even if we only spent time together twice a year, we are as close as ever. Thank you for all your love and support, and mostly for your understanding. Special thanks to Norocel, the craziest and funniest dog on the planet.

And finally, all my love goes to Harri, who has kicked my deriere into gear when I needed to and who had to endure first hand “the making of the thesis” (although he never got to read it). You are my person.

Helsinki,

September 2012

REFERENCES

(2012). Scenarios for the future spread of Schmallenberg virus. *Vet Rec* **170**(10), 245-246.

Abrescia, N. G., J. J. Cockburn, Grimes, J. M., Sutton, G. C., Diprose, J. M., Butcher, S. J., Fuller, S. D., San Martin, C., Burnett, R. M., Stuart, D. I., Bamford, D. H., Bamford, J. K. (2004). Insights into assembly from structural analysis of bacteriophage PRD1. *Nature* **432**(7013), 68-74.

Adrian, M., Dubochet, J., Lepault, J., McDowall, A. W. (1984). Cryo-electron microscopy of viruses. *Nature* **308**(5954), 32-36.

Akita, F., Chong, K. T., Tanaka, H., Yamashita, E., Miyazaki, N., Nakaishi, Y., Suzuki, M., Namba, K., Ono, Y., Tsukihara, T., Nakagawa, A. (2007). The crystal structure of a virus-like particle from the hyperthermophilic archaeon Pyrococcus furiosus provides insight into the evolution of viruses. *J Mol Biol* **368**(5), 1469-1483.

Amos, L. A. and J. T. Finch (2004). Aaron Klug and the revolution in biomolecular structure determination. *Trends Cell Biol* **14**(3), 148-152.

Angert, I., Majorovits, E., Schroder, R. R. (2000). Zero-loss image formation and modified contrast transfer theory in EFTEM. *Ultramicroscopy* **81**(3-4), 203-222.

Atanasova, N. S., Roine, E., Oren, A., Bamford, D. H., Oksanen, H. M. (2012). Global network of specific virus-host interactions in hypersaline environments. *Environ Microbiol* **14**(2), 426-440.

Backovic, M. and F. A. Rey (2012). Virus entry: old viruses, new receptors. *Curr Opin Virol* **2**(1), 4-13.

Baker, M. L., Jiang, W., Bowman, B.R., Zhou, Z. H., Quiocho, F.A., Rixon, F. J., Chiu, W. (2003). Architecture of the herpes simplex virus major capsid protein derived from structural bioinformatics. *J Mol Biol* **331**(2), 447-456.

Baker, T. S.,Olson, N. H., Fuller, S. D. (1999). Adding the third dimension to virus life cycles: three-dimensional reconstruction of icosahedral viruses from cryo-electron micrographs. *Microbiol Mol Biol Rev* **63**(4), 862-922.

Bamford, D. and L. Mindich (1982). Structure of the lipid-containing bacteriophage PRD1: disruption of wild-type and nonsense mutant phage particles with guanidine hydrochloride. *J Virol* **44**(3), 1031-1038.

Bamford, D. H., Caldentey, J., Bamford, J. K. (1995). Bacteriophage PRD1: a broad host range DSDNA tectivirus with an internal membrane. *Adv Virus Res* **45**, 281-319.

Bamford, J. K. and D. H. Bamford (1990). Capsomer proteins of bacteriophage PRD1, a bacterial virus with a membrane. *Virology* **177**(2), 445-451.

Bamford, J. K. and D. H. Bamford (2000). A new mutant class, made by targeted mutagenesis, of phage PRD1 reveals that protein P5 connects the receptor binding protein to the vertex. *J Virol* **74**(17), 7781-7786.

Bamford, J. K., Cockburn, J. J., Diprose, J., Grimes, J. M., Sutton, G., Stuart, D. I., Bamford, D. H. (2002). Diffraction quality crystals of PRD1, a 66-MDa dsDNA virus with an internal membrane. *J Struct Biol* **139**(2), 103-112.

Bammes, B. E., Rochat, R. H., Jakana, J., Chen, D. H., Chiu, W.(2012). Direct electron detection yields cryo-EM reconstructions at resolutions beyond 3/4 Nyquist frequency. *J Struct Biol* **177**(3), 589-601.

Basak, A. K., Gouet, P., Grimes, J., Roy, P., Stuart, D. (1996). Crystal structure of the top domain of African horse sickness virus VP7: comparisons with bluetongue virus VP7. *J Virol* **70**(6), 3797-3806.

Basnak, G., Morton, V. L., Rolfsson, O., Stonehouse, N. J., Ashcroft, A. E., Stockley, P. G. (2010). Viral genomic single-stranded RNA directs the pathway toward a T=3 capsid. *J Mol Biol* **395**(5), 924-936.

Bath, C., Cukalac, T., Porter, K., Dyall-Smith, M., L. (2006). His1 and His2 are distantly related, spindle-shaped haloviruses belonging to the novel virus group, Salterprovirus. *Virology* **350**(1), 228-239.

Baumeister, W. and A. C. Steven (2000). Macromolecular electron microscopy in the era of structural genomics. *Trends Biochem Sci* **25**(12), 624-631.

Beaton, A. R., Rodriguez, J., Reddy, Y. K., Roy, P. (2002). The membrane trafficking protein calpactin forms a complex with bluetongue virus protein NS3 and mediates virus release. *Proc Natl Acad Sci U S A* **99**(20), 13154-13159.

Belhouchet, M., Mohd Jaafar, F., Firth, A. E., Grimes, J. M., Mertens, P. P., Attoui, H. (2011). Detection of a fourth orbivirus non-structural protein. *PLoS One* **6**(10), e25697.

Benjamin, J., Ganser-Pornillos, B. K., Tivol, W. F., Sundquist, W. I., Jensen, G. J.(2005). Three-dimensional structure of HIV-1 virus-like particles by electron cryotomography. *J Mol Biol* **346**(2), 577-588.

Benson, S. D., Bamford, J. K., Bamford, D. H., Burnett, R. M. (1999). Viral evolution revealed by bacteriophage PRD1 and human adenovirus coat protein structures. *Cell* **98**(6), 825-833.

Bentley, L., Fehrsen, J., Jordaan, F., Huismans, H., du Plessis, D. H. (2000). Identification of antigenic regions on VP2 of African horsesickness virus serotype 3 by using phage-displayed epitope libraries. *J Gen Virol* **81**(Pt 4), 993-1000.

Berman, H., Henrick, K., Nakamura, H. (2003). Announcing the worldwide Protein Data Bank. *Nat Struct Biol* **10**(12), 980.

Berman, H. M., Westbrook, J., Feng, Z., Gilliland, G., Bhat, T. N., Weissig, H., Shindyalov, I. N., Bourne, P. E. (2000). The Protein Data Bank. *Nucleic Acids Res* **28**(1), 235-242.

Bertin, A., de Frutos, M., Letellier, L. (2011). Bacteriophage-host interactions leading to genome internalization. *Curr Opin Microbiol* **14**(4), 492-496.

Beumer, J., Hannecart-Pokorni, E., and Godard, C. (1984). Bacteriophages receptors. *Bull Inst Pasteur* **82**, 173-253.

Bhattacharya, B., Noad, R. J., Roy, P. (2007). Interaction between Bluetongue virus outer capsid protein VP2 and vimentin is necessary for virus egress. *Virol J* **4**, 7.

Boisset, N., Taveau, J. C., Lamy, J., Wagenknecht, T., Radermacher, M., Frank, J. (1990). Three-dimensional reconstruction of native Androctonus australis hemocyanin. *J Mol Biol* **216**(3), 743-760.

Bottcher, B., Wynne, S. A., Crowther, R. A. (1997). Determination of the fold of the core protein of hepatitis B virus by electron cryomicroscopy. *Nature* **386**(6620), 88-91.

Boyce, M., Wehrfritz, J., Noad, R., Roy, P. (2004). Purified recombinant bluetongue virus VP1 exhibits RNA replicase activity. *J Virol* **78**(8), 3994-4002.

Brandt, S., Heikkonen, J., Engelhardt, P. (2001). Automatic alignment of transmission electron microscope tilt series without fiducial markers. *J Struct Biol* **136**(3), 201-213.

Bremer, C. W. (1976). A gel electrophoretic study of the protein and nucleic acid components of African horsesickness virus. *Onderstepoort J Vet Res* **43**(4), 193-199.

Brenner, S. and R. W. Horne (1959). A negative staining method for high resolution electron microscopy of viruses. *Biochim Biophys Acta* **34**, 103-110.

Briggs, J. A., Grünewald, K., Glass, B., Forster, F., Krausslich, H. G., Fuller, S. D. (2006). The mechanism of HIV-1 core assembly: insights from three-dimensional reconstructions of authentic virions. *Structure* **14**(1), 15-20.

Briggs, J. A., Huiskonen, J. T., Fernando, K. V., Gilbert, R. J., Scotti, P., Butcher, S. J., Fuller, S. D. (2005). Classification and three-dimensional reconstruction of unevenly distributed or symmetry mismatched features of icosahedral particles. *J Struct Biol* **150**(3), 332-339.

Briggs, J. A. and H. G. Krausslich (2011). The molecular architecture of HIV. *J Mol Biol* **410**(4), 491-500.

Briggs, J. A., Riches, J. D., Glass, B., Bartonova, V., Zanetti, G., Krausslich, H. G. (2009). Structure and assembly of immature HIV. *Proc Natl Acad Sci U S A* **106**(27), 11090-11095.

Brookes, S. M., Hyatt, A. D., Eaton, B. T. (1993). Characterization of virus inclusion bodies in bluetongue virus-infected cells. *J Gen Virol* **74 (Pt 3)**, 525-530.

Brookes, S. M., Hyatt, A. D., Eaton, B. T. (1994). The use of immuno-gold silver staining in bluetongue virus adsorption and neutralisation studies. *J Virol Methods* **46**(2), 117-132.

Bruce, E. A., Medcalf, L., Crump, C. M., Noton, S. L., Stuart, A. D., Wise, H. M., Elton, D., Bowers, K., Digard, P. (2009). Budding of filamentous and non-filamentous influenza A virus occurs via a VPS4 and VPS28-independent pathway. *Virology* **390**(2), 268-278.

Bullough, P. A., Hughson, F. M., Skehel, J. J., Wiley, D. C. (1994). Structure of influenza haemagglutinin at the pH of membrane fusion. *Nature* **371**(6492), 37-43.

Burrage, T. G. and W. W. Laegreid (1994). African horsesickness: pathogenesis and immunity. *Comp Immunol Microbiol Infect Dis* **17**(3-4), 275-285.

Burroughs, J. N., O'Hara, R. S., Smale, C. J., Hamblin, C., Walton, A., Armstrong, R., Mertens, P. P. (1994). Purification and properties of virus particles, infectious subviral particles, cores and VP7 crystals of African horsesickness virus serotype 9. *J Gen Virol* **75 (Pt 8)**, 1849-1857.

Butcher, S. J., Bamford, D. H., Fuller, S. D. (1995). DNA packaging orders the membrane of bacteriophage PRD1. *EMBO J* **14**(24), 6078-6086.

Butcher, S. J., Manole, V, Karhu, N. J. (2012). Lipid-containing viruses: bacteriophage PRD1 assembly. *Adv Exp Med Biol* **726**, 365-377.

Caldentey, J., Bamford, J. K., Bamford, D. H. (1990). Structure and assembly of bacteriophage PRD1, and Escherichia coli virus with a membrane. *J Struct Biol* **104**(1-3), 44-51.

Caldentey, J., Tuma, R., Bamford, D. H. (2000). Assembly of bacteriophage PRD1 spike complex: role of the multidomain protein P5. *Biochemistry* **39**(34), 10566-10573.

Calder, L. J., Wasilewski, S., Berriman, J. A., Rosenthal, P. B. (2010). Structural organization of a filamentous influenza A virus. *Proc Natl Acad Sci U S A* **107**(23), 10685-10690.

Cardone, G., Newcomb, W. W., Cheng, N., Wingfield, P. T., Trus, B. L., Brown, J. C., Steven, A. C. (2012). The UL36 tegument protein of Herpes Simplex Virus 1 has a Composite binding site at the capsid vertices. *J Virol* **86**(8), 4058-64.

Caspar, D. L. (1956). Structure of bushy stunt virus. *Nature* **177**(4506), 475-476.

Caspar, D. L. D., and Klug, A. (1962). Physical principles in the construction of regular viruses. *Cold Spring Harbor Symposia on Quantitative Biology*. **XXVII**.

Chang, J., Liu, X., Rochat, R. H., Baker, M. L., Chiu, W. (2012). Reconstructing virus structures from nanometer to near-atomic resolutions with cryo-electron microscopy and tomography. *Adv Exp Med Biol* **726**, 49-90.

Chang, J. T., Schmid, M. F., Haase-Pettingell, C., Weigele, P. R., King, J. A., Chiu, W. (2010). Visualizing the structural changes of bacteriophage Epsilon15 and its Salmonella host during infection. *J Mol Biol* **402**(4), 731-740.

Chang, J. T., M. F. Schmid, et al. (2007). Electron cryotomography reveals the portal in the herpesvirus capsid. J Virol **81**(4), 2065-2068.

Chen, D. H., Baker, M., L., Hyrc, C. F., DiMaio, F., Jakana, J., Wu, W., Dougherty, M., Haase-Pettingell, C., Schmid, M. F., Jiang, W., Baker, D., King, J. A., Chiu, W. (2011). Structural basis for scaffolding-mediated assembly and maturation of a dsDNA virus. *Proc Natl Acad Sci U S A* **108**(4), 1355-1360.

Chen, J. Z., Settembre, E. C., Aoki, S. T., Zhang, X., Bellamy, A. R., Dormitzer, P. R., Harrison, S. C., Grigorieff, N. (2009). Molecular interactions in rotavirus assembly and uncoating seen by high-resolution cryo-EM. *Proc Natl Acad Sci U S A* **106**(26), 10644-10648.

Cockburn, J. J., Abrescia,N. G., Grimes, J. M., Sutton, G. C., Diprose, J. M., Benevides, J. M., Thomas, G. J. Jr., Bamford, J. K., Bamford, D. H., Stuart, D. I. (2004). Membrane structure and interactions with protein and DNA in bacteriophage PRD1. *Nature* **432**(7013), 122-125.

Cockburn, J. J., Bamford, J. K., Grimes, J. M., Bamford, D. H., Stuart, D. I. (2003). Crystallization of the membrane-containing bacteriophage PRD1 in quartz capillaries by vapour diffusion. *Acta Crystallogr D Biol Crystallogr* **59**(Pt 3), 538-540.

Coetzer, J. A., and Erasmus, B. J. (1994). African horsesickness. *Infectious Disease of Livestock with Special Reference to Southern Africa*. C. R. T. J. A. Coetzer, and R. C. Tustin. Oxford, Oxford University Press. **1,** 460-475.

Conway, J. F., Cheng, N., Zlotnick, A., Wingfield, P. T., Stahl, S. J., Steven, A. C. (1997). Visualization of a 4-helix bundle in the hepatitis B virus capsid by cryo-electron microscopy. *Nature* **386**(6620), 91-94.

Crick, F. H. and J. D. Watson (1956). Structure of small viruses. *Nature* **177**(4506), 473-475.

Crowther, R. A. (1971). Procedures for three-dimensional reconstruction of spherical viruses by Fourier synthesis from electron micrographs. *Philos Trans R Soc Lond B Biol Sci* **261**(837), 221-230.

Crowther, R. A. (1971). Three-dimensional reconstruction and the architecture of spherical viruses. *Endeavour* **30**(111), 124-129.

Crowther, R. A., L. A. Amos, et al. (1970a). Three dimensional reconstructions of spherical viruses by fourier synthesis from electron micrographs. *Nature* **226**(5244), 421-425.

Crowther, R. A., DeRosier, D. J., and Klug, A. (1970b). The reconstruction of a three-dimensional structure from projections and its application to electron microscopy. *Phil Trans Roy Soc Lond A* **317**, 319-340.

D'Herelle, F. (2007). On an invisible microbe antagonistic toward dysenteric bacilli: brief note by Mr. F. D'Herelle, presented by Mr. Roux. 1917. *Res Microbiol* **158**(7), 553-554.

Dai, W., Jia, Q., Bortz, E., Shah, S., Liu, J., Atanasov, I., Li, X., Taylor, K. A., Sun, R., Zhou, Z. H. (2008). Unique structures in a tumor herpesvirus revealed by cryo-electron tomography and microscopy. *J Struct Biol* **161**(3), 428-438.

Dai, X., Zhang, L., Hong, T. (2011). Host cellular signaling induced by influenza virus. *Sci China Life Sci* **54**(1), 68-74.

Darpel, K. E., Langner, K. F., Nimtz, M., Anthony, S. J., Brownlie, J., Takamatsu, H. H., Mellor, P. S., Mertens, P. P. (2011). Saliva proteins of vector Culicoides modify structure and infectivity of bluetongue virus particles. *PLoS One* **6**(3), e17545.

de Haas, F., Paatero, A. O., Mindich, L., Bamford, D. H., Fuller, S. D. (1999). A symmetry mismatch at the site of RNA packaging in the polymerase complex of dsRNA bacteriophage phi6. *J Mol Biol* **294**(2), 357-372.

De Rosier, D. J., and Klug, A. (1968). Reconstruction of three dimensional structures from electron micrographs. *Nature* **217**, 130-134.

de Waal, P. J. and H. Huismans (2005). Characterization of the nucleic acid binding activity of inner core protein VP6 of African horse sickness virus. *Arch Virol* **150**(10), 2037-2050.

Deng, B., O'Connor, C. M., Kedes, D. H., Zhou, Z. H. (2007). Direct visualization of the putative portal in the Kaposi's sarcoma-associated herpesvirus capsid by cryoelectron tomography. *J Virol* **81**(7), 3640-3644.

Diprose, J. M., Burroughs, J. N., Sutton, G. C., Goldsmith, A., Gouet, P., Malby, R., Overton, I., Zientara, S., Mertens, P. P., Stuart, D. I., Grimes, J. M. (2001). Translocation portals for the substrates and products of a viral transcription complex: the bluetongue virus core. *EMBO J* **20**(24), 7229-7239.

Dorig, R. E., Marcil, A., Chopra, A., Richardson, C. D. (1993). The human CD46 molecule is a receptor for measles virus (Edmonston strain). *Cell* **75**(2), 295-305.

Dubochet, J., Adrian, M., Chang, J. J., Homo, J. C., Lepault, J., McDowall, A. W., Schultz, P. (1988). Cryo-electron microscopy of vitrified specimens. *Q Rev Biophys* **21**(2), 129-228.

Eichler, J. (2003). Facing extremes: archaeal surface-layer (glyco)proteins. *Microbiology* **149**(Pt 12), 3347-3351.

Erasmus, B. J. (1973). The pathogenesis of African horse sickness. *Proceedings of Third International Conference on Equine Infectious Diseases: Equine Infectious Diseases*. J. T. B. a. H. Gerber. Paris, S. Karger. **III**.

Erickson, H. P. and A. Klug (1971). Measurement and compensation of defocusing and aberrations by Fourier processing of electron micrographs. *Phil Trans Roy Soc Lond B* **261**, 105-118.

Faruqi, A. R. and S. Subramaniam (2000). CCD detectors in high-resolution biological electron microscopy. *Q Rev Biophys* **33**(1), 1-27.

Fernandez, J. J., Luque, D., Caston, J. R., Carrascosa, J. L. (2008). Sharpening high resolution information in single particle electron cryomicroscopy. *J Struct Biol* **164**(1), 170-175.

Fontana, J., Cardone, G., Heymann, J. B., Winkler, D. C., Steven, A. C. (2012). Structural changes in influenza virus at low pH characterized by cryo-electron tomography. *J Virol* **86**(6), 2919-2929.

Forzan, M., Marsh, M., Roy, P. (2007). Bluetongue virus entry into cells. *J Virol* **81**(9), 4819-4827.

Forzan, M., Wirblich, C., Roy, P. (2004). A capsid protein of nonenveloped Bluetongue virus exhibits membrane fusion activity. *Proc Natl Acad Sci U S A* **101**(7), 2100-2105.

French, T. J., Inumaru, S., Roy, P. (1989). Expression of two related nonstructural proteins of bluetongue virus (BTV) type 10 in insect cells by a recombinant baculovirus: production of polyclonal ascitic fluid and characterization of the gene product in BTV-infected BHK cells. *J Virol* **63**(8), 3270-3278.

Fu, C. Y., Wang, K., Gan, L., Lanman, J., Khayat, R., Young, M. J., Jensen, G. J., Doerschuk, P. C., Johnson, J. E. (2010). In vivo assembly of an archaeal virus studied with whole-cell electron cryotomography. *Structure* **18**(12), 1579-1586.

Fujiyoshi, Y., Kume, N. P., Sakata, K., Sato, S. B. (1994). Fine structure of influenza A virus observed by electron cryo-microscopy. *EMBO J* **13**(2), 318-326.

Fukusho, A., Ritter, G. D., Roy, P. (1987). Variation in the bluetongue virus neutralization protein VP2. *J Gen Virol* **68 (Pt 11),** 2967-2973.

Fuller, S. D., Butcher, S. J., Cheng, R. H., Baker, T. S. (1996). Three-dimensional reconstruction of icosahedral particles--the uncommon line. *J Struct Biol* **116**(1), 48-55.

Ge, P., Tsao, J., Schein, S., Green, T. J., Luo, M., Zhou, Z. H. (2010). Cryo-EM model of the bullet-shaped vesicular stomatitis virus. *Science* **327**(5966), 689-693.

Ghiasi, H., Fukusho, A., Eshita, Y., Roy, P. (1987). Identification and characterization of conserved and variable regions in the neutralization VP2 gene of bluetongue virus. *Virology* **160**(1), 100-109.

Gibbens, N. (2012). Schmallenberg virus: a novel viral disease in northern Europe. *Vet Rec* **170**(2), 58.

Goddard, T. D., Huang, C. C., Ferrin, T. E. (2007). Visualizing density maps with UCSF Chimera. *J Struct Biol* **157**(1), 281-287.

Gonen, T., Cheng, Y., Sliz, P., Hiroaki, Y., Fujiyoshi, Y., Harrison, S. C., Walz, T. (2005). Lipid-protein interactions in double-layered two-dimensional AQP0 crystals. *Nature* **438**(7068), 633-638.

Gouet, P., Diprose, J. M., Grimes, J. M., Malby, R., Burroughs, J. N., Zientara, S., Stuart, D. I., Mertens, P. P. (1999). The highly ordered double-stranded RNA genome of bluetongue virus revealed by crystallography. *Cell* **97**(4), 481-490.

Gould, E. A. and S. Higgs (2009). Impact of climate change and other factors on emerging arbovirus diseases. *Trans R Soc Trop Med Hyg* **103**(2), 109-121.

Gowen, B., Bamford, J. K., Bamford, D. H., Fuller, S. D. (2003). The tailless icosahedral membrane virus PRD1 localizes the proteins involved in genome packaging and injection at a unique vertex. *J Virol* **77**(14), 7863-7871.

Grahn, A. M., Caldentey, J., Bamford, J. K., Bamford, D. H. (1999). Stable packaging of phage PRD1 DNA requires adsorption protein P2, which binds to the IncP plasmid-encoded conjugative transfer complex. *J Bacteriol* **181**(21), 6689-6696.

Grahn, A. M., Daugelavicius, R., Bamford, D. H. (2002a). Sequential model of phage PRD1 DNA delivery: active involvement of the viral membrane. *Mol Microbiol* **46**(5), 1199-1209.

Grahn, A. M., Daugelavicius, R., Bamford, D. H. (2002b). The small viral membrane-associated protein P32 is involved in bacteriophage PRD1 DNA entry. *J Virol* **76**(10), 4866-4872.

Grimes, J. M., Burroughs, J. N., Gouet, P., Diprose, J. M., Malby, R., Zientara, S., Mertens, P. P., Stuart, D. I. (1998). The atomic structure of the bluetongue virus core. *Nature* **395**(6701), 470-478.

Grubman, M. J. and S. A. Lewis (1992). Identification and characterization of the structural and nonstructural proteins of African horsesickness virus and determination of the genome coding assignments. *Virology* **186**(2), 444-451.

Grünewald, K., Desai, P., Winkler, D. C., Heymann, J. B., Belnap, D. M., Baumeister, W., Steven, A. C. (2003). Three-dimensional structure of herpes simplex virus from cryo-electron tomography. *Science* **302**(5649), 1396-1398.

Grünewald, K., Medalia, O., Gross, A., Steven, A. C., Baumeister, W. (2003). Prospects of electron cryotomography to visualize macromolecular complexes inside cellular compartments: implications of crowding. *Biophys Chem* **100**(1-3), 577-591.

Hadfield, A. T., Lee, W., Zhao, R., Oliveira, M. A., Minor, I., Rueckert, R. R., Rossmann, M. G. (1997). The refined structure of human rhinovirus 16 at 2.15 Å resolution: implications for the viral life cycle. *Structure* **5**(3), 427-441.

Hänninen, A. L., Bamford, D. H., Bamford, J. K. (1997). Probing phage PRD1-specific proteins with monoclonal and polyclonal antibodies. *Virology* **227**(1), 198-206.

Happonen, L. J., Redder, P., Peng, X., Reigstad, L. J., Prangishvili, D., Butcher, S. J. (2010). Familial relationships in hyperthermo- and acidophilic archaeal viruses. *J Virol* **84**(9), 4747-4754.

Haring, M., Rachel, R., Peng, X., Garrett, R. A., Prangishvili, D. (2005). Viral diversity in hot springs of Pozzuoli, Italy, and characterization of a unique archaeal virus, Acidianus bottle-shaped virus, from a new family, the Ampullaviridae. *J Virol* **79**(15), 9904-9911.

Haring, M., Vestergaard, G., Brugger, K., Rachel, R., Garrett, R. A., Prangishvili, D. (2005). Structure and genome organization of AFV2, a novel archaeal lipothrixvirus with unusual terminal and core structures. *J Bacteriol* **187**(11), 3855-3858.

Harris, A., Borgnia, M. J., Shi, D., Bartesaghi, A., He, H., Pejchal, R., Kang, Y. K., Depetris, R., Marozsan, A. J., Sanders, R. W., Klasse, P. J., Milne, J. L., Wilson, I. A., Olson, W. C., Moore, J. P., Subramaniam, S. (2011). Trimeric HIV-1 glycoprotein gp140 immunogens and native HIV-1 envelope glycoproteins display the same closed and open quaternary molecular architectures. *Proc Natl Acad Sci U S A* **108**(28), 11440-11445.

Harris, A., Cardone, G., Winkler, D. C., Heymann, J. B., Brecher, M., White, J. M., Steven, A. C. (2006). Influenza virus pleiomorphy characterized by cryoelectron tomography. *Proc Natl Acad Sci U S A* **103**(50), 19123-19127.

Harris, J. R. and D. Scheffler (2002). Routine preparation of air-dried negatively stained and unstained specimens on holey carbon support films: a review of applications. *Micron* **33**(5), 461-480.

Hashiguchi, T., Ose, T., Kubota, M., Maita, N., Kamishikiryo, J., Maenaka, K., Yanagi, Y. (2011). Structure of the measles virus hemagglutinin bound to its cellular receptor SLAM. *Nat Struct Mol Biol* **18**(2), 135-141.

Hassan, S. H., Wirblich, C., Forzan, M., Roy, P. (2001). Expression and functional characterization of bluetongue virus VP5 protein: role in cellular permeabilization. *J Virol* **75**(18), 8356-8367.

Hayward, S. B. and R. M. Glaeser (1979). Radiation damage of purple membrane at low temperature. *Ultramicroscopy* **04**(2), 201-210.

Hewat, E. A., Booth, T. F., Loudon, P. T., Roy, P. (1992). Structure of bluetongue virus particles by cryoelectron microscopy. *J Struct Biol* **109**(1), 61-69.

Hogle, J. M., Chow, M., Filman, D. J. (1985). Three-dimensional structure of poliovirus at 2.9 Å resolution. *Science* **229**(4720), 1358-1365.

Horne, P., and R. W. Wildy (1961). Symmetry in virus architecture. *Virology* **15**, 348-373.

Horne, R. W. and I. P. Ronchetti (1974). A negative staining-carbon film technique for studying viruses in the electron microscope. I. Preparative procedures for examining icosahedral and filamentous viruses. *J Ultrastruct Res* **47**(3), 361-383.

Hosokawa, F., Tomita, T., Naruse, M., Honda, T., Hartel, P., Haider, M. (2003). A spherical aberration-corrected 200 kV TEM. *J Electron Micros*c (Tokyo) **52**(1), 3-10.

Howell, P. G. (1962). The isolation and identification of further antigenic types of African horsesickness virus. *Onderstepoort J Vet Res* **29**, 139-149.

Huiskonen, J. T., Jäälinoja, H. T., Briggs, J. A., Fuller, S. D., Butcher, S. J. (2007). Structure of a hexameric RNA packaging motor in a viral polymerase complex. *J Struct Biol* **158**(2), 156-164.

Huiskonen, J. T., Laakkonen, L., Toropainen, M., Sarvas, M., Bamford, D. H., Bamford, J. K. (2003). Probing the ability of the coat and vertex protein of the membrane-containing bacteriophage PRD1 to display a meningococcal epitope. *Virology* **310**(2), 267-279.

Huiskonen, J. T., Manole, V., Butcher, S. J. (2007). Tale of two spikes in bacteriophage PRD1. *Proc Natl Acad Sci U S A* **104**(16), 6666-6671.

Huismans, H. and B. J. Erasmus (1981). Identification of the serotype-specific and group-specific antigens of bluetongue virus. *Onderstepoort J Vet Res* **48**(2), 51-58.

Hyatt, A. D., Zhao, Y., Roy, P. (1993). Release of bluetongue virus-like particles from insect cells is mediated by BTV nonstructural protein NS3/NS3A. *Virology* **193**(2), 592-603.

Ibiricu, I., Huiskonen, J. T., Dohner, K., Bradke, F., Sodeik, B., Grünewald, K. (2011). Cryo electron tomography of Herpes Simplex Virus during axonal transport and secondary envelopment in primary neurons. *PLoS Pathog* **7**(12), e1002406.

Jaatinen, S. T., Viitanen, S. J., Bamford, D. H., Bamford, J. K. (2004). Integral membrane protein P16 of bacteriophage PRD1 stabilizes the adsorption vertex structure. *J Virol* **78**(18), 9790-9797.

Jensen, M. R., Communie, G., Ribeiro, E. A. Jr., Martinez, N., Desfosses, A., Salmon, L., Mollica, L., Gabel, F., Jamin, M., Longhi, S., Ruigrok, R. W., Blackledge, M. (2011). Intrinsic disorder in measles virus nucleocapsids. *Proc Natl Acad Sci U S A* **108**(24), 9839-9844.

Jiang, W., Baker, M. L., Jakana, J., Weigele, P. R., King, J., Chiu, W. (2008). Backbone structure of the infectious epsilon15 virus capsid revealed by electron cryomicroscopy. *Nature* **451**(7182), 1130-1134.

Juez, G., Rodriguez-Valera, F., Ventosa, A., Kushner, D. J. (1986). Haloarcula hispanica spec. nov. and Haloferax gibbonsii spec. nov., two new species of extremely halophilic archaebacteria. *System Appl Microbiol* **8**, 75-79.

Jäälinoja, H. T., Roine, E., Laurinmäki, P., Kivelä, H. M., Bamford, D. H., Butcher, S. J. (2008). Structure and host-cell interaction of SH1, a membrane-containing, halophilic euryarchaeal virus. *Proc Natl Acad Sci U S A* **105**(23), 8008-8013.

Kar, A. K. and P. Roy (2003). Defining the structure-function relationships of bluetongue virus helicase protein VP6. *J Virol* **77**(21), 11347-11356.

Kim, H. S., Huang, E., Desai, J., Sole, M., Pryce, E. N., Okoye, M. E., Person, S., Desai, P. J. (2011). A domain in the herpes simplex virus 1 triplex protein VP23 is essential for closure of capsid shells into icosahedral structures. *J Virol* **85**(23), 12698-12707.

Kivioja, T., Ravantti, J., Verkhovsky, A., Ukkonen, E., Bamford, D. H. (2000). Local average intensity-based method for identifying spherical particles in electron micrographs. *J Struct Biol* **131**(2), 126-134.

Klug, A., and D.L.D Caspar (1960). The structure of small viruses. *Advances in Virus Research* **7,** 225-325.

Kruger, D. H., Schneck, P., Gelderblom, H. R. (2000). Helmut Ruska and the visualisation of viruses. *Lancet* **355**(9216), 1713-1717.

Kuhn, R. J., Zhang, W., Rossmann, M. G., Pletnev, S. V., Corver, J., Lenches, E., Jones, C. T., Mukhopadhyay, S., Chipman, P. R., Strauss, E. G., Baker, T. S., Strauss, J. H. (2002). Structure of dengue virus: implications for flavivirus organization, maturation, and fusion. *Cell* **108**(5), 717-725.

Kukura, P., Ewers, H., Muller, C., Renn, A., Helenius, A., Sandoghdar, V. (2009). High-speed nanoscopic tracking of the position and orientation of a single virus. *Nat Methods* **6**(12), 923-927.

Kunding, A. H., Mortensen, M. W., Christensen, S. M., Bhatia, V. K., Makarov, I., Metzler, R., Stamou, D. (2011). Intermembrane docking reactions are regulated by membrane curvature. *Biophys J* **101**(11), 2693-2703.

Kuo, I. A. and R. M. Glaeser (1975). Development of methodology for low exposure, high resolution electron microscopy of biological specimens. *Ultramicroscopy* **1**(1), 53-66.

Lander, G. C., Khayat, R., Li, R., Prevelige, P. E., Potter, C. S., Carragher, B., Johnson, J. E. (2009). The P22 tail machine at subnanometer resolution reveals the architecture of an infection conduit. *Structure* **17**(6), 789-799.

Lee, K. K. (2010). Architecture of a nascent viral fusion pore. *EMBO J* **29**(7), 1299-1311.

Leiman, P. G., Arisaka, F., van Raaij, M. J., Kostyuchenko, V. A., Aksyuk, A. A., Kanamaru, S., Rossmann, M. G. (2010). Morphogenesis of the T4 tail and tail fibers. *Virol J* **7**, 355.

Lentz, T. L. (1990). The recognition event between virus and host cell receptor: a target for antiviral agents. *J Gen Virol* **71 (Pt 4),** 751-766.

Li, L., Lok, S. M., Yu, I. M., Zhang, Y., Kuhn, R. J., Chen, J., Rossmann, M. G. (2008). The flavivirus precursor membrane-envelope protein complex: structure and maturation. *Science* **319**(5871), 1830-1834.

Liddington, R. C., Yan, Y., Moulai, J., Sahli, R., Benjamin, T. L., Harrison, S. C. (1991). Structure of simian virus 40 at 3.8-Å resolution. *Nature* **354**(6351), 278-284.

Liljeroos, L., Huiskonen, J. T., Ora, A., Susi, P., Butcher, S. J. (2011). Electron cryotomography of measles virus reveals how matrix protein coats the ribonucleocapsid within intact virions. *Proc Natl Acad Sci U S A* **108**(44), 18085-18090.

Liu, H., Jin, L., Koh, S. B., Atanasov, I., Schein, S., Wu, L., Zhou, Z. H. (2010). Atomic structure of human adenovirus by cryo-EM reveals interactions among protein networks. *Science* **329**(5995), 1038-1043.

Liu, J., Bartesaghi, A., Borhnia, M. J., Sapiro, G., Subramaniam, S. (2008). Molecular architecture of native HIV-1 gp120 trimers. *Nature* **455**(7209), 109-113.

Liu, J., Wright, E. R., Winkler, H. (2010). 3D visualization of HIV virions by cryoelectron tomography. *Methods Enzymol* **483**, 267-290.
Liu, X., Jiang, W., Jakana, J., Chiu, W. (2007). Averaging tens to hundreds of icosahedral particle images to resolve protein secondary structure elements using a Multi-Path Simulated Annealing optimization algorithm. *J Struct Biol* **160**(1), 11-27.
Liu, X., Zhang, Q., Murata, K., Baker, M. L., Sullivan, M. B., Fu, C., Dougherty, M. T., Schmid, M. F., Osburne, M. S., Chisholm, S. W., Chiu, W. (2010). Structural changes in a marine podovirus associated with release of its genome into Prochlorococcus. *Nat Struct Mol Biol* **17**(7), 830-836.
Liu, Y., Penczek, P. A., McEwen, B. F., Frank, J. (1995). A marker-free alignment method for electron tomography. *Ultramicroscopy* **58**(3-4), 393-402.
Lo, P., Yu, X., Atanasov, I., Chandran, B., Zhou, Z. H. (2003). Three-dimensional localization of pORF65 in Kaposi's sarcoma-associated herpesvirus capsid. *J Virol* **77**(7), 4291-4297.
Loney, C., Mottet-Osman, G., Roux, L., Bhella, D. (2009). Paramyxovirus ultrastructure and genome packaging: cryo-electron tomography of sendai virus. *J Virol* **83**(16), 8191-8197.
Lupas, A., Van Dyke, M., Stock, J. (1991). Predicting coiled coils from protein sequences. *Science* **252**(5009), 1162-1164.
Lymperopoulos, K., Wirblich, C., Brierley, I., Roy, P. (2003). Sequence specificity in the interaction of Bluetongue virus non-structural protein 2 (NS2) with viral RNA. *J Biol Chem* **278**(34), 31722-31730.
Macpherson, I. (1963). Characteristics of a hamster cell clone transformed by polyoma virus. *J Natl Cancer Inst* **30**, 795-815.
Mancini, E. J., Clarke, M., Gowen, B. E., Rutten, T., Fuller, S. D. (2000). Cryo-electron microscopy reveals the functional organization of an enveloped virus, Semliki Forest virus. *Mol Cell* **5**(2), 255-266.
Manole, V., Laurinmäki, P., Van Wyngaardt, W., Potgieter, C. A., Wright, I. M., Venter, G. J., van Dijk, A. A., Sewell, B. T., Butcher, S. J. (2012). Structural insight into African horsesickness virus infection. *J Virol* **86**(15), 7858-66.
Marchi, P. R., Rawlings, P., Burroughs, J. N., Wellby, M., Mertens, P. P., Mellor, P. S., Wade-Evans, A. M. (1995). Proteolytic cleavage of VP2, an outer capsid protein of African horse sickness virus, by species-specific serum proteases enhances infectivity in Culicoides. *J Gen Virol* **76 (Pt 10)**, 2607-2611.
Maree, F. F. and H. Huismans (1997). Characterization of tubular structures composed of nonstructural protein NS1 of African horsesickness virus expressed in insect cells. *J Gen Virol* **78 (Pt 5)**, 1077-1082.
Marinescu, D. C., Ji, Y. (2003). A computational framework for the 3D structure determination of viruses with unknown symmetry. *J. Parallel Distrib. Comput.* **63**, 738-758.
Martinez-Costas, Sutton, G., Ramadevi, N., Roy, P. (1998). Guanylyltransferase and RNA 5'-triphosphatase activities of the purified expressed VP4 protein of bluetongue virus. *J Mol Biol* **280**(5), 859-866.
Martinez-Torrecuadrada, J. L. and J. I. Casal (1995). Identification of a linear neutralization domain in the protein VP2 of African horse sickness virus. *Virology* **210**(2), 391-399.
Martinez-Torrecuadrada, J. L., Diaz-Laviada, M., Roy, P., Sanchez, C., Vela, C., Sanchez-Vizcaino, J. M., Casal, J. I. (1997). Serologic markers in early stages of African horse sickness virus infection. *J Clin Microbiol* **35**(2), 531-535.
Masich, S., Ostberg, T., Norlen, L., Shupliakov, O., Daneholt, B. (2006). A procedure to deposit fiducial markers on vitreous cryo-sections for cellular tomography. *J Struct Biol* **156**(3), 461-468.
Mastronarde, D. N. (2005). Automated electron microscope tomography using robust prediction of specimen movements. *J Struct Biol* **152**(1), 36-51.
Matsuo, E., Celma, C. C., Roy, P. (2010). A reverse genetics system of African horsesickness virus reveals existence of primary replication. *FEBS Lett* **584**(15), 3386-3391.
Matthews, B. W. (2007). Protein Structure Initiative: getting into gear. *Nat Struct Mol Biol* **14**(6), 459-460.
Meiring, T. L., Huismans, H., van Staden, V. (2009). Genome segment reassortment identifies non-structural protein NS3 as a key protein in African horsesickness virus release and alteration of membrane permeability. *Arch Virol* **154**(2), 263-271.

Mellor, P. S. (1992). Culicoides as potential orbivirus vectors in Europe. *Bluetongue, African horsesickness, and related orbiviruses*. E. W. a. B. I. Osburn. Boca Raton, CRC Press Inc.**,** 278-283.

Mellor, P. S., Boorman, J., Baylis, M. (2000). Culicoides biting midges: their role as arbovirus vectors. *Annu Rev Entomol* **45**, 307-340.

Mellor, P. S. and C. Hamblin (2004). African horse sickness. *Vet Res* **35**(4), 445-466.

Merckel, M. C., Huiskonen, J. T., Bamford, D. H., Goldman, A., Tuma, R. (2005). The structure of the bacteriophage PRD1 spike sheds light on the evolution of viral capsid architecture. *Mol Cell* **18**(2), 161-170.

Mesyanzhinov, V. V. (2004). Bacteriophage T4: structure, assembly, and initiation infection studied in three dimensions. *Adv Virus Res* **63**, 287-352.

Mesyanzhinov, V. V., Leiman, P. G., Kostyuchenko, V. A., Kurochkina, L. P., Miroshnikov, K. A., Sykilinda, N. N., Shneider, M. M. (2004). Molecular architecture of bacteriophage T4. *Biochemistry (Mosc)* **69**(11), 1190-1202.

Mindell, J. A. and N. Grigorieff (2003). Accurate determination of local defocus and specimen tilt in electron microscopy. *J Struct Biol* **142**(3), 334-347.

Mindich, L., Bamford, D. H., McGraw, T., Mackenzie, G. (1982a). Assembly of bacteriophage PRD1: particle formation with wild-type and mutant viruses. *J Virol* **44**(3), 1021-1030.

Mindich, L., Bamford, D. H., Goldthwaite, C., Laverty, M., Mackenzie, G. (1982b)."Isolation of nonsense mutants of lipid-containing bacteriophage PRD1. *J Virol* **44**(3), 1013-1020.

Mizukoshi, N., Sakamoto, K., Iwata, A., Tsuchiya, T., Ueda, S., Apiwatnakorn, B., Kamada, M., Fukusho, A. (1993). The complete nucleotide sequence of African horsesickness virus serotype 4 (vaccine strain) segment 4, which encodes the minor core protein VP4. *Virus Res* **28**(3), 299-306.

Modis, Y., Trus, B. L., Harrison, S. C. (2002). Atomic model of the papillomavirus capsid. *EMBO J* **21**(18), 4754-4762.

Morton, V. L., Dykeman, E. C., Stonehouse, N. J., Ashcroft, A. E., Twarock, R., Stockley, P. G. (2010). The impact of viral RNA on assembly pathway selection. *J Mol Biol* **401**(2), 298-308.

Muhlebach, M. D., Mateo, M., Sinn, P. L., Prufer, S., Uhlig, K. M., Leonard, V. H., Navaratnarajah, C. K., Frenzke, M., Wong, X. X., Sawatsky, B., Ramachandran, S., McCray, P. B. Jr., Cichutek, K., von Messling, V., Lopez, M., Cattaneo, R. (2011). Adherens junction protein nectin-4 is the epithelial receptor for measles virus. *Nature* **480**(7378), 530-533.

Murata, K., Liu, X., Danev, R., Jakana, J., Schmid, M. F., King, J., Nagayama, K., Chiu, W. (2010). Zernike phase contrast cryo-electron microscopy and tomography for structure determination at nanometer and subnanometer resolutions. *Structure* **18**(8), 903-912.

Nason, E. L., Rothagel, R., Mukherjee, S. K., Kar, A. K., Forzan, M., Prasad, B. V., Roy, P. (2004). Interactions between the inner and outer capsids of bluetongue virus. *J Virol* **78**(15), 8059-8067.

Newcomb, W. W. and J. C. Brown (2010). Structure and capsid association of the herpesvirus large tegument protein UL36. *J Virol* **84**(18), 9408-9414.

Noyce, R. S., Bondre, D. G., Ha, M. N., Lin, L. T., Sisson, G., Tsao, M. S., Richardson, C. D. (2011). Tumor cell marker PVRL4 (nectin 4) is an epithelial cell receptor for measles virus. *PLoS Pathog* **7**(8), e1002240.

Oellermann, R. A. (1970). Plaque formation by African horsesickness virus and characterization of its RNA. Onderstepoort J Vet Res **37**(2), 137-143.

Ojala, P. M., Sodeik, B., Ebersold, M. W., Kutay, U., Helenius, A. (2000). Herpes simplex virus type 1 entry into host cells: reconstitution of capsid binding and uncoating at the nuclear pore complex in vitro. *Mol Cell Biol* **20**(13), 4922-4931.

Orlova, E. V., Dube, P., Beckmann, E., Zemlin, F., Lurz, R., Trautner, T. A., Tavares, P., van Heel, M. (1999). Structure of the 13-fold symmetric portal protein of bacteriophage SPP1. *Nat Struct Biol* **6**(9), 842-846.

Orlova, E. V., Gowen, B., Droge, A., Stiege, A., Weise, F., Lurz, R., van Heel, M., Tavares, P. (2003). Structure of a viral DNA gatekeeper at 10 Å resolution by cryo-electron microscopy. *EMBO J* **22**(6), 1255-1262.

Orlova, E. V. and H. R. Saibil (2004). Structure determination of macromolecular assemblies by single-particle analysis of cryo-electron micrographs. *Curr Opin Struct Biol* **14**(5), 584-590.

Pagaling, E., Haigh, R. D., Grant, W. D., Cowan, D. A., Jones, B. E., Ma, Y., Ventosa, A., Heaphy, S. (2007). Sequence analysis of an Archaeal virus isolated from a hypersaline lake in Inner Mongolia, China. *BMC Genomics* **8,** 410.

Parent, K. N., Khayat, R., Tu, L. H., Suhanovsky, M. M., Cortines, J. R., Tesche, C. M., Johnson, J. E., Baker, T. S. (2010). P22 coat protein structures reveal a novel mechanism for capsid maturation: stability without auxiliary proteins or chemical crosslinks. *Structure* **18**(3), 390-401.

Paweska, J. T., Venter, G. J., Mellor, P. S. (2002). Vector competence of South African Culicoides species for bluetongue virus serotype 1 (BTV-1) with special reference to the effect of temperature on the rate of virus replication in C. imicola and C. bolitinos. *Med Vet Entomol* **16**(1), 10-21.

Pedgley, D. E. and M. R. Tucker (1977). Possible spread of African horse sickness on the wind. *J Hyg (Lond)* **79**(2), 279-298.

Peng, L., Ryazantsev, S., Sun, R., Zhou, Z. H. (2010). Three-dimensional visualization of gammaherpesvirus life cycle in host cells by electron tomography. *Structure* **18**(1), 47-58.

Pepin, K. M., Domsic, J., McKenna, R. (2008). Genomic evolution in a virus under specific selection for host recognition. *Infect Genet Evol* **8**(6), 825-834.

Pettersen, E. F., Goddard, T. D., Huang, C. C., Couch, G. S., Greenblatt, D. M., Meng, E. C., Ferrin, T. E. (2004). UCSF Chimera--a visualization system for exploratory research and analysis. *J Comput Chem* **25**(13), 1605-1612.

Pietilä, M. K., Atanasova, N. S., Manole, V., Liljeroos, L., Butcher, S. J., Oksanen, H. M., Bamford, D. H. (2012). Virion architecture unifies globally distributed pleolipoviruses infecting halophilic archaea. *J Virol* **86**(9), 5067-5079.

Pietilä, M. K., Laurinavicius, S., Sund, J., Roine, E., Bamford, D. H. (2010). The single-stranded DNA genome of novel archaeal virus halorubrum pleomorphic virus 1 is enclosed in the envelope decorated with glycoprotein spikes. *J Virol* **84**(2), 788-798.

Pietilä, M. K., Roine, E., Paulin, L., Kalkkinen, N., Bamford, D. H. (2009). An ssDNA virus infecting archaea: a new lineage of viruses with a membrane envelope. *Mol Microbiol* **72**(2), 307-319.

Pohl, C., Duprex, W. P., Krohne, G., Rima, B. K., Schneider-Schaulies, S. (2007). Measles virus M and F proteins associate with detergent-resistant membrane fractions and promote formation of virus-like particles. *J Gen Virol* **88**(Pt 4), 1243-1250.

Polson, A. and D. Deeks (1963). Electron microscopy of neurotropic African horse-sickness virus. *J Hyg (Lond)* **61**, 149-153.

Pope, W. H., Weigele, P. R., Chang, J., Pedulla, M. L., Ford, M. E., Houtz, J. M., Jiang, W., Chiu, W., Hatfull, G. F., Hendrix, R. W., King, J. (2007). Genome sequence, structural proteins, and capsid organization of the cyanophage Syn5: a "horned" bacteriophage of marine synechococcus. *J Mol Biol* **368**(4), 966-981.

Potgieter, A. C., Page, N. A., Liebenberg, L., Wright, I. M., Landt, O., van Dijk, A. A. (2009). Improved strategies for sequence-independent amplification and sequencing of viral double-stranded RNA genomes. *J Gen Virol* **90**(Pt 6), 1423-1432.

Prangishvili, D., Arnold, H. P., Gotz, D., Ziese, U., Holz, I., Kristjansson, J. K., Zillig, W. (1999). A novel virus family, the Rudiviridae: Structure, virus-host interactions and genome variability of the sulfolobus viruses SIRV1 and SIRV2. *Genetics* **152**(4), 1387-1396.

Prangishvili, D., Vestergaard, G., Haring, M., Aramayo, R., Basta, T., Rachel, R., Garett, R. A. (2006). Structural and genomic properties of the hyperthermophilic archaeal virus ATV with an extracellular stage of the reproductive cycle. *J Mol Biol* **359**(5), 1203-1216.

Prasad, B. V.,Rothnagel, R., Zeng, C. Q., Jakana, J., Lawton, J. A., Chiu, W., Estes, M. K. (1996). Visualization of ordered genomic RNA and localization of transcriptional complexes in rotavirus. *Nature* **382**(6590), 471-473.

Quax, T. E., Krupovic, M., Lucas, S., Forterre, P., Prangishvili, D. (2010). The Sulfolobus rod-shaped virus 2 encodes a prominent structural component of the unique virion release system in Archaea. *Virology* **404**(1), 1-4.

Quax, T. E., Lucas, S., Reimann, J., Pehau-Arnaudet, G., Prevost, M. C., Forterre, P., Albers, S. V., Prangishvili, D. (2011). Simple and elegant design of a virion egress structure in Archaea. *Proc Natl Acad Sci U S A* **108**(8), 3354-3359.

Quiberoni, A., Stiefel, J. I., Reinheimer, J. A. (2000). Characterization of phage receptors in Streptococcus thermophilus using purified cell walls obtained by a simple protocol. *J Appl Microbiol* **89**(6), 1059-1065.

Radermacher, M. (1988). Three-dimensional reconstruction of single particles from random and nonrandom tilt series. *J Electron Microsc Tech* **9**(4), 359-394.

Ramadevi, N., Burroughs, N. J., Mertens, P. P., Jones, I. M., Roy, P. (1998a). Capping and methylation of mRNA by purified recombinant VP4 protein of bluetongue virus. *Proc Natl Acad Sci U S A* **95**(23), 13537-13542.

Ramadevi, N. and P. Roy (1998b). Bluetongue virus core protein VP4 has nucleoside triphosphate phosphohydrolase activity. *J Gen Virol* **79 (Pt 10),** 2475-2480.

Ramadevi, N., Rodriguez, J., Roy, P. (1998c). A leucine zipper-like domain is essential for dimerization and encapsidation of bluetongue virus nucleocapsid protein VP4. *J Virol* **72**(4), 2983-2990.

Ramos, I. and A. Fernandez-Sesma (2012). Cell receptors for influenza a viruses and the innate immune response. *Front Microbiol* **3**, 117.

Rayment, I., Baker, T. S., Caspar, D. L., Murakamai, W. T. (1982). Polyoma virus capsid structure at 22.5 Å resolution. *Nature* **295**(5845), 110-115.

Reddy, V. S., Natchiar, S. K., Stewart, P. L., Nemerow, G. R. (2010). Crystal structure of human adenovirus at 3.5 Å resolution. *Science* **329**(5995), 1071-1075.

Reinisch, K. M., Nibert, M. L., Harrison, S. C. (2000). Structure of the reovirus core at 3.6 Å resolution. *Nature* **404**(6781), 960-967.

Rice, G., Tang, L., Stedman, K., Roberto, F., Spuhler, J., Gillitzer, E., Johnson, J. E., Douglas, T., Young, M. (2004). The structure of a thermophilic archaeal virus shows a double-stranded DNA viral capsid type that spans all domains of life. *Proc Natl Acad Sci U S A* **101**(20), 7716-7720.

Riedl, P., Moll, M., Klenk, H. D., Maisner, A. (2002). Measles virus matrix protein is not cotransported with the viral glycoproteins but requires virus infection for efficient surface targeting. *Virus Res* **83**(1-2), 1-12.

Rochat, R. H., Liu, X., Murata, K., Nagayama, K., Rixon, F. J., Chiu, W.(2011). Seeing the portal in herpes simplex virus type 1 B capsids. *J Virol* **85**(4), 1871-1874.

Rogers, G. N. and J. C. Paulson (1983). Receptor determinants of human and animal influenza virus isolates: differences in receptor specificity of the H3 hemagglutinin based on species of origin. *Virology* **127**(2), 361-373.

Roine, E., Kukkaro, P., Paulin, L., Laurinavicius, S., Domanska, A., Somerharju, P., Bamford, D. H. (2010). New, closely related haloarchaeal viral elements with different nucleic Acid types. *J Virol* **84**(7), 3682-3689.

Rolfsson, O., Toropova, K., Ranson, N. A., Stockley, P. G. (2010). Mutually-induced conformational switching of RNA and coat protein underpins efficient assembly of a viral capsid. *J Mol Biol* **401**(2), 309-22.

Rosenthal, P. B. and R. Henderson (2003). Optimal determination of particle orientation, absolute hand, and contrast loss in single-particle electron cryomicroscopy. *J Mol Biol* **333**(4), 721-745.

Rossman, J. S. and R. A. Lamb (2011). Influenza virus assembly and budding. *Virology* **411**(2), 229-236.

Roy, A., Kucukural, A., Zhang, Y. (2010). I-TASSER: a unified platform for automated protein structure and function prediction. *Nat Protoc* **5**(4), 725-738.

Roy, P. (2005). Bluetongue virus proteins and particles and their role in virus entry, assembly, and release. *Adv Virus Res* **64**, 69-123.

Roy, P. (2008). Functional mapping of bluetongue virus proteins and their interactions with host proteins during virus replication. *Cell Biochem Biophys* **50**(3), 143-157.

Rydman, P. S., Bamford, J. K., Bamford, D. H. (2001). A minor capsid protein P30 is essential for bacteriophage PRD1 capsid assembly. *J Mol Biol* **313**(4), 785-795.

Rydman, P. S., Caldentey, J., Butcher, S. J., Fuller, S. D., Rutten, T., Bamford, D. H. (1999). Bacteriophage PRD1 contains a labile receptor-binding structure at each vertex. *J Mol Biol* **291**(3), 575-587.

Sachse, C., Chen, J. Z., Coureux, P. D., Stroupe, M. E., Fandrich, M., Grigorieff, N. (2007). High-resolution electron microscopy of helical specimens: a fresh look at tobacco mosaic virus. *J Mol Biol* **371**(3), 812-835.

San Martin, C., Burnett, R. M., de Haas, F., Heinkel, R., Rutten, T., Fuller, S. D., Butcher, S. J., Bamford, D. H. (2001). Combined EM/X-ray imaging yields a quasi-atomic model of the adenovirus-related bacteriophage PRD1 and shows key capsid and membrane interactions. *Structure* **9**(10), 917-930.

San Martin, C., Huiskonen, J. T., Bamford, J. K., Butcher, S. J., Fuller, S. D., Bamford, D. H., Burnett, R. M. (2002). Minor proteins, mobile arms and membrane-capsid interactions in the bacteriophage PRD1 capsid. *Nat Struct Biol* **9**(10), 756-763.

Sanz-Garcia, E., Stewart, A. B., Belnap, D. M. (2010). The random-model method enables ab initio 3D reconstruction of asymmetric particles and determination of particle symmetry. *J Struct Biol* **171**(2), 216-222.

Schief, W. R., Ban, Y. E., Stamatatos, L. (2009). Challenges for structure-based HIV vaccine design. *Curr Opin HIV AIDS* **4**(5), 431-440.

Schmid, M. F. (2011). Single-particle electron cryotomography (cryoET). *Adv Protein Chem Struct Biol* **82**, 37-65.

Schoehn, G., Moss, S. R., Nuttall, P. A., Hewat, E. A. (1997). Structure of Broadhaven virus by cryoelectron microscopy: correlation of structural and antigenic properties of Broadhaven virus and bluetongue virus outer capsid proteins. *Virology* **235**(2), 191-200.

Schroder, R. R. (1992). Zero-loss energy-filtered imaging of frozen-hydrated proteins: model calculations and implications for future developments. *J Microsc* **166**(Pt 3), 389-400.

Schwede, T., Kopp, J., Guex, N., Peitsch, M. C. (2003). SWISS-MODEL: An automated protein homology-modeling server. *Nucleic Acids Res* **31**(13), 3381-3385.

Seitsonen, J., Susi, P., Heikkilä, O., Sinkovits, R. S., Laurinmäki, P., Hyypiä, T., Butcher, S. J. (2010). Interaction of alphaVbeta3 and alphaVbeta6 integrins with human parechovirus 1. *J Virol* **84**(17), 8509-8519.

Sellers, R. F. (1980). Weather, host and vector--their interplay in the spread of insect-borne animal virus diseases. *J Hyg (Lond)* **85**(1), 65-102.

Sencilo, A., Paulin, L., Kellner, S., Helm, M., Roine, E. (2012). Related haloarchaeal pleomorphic viruses contain different genome types. *Nucleic Acids Res* **40**(12), 5523-5534.

Settembre, E. C., Chen, J. Z., Dormitzer, P. R., Grigorieff, N., Harrison, S. C. (2011). Atomic model of an infectious rotavirus particle. *EMBO J* **30**(2), 408-416.

Siegel, B. M. (1971). Current and future prospects in electron microscopy for observations in biomolecular structure. *Philos Trans R Soc Lond B Biol Sci* **261**(837), 5-14.

Slenning, B. D. (2010). Global climate change and implications for disease emergence. *Vet Pathol* **47**(1), 28-33.

Sokolova, A., Malfois, M., Caldentey, J., Svergun, D. I., Koch, M. H., Bamford, D. H., Tuma, R. (2001). Solution structure of bacteriophage PRD1 vertex complex. *J Biol Chem* **276**(49), 46187-46195.

Strömsten, N. J., Bamford, D. H., Bamford, J. K. (2003). The unique vertex of bacterial virus PRD1 is connected to the viral internal membrane. *J Virol* **77**(11), 6314-6321.

Tang, J., Olson, N., Jardine, P. J., Grimes, S., Anderson, D. L., Baker, T. S. (2008). DNA poised for release in bacteriophage phi29. *Structure* **16**(6), 935-943.

Thomas, C. P., Booth, T. F., Roy, P. (1990). Synthesis of bluetongue virus-encoded phosphoprotein and formation of inclusion bodies by recombinant baculovirus in insect cells: it binds the single-stranded RNA species. *J Gen Virol* **71 (Pt 9)**, 2073-2083.

Thon, F. (1971). Phase contrast electron microscopy , *Electron microscopy in material science*, Academic Press, New York.

Thuman-Commike, P. A. and W. Chiu (2000). Reconstruction principles of icosahedral virus structure determination using electron cryomicroscopy. *Micron* **31**(6), 687-711.

Toropova, K., Stockley, P. G., Ranson, N. A. (2011). Visualising a viral RNA genome poised for release from its receptor complex. *J Mol Biol* **408**(3), 408-419.

Toyoshima, C. and N. Unwin (1988). Contrast transfer for frozen-hydrated specimens: determination from pairs of defocused images. *Ultramicroscopy* **25**(4), 279-291.

Twarock, R. (2004). A tiling approach to virus capsid assembly explaining a structural puzzle in virology. *J Theor Biol* **226**(4), 477-482.

Twort, F. W. (1915). An investigation on the nature of ultra-microscopic viruses. *The Lancet* **186**(4814), 1241-1243.

Ubarretxena-Belandia, I. and D. L. Stokes (2012). Membrane protein structure determination by electron crystallography. *Curr Opin Struct Biol* **22**(4),520-8.

Uitenweerde, J. M., Theron, J., Stoltz, M. A., Huismans, H. (1995). The multimeric nonstructural NS2 proteins of bluetongue virus, African horsesickness virus, and epizootic hemorrhagic disease virus differ in their single-stranded RNA-binding ability. *Virology* **209**(2), 624-632.

van Heel, M., Gowen, B., Matadeen, R., Orlova, E. V., Finn, R., Pape, T., Cohen, D., Stark, H., Schmidt, R., Schatz, M., Patwardhan, A. (2000). Single-particle electron cryo-microscopy: towards atomic resolution. *Q Rev Biophys* **33**(4), 307-369.

van Raaij, M. J., Mitraki, A., Lavigne, G., Cusack, S. (1999). A triple beta-spiral in the adenovirus fibre shaft reveals a new structural motif for a fibrous protein. *Nature* **401**(6756), 935-938.

Varghese, J. N., Laver, W. G., Colman, P. M. (1983). Structure of the influenza virus glycoprotein antigen neuraminidase at 2.9 Å resolution. *Nature* **303**(5912), 35-40.

Venter, J. C., Adams, M. D., Myers, E. W., Li, P. W., Mural, R. J., Sutton, G. G., Smith, H. O., Yandell, M., Evans, C. A., Holt, R. A., Gocayne, J. D., Amanatides, P., Ballew, R. M., Huson, D. H., Wortman, J. R., Zhang, Q., Kodira, C. D., Zheng, X. H., Chen, L., Skupski, M., Subramanian, G., Thomas, P. D., Zhang, J., Gabor Miklos, G. L., Nelson, C., Broder, S., Clark, A. G., Nadeau, J., McKusick, V. A., Zinder, N., Levine, A. J., Roberts, R. J., Simon, M., Slayman, C., Hunkapiller, M., Bolanos, R., Delcher, A., Dew, I., Fasulo, D., Flanigan, M., Florea, L., Halpern, A., Hannenhalli, S., Kravitz, S., Levy, S., Mobarry, C., Reinert, K., Remington, K., Abu-Threideh, J., Beasley, E., Biddick, K., Bonazzi, V., Brandon, R., Cargill, M., Chandramouliswaran, I., Charlab, R., Chaturvedi, K., Deng, Z., Di Francesco, V., Dunn, P., Eilbeck, K., Evangelista, C., Gabrielian, A. E., Gan, W., Ge, W., Gong, F., Gu, Z., Guan, P., Heiman, T. J., Higgins, M. E., Ji, R. R., Ke, Z., Ketchum, K. A., Lai, Z., Lei, Y., Li, Z., Li, J., Liang, Y., Lin, X., Lu, F., Merkulov, G. V., Milshina, N., Moore, H. M., Naik, A. K., Narayan, V. A., Neelam, B., Nusskern, D., Rusch, D. B., Salzberg, S., Shao, W., Shue, B., Sun, J., Wang, Z., Wang, A., Wang, X., Wang, J., Wei, M., Wides, R., Xiao, C., Yan, C., Yao, A., Ye, J., Zhan, M., Zhang, W., Zhao, Q., Zheng, L., Zhong, F., Zhong, W., Zhu, S., Zhao, S., Gilbert, D., Baumhueter, S., Spier, G., Carter, C., Cravchik, A., Woodage, T., Ali, F., An, H., Awe, A., Baldwin, D., Baden, H., Barnstead, M., Barrow, I., Beeson, K., Busam, D., Carver, A., Center, A., Cheng, M. L., Curry, L., Danaher, S., Davenport, L., Desilets, R., Dietz, S., Dodson, K., Doup, L., Ferriera, S., Garg, N., Gluecksmann, A., Hart, B., Haynes, C., Heiner, C., Hladun, S., Hostin, D., Houck, J., Howland, T., Ibegwam, C., Johnson, J., Kalush, F., Kline, L., Koduru, S., Love, A., Mann, F., May, D., McCawley, S., McIntosh, T., McMullen, I., Moy, M., Moy, L., Murphy, B., Nelson, K., Pfannkoch, C., Pratts, E., Puri, V., qureshi, H., Reardon, M., Rodriguez, R., Rogers, Y. H., Romblad, D., Ruhfel, B., Scott, R., Sitter, C., Smallwood, M., Stewart, E., Strong, R., Suh, E., Thomas, R., Tint, N. N., Tse, S., Vech, C., Wang, G., Wetter, J., Williams, S., Williams, M, Windsor, S., Winn-Deen, E., Wolfe, K., Zaveri, J., Zaveri, K., Abril, J. F., Guigo, R., Campbell, M. J., Sjolander, K. V., Karlak, B., Kejariwal, A., Mi, H., Lazareva, B., Hatton, T., Narechania, A., Diemer, K., Muruganujan, A., Guo, N., Sato, S., Bafna, V., Istrail, S., Lippert, R., Schwartz, R., Walenz, B., Yooseph, S., Allen, D., Basu, A., Baxendale, J., Blick, L., Caminha, M., Carnes-Stine, J., Caulk, P., Chiang, Y. H., Coyne, M., Dahlk, C., Mays, A., Dombroski, M., Donnelly, M., Ely, D., Esparham, S., Fosler, C., Gire, H., Glanowski, S., Glasser, K., Glodek, A., Gorokhov, M., Graham, K., Gropman, B., Harris, M., Heil, J., Henderson, S., Hoover, J., Jennings, D., Jordan, C., Jordan, J., Kasha, J., Kagan, L., Kraft, C., Levitsky, A., Lewis, M., Liu, X., Lopez, J., Ma, D., Majoros, W., McDaniel, J., Murphy, S., Newman, M., Nguyen, T., Nguyen, N., Nodell, M., Pan, S., Peck, J., Peterson, M., Rowe, W., Sanders, R., Scott, J., Simpson, M., Smith, T., Sprague, A., Stockwell, T., Turner, R., Venter, E., Wang, M., Wen, M., Wu, D., Wu, M., Xia, A., Zandieh, A., Zhu, X. (2001). The sequence of the human genome. *Science* **291**(5507), 1304-1351.

Vestergaard, G., Haring, M., Peng, X., Rachel, R., Garett, R. A., Prangishvili, D. (2005). A novel rudivirus, ARV1, of the hyperthermophilic archaeal genus Acidianus. *Virology* **336**(1), 83-92.

Vinga, I., Baptista, C., Auzat, I., Petipas, I., Lurz, R., Tavares, P., Santos, M. A., Sao-Jose, C. (2012). Role of bacteriophage SPP1 tail spike protein gp21 on host cell receptor binding and trigger of phage DNA ejection. *Mol Microbiol* **83**(2), 289-303.

Vreede, F. T. and H. Huismans (1998). Sequence analysis of the RNA polymerase gene of African horsesickness virus. *Arch Virol* **143**(2), 413-419.

Watanabe, R. and R. A. Lamb (2010). Influenza virus budding does not require a functional AAA+ ATPase, VPS4. *Virus Res* **153**(1), 58-63.

White, T. A., Bartesaghi, A., Borgnia, M. J., Meyerson, J. R., de la Cruz, M. J., Bess, J. W., Nandwani, R., Hoxie, J. A., Lifson, J. D., Milne, J. L., Subramaniam, S. (2010). Molecular architectures of trimeric SIV and HIV-1 envelope glycoproteins on intact viruses: strain-dependent variation in quaternary structure. *PLoS Pathog* **6**(12), e1001249.

Williams, C. F., Inoue, T., Lucus, A. M., Zanotto, P. M., Roy, P. (1998). The complete sequence of four major structural proteins of African horsesickness virus serotype 6: evolutionary relationships within and between the orbiviruses. *Virus Res* **53**(1), 53-73.

Wilson, I. A., Skehel, J. J., Wiley, D. C. (1981). Structure of the haemagglutinin membrane glycoprotein of influenza virus at 3 Å resolution. *Nature* **289**(5796), 366-373.

Winkler, H. (2007). 3D reconstruction and processing of volumetric data in cryo-electron tomography. *J Struct Biol* **157**(1), 126-137.

Witte, A., Baranyi, U., Klein, R., Sulzner, M., Luo, C., Wanner, G., Kruger, D. H., Lubitz, W. (1997). Characterization of Natronobacterium magadii phage phi Ch1, a unique archaeal phage containing DNA and RNA. *Mol Microbiol* **23**(3), 603-616.

Wright, E. R., Schooler, J. B., Ding, H. J., Kieffer, C., Fillmore, C., Sundquist, W. I., Jensen, G. J. (2007). Electron cryotomography of immature HIV-1 virions reveals the structure of the CA and SP1 Gag shells. *EMBO J* **26**(8), 2218-2226.

Wurtz, M. (1992). Bacteriophage structure. *Electron Microsc Rev* **5**(2), 283-309.

Xiong, Q., Morphew, M. K., Scwartz, C. L., Hoenger, A. H., Mastronarde, D. N. (2009). CTF determination and correction for low dose tomographic tilt series. *J Struct Biol* **168**(3), 378-387.

Xu, L., Benson, S. D., Butcher, S. J., Bamford, D. H., Burnett, R. M. (2003). The receptor binding protein P2 of PRD1, a virus targeting antibiotic-resistant bacteria, has a novel fold suggesting multiple functions. *Structure* **11**(3), 309-322.

Yan, X., Dryden, K. A., Tang, J., Baker, T. S. (2007). Ab initio random model method facilitates 3D reconstruction of icosahedral particles. *J Struct Biol* **157**(1), 211-225.

Yan, X., Sinkovits, R. S., Baker, T. S. (2007). AUTO3DEM--an automated and high throughput program for image reconstruction of icosahedral particles. *J Struct Biol* **157**(1), 73-82.

Yasumura, Y., and Kawakita, Y. (1963). *Nippon Rinsho* **21**, 1209.

Yu, R., Lentzen, M., Zhu, J. (2012). Effective object planes for aberration-corrected transmission electron microscopy. *Ultramicroscopy* **112**(1), 15-21.

Yu, X., Jin, L., Zhou, Z. H. (2008). 3.88 A structure of cytoplasmic polyhedrosis virus by cryo-electron microscopy. *Nature* **453**(7193), 415-419.

Yu, X., Shah, S., Atanasov, I., Lo, P., Liu, F., Britt, W. J., Zhou, Z. H. (2005). Three-dimensional localization of the smallest capsid protein in the human cytomegalovirus capsid. *J Virol* **79**(2), 1327-1332.

Yu, X., Shah, S., Lee, M., Dai, W., Lo, P., Britt, W., Zhu, H., Liu, F., Zhou, Z. H. (2011). Biochemical and structural characterization of the capsid-bound tegument proteins of human cytomegalovirus. *J Struct Biol* **174**(3), 451-460.

Yu, X. K., O'Connor, C. M., Atanasov, I., Damania, B., Kedes, D. H., Zhou, Z. H.(2003). Three-dimensional structures of the A, B, and C capsids of rhesus monkey rhadinovirus: insights into gammaherpesvirus capsid assembly, maturation, and DNA packaging. *J Virol* **77**(24), 13182-13193.

Zanetti, G., Briggs, J. A., Grünewald, K., Sattentau, Q. J., Fuller, S. D. (2006). Cryo-electron tomographic structure of an immunodeficiency virus envelope complex in situ. *PLoS Pathog* **2**(8), e83.

Zanetti, G., Riches, J. D., Fuller, S. D., Briggs, J. A. (2009). Contrast transfer function correction applied to cryo-electron tomography and sub-tomogram averaging. *J Struct Biol* **168**(2), 305-312.

Zhang, R., Hryc, C. F., Cong, Y., Liu, X., Jakana, J., Gorchakov, R., Baker, M. L., Weaver, S. C., Chiu, W. (2011). 4.4 Å cryo-EM structure of an enveloped alphavirus Venezuelan equine encephalitis virus. *EMBO J* **30**(18), 3854-3863.

Zhang, X., Boyce, M., Bhattacharya, B., Schein, S., Roy, P., Zhou, Z. H. (2010). Bluetongue virus coat protein VP2 contains sialic acid-binding domains, and VP5 resembles enveloped virus fusion proteins. *Proc Natl Acad Sci U S A* **107**(14), 6292-6297.

Zhang, X., Jin, L., Fang, Q., Hui, W. H., Zhou, Z. H. (2010). 3.3 Å cryo-EM structure of a nonenveloped virus reveals a priming mechanism for cell entry. *Cell* **141**(3), 472-482.

Zhang, X., Settembre, E., Xu, C., Dormitzer, P. R., Bellamy, R., Harrison, S. C., Grogorieff, N. (2008)."Near-atomic resolution using electron cryomicroscopy and single-particle reconstruction. *Proc Natl Acad Sci U S A* **105**(6), 1867-1872.

Zhang, X., Walker, S. B., Chipman, P. R., Nibert, M. L., Baker, T. S.(2003). Reovirus polymerase lambda 3 localized by cryo-electron microscopy of virions at a resolution of 7.6 Å. *Nat Struct Biol* **10**(12), 1011-1018.

Zhang, Y. (2008). I-TASSER server for protein 3D structure prediction. *BMC Bioinformatics* **9**, 40.

Zhou, Z. H., Chen, D. H., Jakana, J., Rixon, F. J., Chiu, W. (1999). Visualization of tegument-capsid interactions and DNA in intact herpes simplex virus type 1 virions. *J Virol* **73**(4), 3210-3218.

Zhou, Z. H., Chiu, W., Haskell, K., Spears, H. Jr., Jakana, J., Rixon, F. J., Scott, L. R. (1998). Refinement of herpesvirus B-capsid structure on parallel supercomputers. *Biophys J* **74**(1), 576-588.

Zhou, Z. H., Dougherty, M., Jakana, J., He, J., Rixon, F. J., Chiu, W. (2000). Seeing the herpesvirus capsid at 8.5 Å. *Science* **288**(5467), 877-880.

Zhu, P., Chertova, E., Bess, J. Jr., Lifson, J. D., Arthur, L. O., Liu, J., Taylor, K. A., Roux, K. H. (2003). Electron tomography analysis of envelope glycoprotein trimers on HIV and simian immunodeficiency virus virions. *Proc Natl Acad Sci U S A* **100**(26), 15812-15817.

Zhu, P., Winkler, H., Chertova, E., Taylor, K. A., Roux, K. H. (2008). Cryoelectron tomography of HIV-1 envelope spikes: further evidence for tripod-like legs. *PLoS Pathog* **4**(11), e1000203.

Zubieta, C., Schoehn, G., Chroboczek, J., Cusack, S. (2005). The structure of the human adenovirus 2 penton. *Mol Cell* **17**(1), 121-135.